




2017

PROPERTIES AND OPTIMIZATION OF RESPIRATORY NAVIGATOR GATING FOR SPIRAL CINE DENSE CARDIAC MRI

Sean Michael Hamlet

University of Kentucky, seanmhamlet@gmail.com

Author ORCID Identifier:

 <https://orcid.org/0000-0002-5452-3224>

Digital Object Identifier: <https://doi.org/10.13023/ETD.2017.349>

[Right click to open a feedback form in a new tab to let us know how this document benefits you.](#)

Recommended Citation

Hamlet, Sean Michael, "PROPERTIES AND OPTIMIZATION OF RESPIRATORY NAVIGATOR GATING FOR SPIRAL CINE DENSE CARDIAC MRI" (2017). *Theses and Dissertations--Electrical and Computer Engineering*. 106.

https://uknowledge.uky.edu/ece_etds/106

This Doctoral Dissertation is brought to you for free and open access by the Electrical and Computer Engineering at UKnowledge. It has been accepted for inclusion in Theses and Dissertations--Electrical and Computer Engineering by an authorized administrator of UKnowledge. For more information, please contact UKnowledge@lsv.uky.edu.

STUDENT AGREEMENT:

I represent that my thesis or dissertation and abstract are my original work. Proper attribution has been given to all outside sources. I understand that I am solely responsible for obtaining any needed copyright permissions. I have obtained needed written permission statement(s) from the owner(s) of each third-party copyrighted matter to be included in my work, allowing electronic distribution (if such use is not permitted by the fair use doctrine) which will be submitted to UKnowledge as Additional File.

I hereby grant to The University of Kentucky and its agents the irrevocable, non-exclusive, and royalty-free license to archive and make accessible my work in whole or in part in all forms of media, now or hereafter known. I agree that the document mentioned above may be made available immediately for worldwide access unless an embargo applies.

I retain all other ownership rights to the copyright of my work. I also retain the right to use in future works (such as articles or books) all or part of my work. I understand that I am free to register the copyright to my work.

REVIEW, APPROVAL AND ACCEPTANCE

The document mentioned above has been reviewed and accepted by the student's advisor, on behalf of the advisory committee, and by the Director of Graduate Studies (DGS), on behalf of the program; we verify that this is the final, approved version of the student's thesis including all changes required by the advisory committee. The undersigned agree to abide by the statements above.

Sean Michael Hamlet, Student

Dr. Brandon Fornwalt, Major Professor

Dr. Caicheng Lu, Director of Graduate Studies

PROPERTIES AND OPTIMIZATION OF RESPIRATORY NAVIGATOR
GATING FOR SPIRAL CINE DENSE CARDIAC MRI

DISSERTATION

A dissertation submitted in partial fulfillment of the
requirements of the degree of Doctor of Philosophy in the
College of Engineering
at the University of Kentucky

By

Sean Michael Hamlet

Lexington, Kentucky

Co-Directors: Dr. Brandon Fornwalt, Assistant Professor of Electrical Engineering
and Dr. Kevin Donohue, Professor of Electrical Engineering

Lexington, Kentucky

2017

Copyright © Sean Michael Hamlet 2017

ABSTRACT OF DISSERTATION

PROPERTIES AND OPTIMIZATION OF RESPIRATORY NAVIGATOR GATING FOR SPIRAL CINE DENSE CARDIAC MRI

Cardiac magnetic resonance (MR) imaging can non-invasively assess heart function. Displacement encoding with stimulated echoes (DENSE) is an advanced cardiac MR imaging technique that measures tissue displacement and can be used to quantify cardiac mechanics (e.g. strain and torsion). When combined with clinical risk factors, cardiac mechanics have been shown to be better predictors of mortality than traditional measures of heart function.

End-expiratory breath-holds are typically used to minimize respiratory motion artifacts. Unfortunately, requiring subjects to breath-hold introduces limitations with the duration of image acquisition and quality of data acquired, especially in patients with limited ability to hold their breath. Thus, DENSE acquisitions often require respiratory navigator gating, which works by measuring the diaphragm during normal breathing and only acquiring data when the diaphragm is within a pre-defined acceptance window.

Unfortunately, navigator gating results in long scan durations due to inconsistent breathing patterns. Also, the navigator echo can be used in different ways to accept or reject image data, which creates several navigator configuration options. Each respiratory navigator configuration has distinct advantages and disadvantages that directly affect scan duration and image quality, which can affect derived cardiac mechanics. Scan duration and image quality need to be optimized to improve the clinical utility of DENSE. Thus, the goal of this project was to optimize those parameters. To accomplish this goal, we set out to complete 3 aims: 1) understand how respiratory gating affects the reproducibility of measures of cardiac mechanics, 2) determine the optimal respiratory navigator configuration, and 3) reduce scan duration by developing and using an interactive videogame to optimize navigator efficiency.

Aim 1 of this project demonstrated that the variability in torsion, but not strain, could be significantly reduced through the use of a respiratory navigator compared to traditional breath-holds. Aim 2 demonstrated that, among the configuration options,

the dual-navigator configuration resulted in the best image quality compared to the reference standard (traditional breath-holds), but also resulted in the longest scan duration. In Aim 3, we developed an interactive breathing-controlled videogame and demonstrated that its use during cardiac MR can significantly reduce scan duration compared to traditional free-breathing and also led to a small improvement in signal-to-noise ratio of the acquired images.

In summary, respiratory navigator gating with DENSE 1) reduces the variability in measured LV torsion, 2) results in the best image quality with the dual-navigator configuration, and 3) results in significantly shorter scan durations through the use of an interactive videogame. Selecting the optimal navigator configuration and using an interactive videogame can improve the clinical utility of DENSE.

KEYWORDS: Respiratory Navigator Gating, Cardiac Magnetic Resonance Imaging, Displacement Encoding with Stimulated Echoes, Cardiac Mechanics, Interactive Videogame

Sean Michael Hamlet

14 June 2017

Date

PROPERTIES AND OPTIMIZATION OF RESPIRATORY NAVIGATOR
GATING FOR SPIRAL CINE DENSE CARDIAC MRI

By

Sean Michael Hamlet

Dr. Brandon Fornwalt, MD, PhD
Co-Director of Dissertation

Dr. Kevin Donohue, PhD
Co-Director of Dissertation

Dr. Caicheng Lu, PhD
Director of Graduate Studies

14 June 2017

Date

To Regina

Once again, I could not have done this without your love and support.
Thank you for your continuing positivity and encouragement.

ACKNOWLEDGMENTS

As in the dedication, I want to thank my wife. Throughout this entire process, including all of my education, she has pushed me forward and supported me in more ways than I can count. This dissertation is a summary of the work I've completed. I sincerely appreciated her support, especially since a lot my time was spent with my eyes glued to the computer screen at home or gone from home all together. This was the hardest thing I've ever completed and her support was what got me through it.

Although this research was completed with my individual effort, its progress could not have been completed without the efforts of several people. I'd like to thank...

1. Brandon Fornwalt for being very motivating and passionate about the overall goals in his lab, which was definitely something that drew me to him. He's always thinking about how we can improve. Most importantly, he's always pushing us to do our best work and I sincerely appreciate that. He's also focused on making sure that his graduate students work on impactful and exciting projects and looked for any way he could help. I'll always appreciate that about him. I'm happy to have been a part of his lab, which has shaped my thoughts and perspectives as well as pushed me to be a better researcher.
2. Chris Haggerty for the time he has taken to work with me on my projects and publications. He was always there to answer any questions about my ideas for experiments and analysis as well as to help me solidify my thoughts on paper.
3. Jonathan Suever for sharing his extensive programming knowledge (which I'm working to get to) with me. Whether it was talking about the technical details of how to implement an idea or discussing the appropriate hardware/software for the job, I enjoyed learning from and with him.
4. Greg Wehner for sharing this entire process together as graduate students. It's been a long road and we've both definitely grown from it. Greg and I had the

opportunity to lean on each other when we needed help. More importantly, Greg and I have become good friends. Although he is moving on to finish his MD degree and I am moving on to be a software engineer, I'm happy we were able to share this journey and I hope our paths cross again someday.

5. David Powell for teaching me about MRI in the classroom and informal settings along with troubleshooting problems with our scans. Dave has been so helpful with everything MRI (which is pretty much everything that we do in this lab). I can't thank him enough for his kindness and wish him the best.
6. Jonathan Grabau for spending all his time working to help me with my videogame project. Jonathan was responsible for the high throughput of children volunteers we were able to scan for the videogame project. I'm extremely grateful for his kindness and helpfulness along with his friendship.
7. Moriel Vandsburger for working with Greg and I so that we could continue our projects and efforts at UK. More importantly, Moriel is a great person who really cares to help out. Lastly, I'll miss having someone I can discuss food with (and I am a lover of food). I can't thank him enough and wish him the best of luck at Berkeley.
8. Darin Cecil for being extremely helpful in making sure Greg and I don't have to deal with all the paperwork with our grants and funding. Darin has always been willing to help out me with a problem (no matter how small). I sincerely thank Darin for this.
9. Tanya Graf for doing so much to make sure my life as a graduate student and researcher goes smoothly. She was always someone I could come to with a problem and she would know immediately how or who could solve it. I sincerely appreciate her kindness and helpfulness.

10. Other labmates (Linyuan Jing, Sam Fielden, David van Maanen, Chris Nevius, Arichanah Pulenthiran, and others) for being extremely helpful with reviews of my work and critiques of projects and presentations. Most importantly, I've appreciated the overall friendliness, helpfulness, and drive of everyone. Brandon and the lab does a great job of selecting fantastic candidates. I wish them and future labmates, good luck.
11. Kevin Donohue for being my Master's advisor, which allowed me the opportunity to meet Brandon and eventually become a graduate student in his lab. I've always appreciated Dr. Donohue's guidance and helpfulness in the entirety of the graduate student process as well as for serving as co-Chair on my committee.
12. Laurence Hassebrook for serving on my committee, for his insightful comments about the training system for the videogame project, and for the opportunity to learn more about signal processing in his courses.
13. Abhijit Patwardhan for serving on my committee, for his suggestions regarding how to test the videogame, and for the opportunity to learn more about biomedical signal processing his class.
14. Gabe Dadi for serving as external examiner on my committee for my defense.

TABLE OF CONTENTS

Acknowledgments.....	iii
List of Tables	x
List of Figures	xii
Chapter 1: Background.....	1
1.1 Heart Disease	1
1.2 Standard Cardiac Magnetic Resonance Imaging (MRI) and Traditional Measures of Cardiac Function	1
1.3 Advanced Measures of Function: Cardiac Mechanics	2
1.4 Displacement Encoded Cardiac MRI.....	2
1.5 Respiratory Motion and Blurring.....	3
1.6 Inconsistent Breath-holds	4
1.7 Respiratory Navigator Gating	5
1.8 Navigator Efficiency	6
1.9 Dissertation Outline	6
Chapter 2: Effects of Patient-Specific Variability in Inconsistent End-Expiratory Diaphragm Position on the Quantification of Left Ventricular Cardiac Strains	10
2.1 Background	10
2.2 Methods	12
2.2.1 Subjects	12
2.2.2 Quantification of Inconsistent End-Expiratory Positions	12
2.2.3 DENSE Acquisition	12
2.2.4 DENSE Post-Processing	14
2.2.5 Statistics	15
2.3 Results.....	17
2.3.1 Inconsistent End-Expiratory Positions	17

2.3.2	Differences and Variability in Peak Strains	17
2.4	Discussion	22
2.4.1	Limitations	25
2.5	Conclusion.....	26
Chapter 3: Using a Respiratory Navigator Reduces Variability when		
Quantifying Left Ventricular Torsion		
3.1	Background	27
3.2	Methods	28
3.2.1	LV Motion Quantification.....	30
3.2.2	Experiment 1: Enforced End-Expiratory Variability.....	31
3.2.3	Experiment 2: Natural End-Expiratory Variability	32
3.2.4	Statistics	34
3.2.5	Theoretical Sample Size Calculation	35
3.3	Results.....	35
3.3.1	Inconsistent End-Expiratory Positions	36
3.3.2	Torsion	37
3.3.3	Theoretical Sample Sizes.....	37
3.4	Discussion	40
3.4.1	Limitations and Future Directions	44
3.5	Conclusion.....	44
Chapter 4: Optimal Respiratory Navigator Configuration.....		
4.1	Introduction.....	45
4.2	Methods	47
4.2.1	Subjects	47
4.2.2	Image Acquisition	47
4.2.3	Navigator Feedback	50
4.2.4	DENSE Post-Processing	50

4.2.5	Analysis	51
4.2.6	Comparison of Acquisition Configurations.....	52
4.3	Results.....	53
4.3.1	Average Peak Strains.....	53
4.3.2	Signal-to-Noise Ratio.....	53
4.3.3	Navigator Efficiency	57
4.4	Discussion	58
4.4.1	Limitations and Future Directions	62
4.5	Conclusion.....	63
Chapter 5: Interactive Feedback Game Designed to Improve Navigator		
	Efficiency.....	64
5.1	Background	64
5.2	Methods	67
5.2.1	Feedback videogame overview	67
5.2.2	Motivation for Design	68
5.2.3	Hardware Design	68
5.2.4	Overall Software Design.....	69
5.2.5	Algorithm	70
5.2.6	Participants	72
5.2.7	Imaging.....	73
5.2.8	Calculation of cardiac strains from DENSE	74
5.2.9	Analysis	75
5.2.10	Training	76
5.2.11	Training Protocol.....	77
5.2.12	Statistics	77
5.3	Results.....	78
5.3.1	Navigator Efficiency	78

5.3.2	SNR	78
5.3.3	Heart rate	81
5.3.4	Strain	83
5.3.5	Survey Responses	83
5.4	Discussion	90
5.4.1	Navigator Efficiency	90
5.4.2	SNR	91
5.4.3	Heart Rate	91
5.4.4	Strains	92
5.4.5	Clinical Implications	93
5.4.6	Comparison with Previous Work	93
5.4.7	Limitations	94
5.5	Conclusion	97
Chapter 6:	Conclusions and Future Work	98
6.1	Summary	98
6.1.1	Aim 1	98
6.1.2	Aim 2	100
6.1.3	Aim 3	101
6.2	Clinical Implications	102
6.3	Future Directions	104
Bibliography	107
Vita	117

LIST OF TABLES

2.1	Global and regional peak strains (mean ± standard deviation) from the three acceptance window positions (minimum, middle, and maximum) for all subjects combined	19
2.2	Segmental circumferential strain (% , mean ± standard deviation) from the three acceptance window positions (minimum, middle, and maximum) for all subjects combined	20
2.3	Segmental radial strain (% , mean ± standard deviation) from the three acceptance window positions (minimum, middle, and maximum) for all subjects combined.....	21
2.4	Standard deviation of global and regional peak strains across inconsistent (maximum, middle, minimum) and consistent (middle and repeated middle) acceptance window positions.....	23
2.5	Power analyses for the ability to detect a difference in global and regional strain between different end-expiratory positions.....	23
3.1	Mean (± standard deviation) of torsion across the volunteers within each experiment	38
3.2	Mean (± standard deviation) of torsion across the volunteers within each experiment	40
4.1	Average strains for different acquisition techniques.....	54
4.2	Segmental strain results for navigator gating and breath-holds in adults	54
4.3	Segmental strain agreement between navigator gating and breath-holds from spiral cine DENSE	56
4.4	CI Results for Differences in Strain Between Navigator Gating and Breathhold DENSE.....	56

4.5	Signal-to-noise ratios for different navigator gating configurations in adults and children	57
4.6	Navigator efficiencies for different navigator gating configurations in adults and children	58
5.1	Average Heart Rate for Off-scanner Trained and Untrained groups.....	82
5.2	Global peak strain results for NF and FG scans.....	83

LIST OF FIGURES

1.1	Measuring cardiac strains dramatically improves the ability to predict mortality.....	2
1.2	Strain analysis of myocardial segments in three orthogonal directions	3
1.3	During respiration, diaphragm motion causes the heart to translate a significant distance while the imaging plane remains fixed.....	4
1.4	High-quality image vs image with breathing artifacts that results in unusable data	5
1.5	Respiratory navigator gating.....	7
1.6	Consistent vs Inconsistent Breathing	7
2.1	During respiration, diaphragm motion causes the heart to translate a significant distance while the imaging plane remains fixed.....	11
2.2	Respiratory navigator gating.....	13
2.3	A respiratory navigator was used to measure end-expiratory positions to define the patient-specific minimum, middle, and maximum end-expiratory positions	13
3.1	Computation of LV torsion from basal and apical images.....	29
3.2	Real time images of the diaphragm as it translates during a respiratory cycle	29
3.3	Respiratory navigator gating.....	32
3.4	Measured end expiratory diaphragm positions were used to define subject specific maximum, middle, and minimum end expiratory positions	33
3.5	The nine possible torsion permutations were constructed from three basal and three apical images	33
3.6	Inconsistent end expiratory positions across ten consecutive breath holds in patients and healthy controls.....	36

3.7	DENSE images from a representative subject show the relative twist differences between the basal and apical images at end systole	38
3.8	Variability of torsion due to enforced inconsistent end-expiratory positions versus the subject specific range of end-expiratory position	39
3.9	Variability of torsion due to naturally inconsistent end-expiratory positions versus the standard deviation of end-expiratory position.....	39
4.1	Different navigator gating configurations used to acquire DENSE image data.....	48
4.2	Theoretical example to demonstrate the disadvantages of single- and dual-navigator gating configurations.....	49
4.3	Bland-Altman plots of average peak circumferential (Ecc), radial (Err), and longitudinal (Ell) strains for retrospective, prospective, and dual navigator gating vs breath-hold	55
5.1	Feedback videogame.....	66
5.2	MRI Feedback Setup	68
5.3	Overall hardware block diagram for Bubble Gulp (Feedback Game)	70
5.4	Overall software block diagram for Bubble Gulp (Feedback Game)	70
5.5	Overall image processing algorithm block diagram for Bubble Gulp (Feedback Game).....	71
5.6	Example Navigator Image to be Processed	72
5.7	Basic text feedback block diagram	73
5.8	Navigator Efficiency for Feedback Game vs No Feedback.....	79
5.9	Average navigator efficiency for Off-scanner Trained and Untrained groups	80
5.10	SNR for all No Feedback and Feedback Game images.....	80
5.11	Mean and standard deviation of heart rate for No Feedback and Feedback Game acquisitions	81

5.12	Feedback Videogame Survey Question 1.....	84
5.13	Feedback Videogame Survey Question 2.....	85
5.14	Feedback Videogame Survey Question 3.....	86
5.15	Feedback Videogame Survey Question 4.....	87
5.16	Feedback Videogame Survey Question 6.....	88
5.17	Feedback Videogame Survey Question 7.....	89

CHAPTER 1

BACKGROUND

1.1 Heart Disease

Heart disease is the leading cause of death for both adult men and women [1]. The term "heart disease" refers to conditions that involve narrow or blocked blood vessels, which can lead to a heart attack, or conditions that affect the heart muscle, valves, or rhythm, which can lead to inefficient pumping and heart failure [1]. In addition to adults, there are children who are born with congenital heart disease (CHD), heart defects that can be present at birth, which is a growing problem that affects over 2 million people in the US alone [2]. As surgical and medical therapies have improved, children with CHD are living to adulthood. For both adults and children, in order to develop improved techniques for treatment and therapy, heart disease and cardiac function need to be accurately monitored.

1.2 Standard Cardiac Magnetic Resonance Imaging (MRI) and Traditional Measures of Cardiac Function

Magnetic resonance imaging (MRI), a non-invasive, non-ionizing medical imaging technique, has become standard protocol for diagnosis, prognosis, and management of acquired and congenital heart diseases. Traditional measures of cardiac function, such as ventricular volumes, ventricular mass, and ejection fraction, can be derived from standard cardiac MRI. Whole heart function is typically assessed with these traditional metrics, but unfortunately, they may not contain enough information to explain the complex nature of some heart diseases. Moreover, there is a growing body of evidence that suggests that, when combined with clinical risk factors (e.g. hypertension), advanced measures of cardiac mechanics (e.g. cardiac strains and torsion) are better predictors of mortality

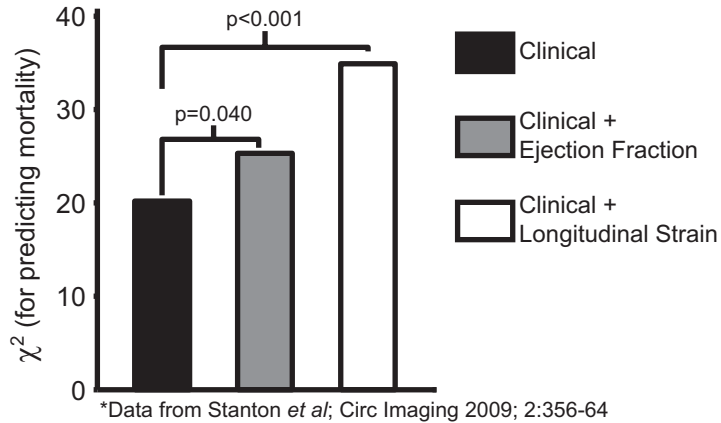


Figure 1.1: Measuring cardiac strains dramatically improves the ability to predict mortality.

compared to traditional measures [3] (Figure 1.1).

1.3 Advanced Measures of Function: Cardiac Mechanics

Cardiac mechanics, such as strain and torsion, measure the deformation of the heart as it contracts and relaxes throughout the cardiac cycle. Strain is a measure of how small segments of the myocardium shorten or lengthen during contraction and relaxation [4, 5]. In segments of the left ventricle, strain is commonly measured in three orthogonal directions: circumferential, radial, and longitudinal (Figure 1.2). Torsion is a measure of the twisting motion along the longitudinal axis of the heart throughout the cardiac cycle [6, 7]. Cardiac mechanics can be quantified from analyzing the motion of small regions of the heart, which can be achieved by using an advanced imaging technique called spiral cine Displacement ENcoding with Stimulated Echoes (DENSE) [8].

1.4 Displacement Encoded Cardiac MRI

Spiral cine DENSE is an advanced cardiac magnetic resonance imaging technique that directly encodes the displacement of the myocardial tissue into the phase of the MR signal [8]. DENSE allows for simple and accurate quantification of cardiac

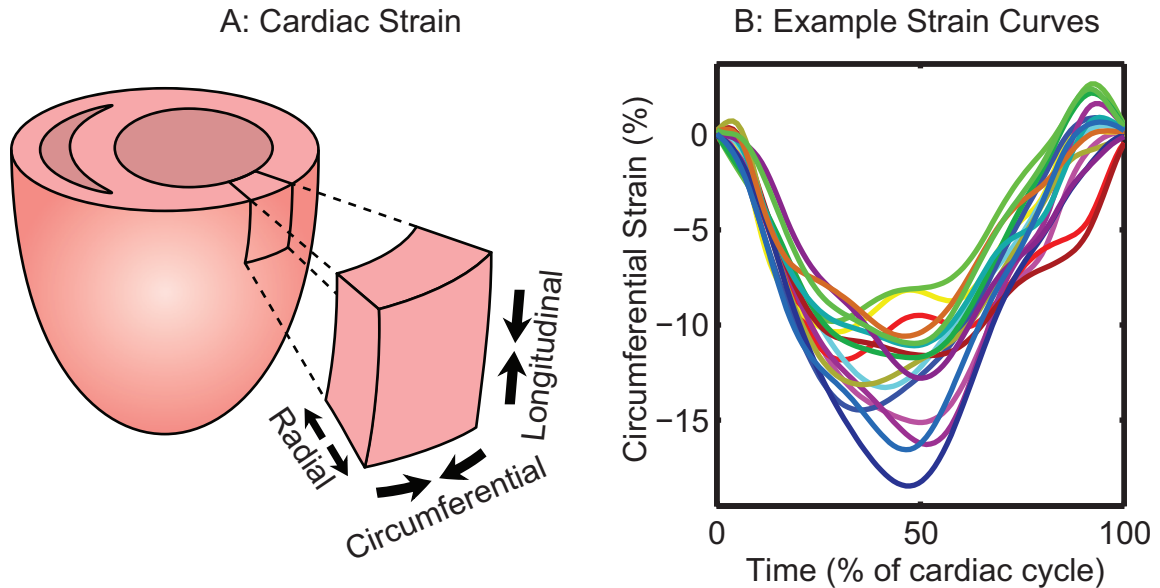


Figure 1.2: Strain analysis of myocardial segments in three orthogonal directions. A) Definition of the three orthogonal strain components: radial, circumferential, and longitudinal. B) Example circumferential strain curves over time throughout the cardiac cycle. Each curve represents the strain for a single myocardial segment. Negative values denote shortening.

mechanics. In addition, DENSE has good spatial resolution and good reproducibility [9, 10]. Moreover, DENSE has been used to quantify cardiac mechanics in both healthy and diseased animals and humans [8, 11, 12, 13, 9]

1.5 Respiratory Motion and Blurring

Due to the heart's position resting on the diaphragm (Figure 1.3), breathing during CMR acquisition results in respiratory image artifacts [14], which make images blurry and unusable (Figure 1.4). Thus, cardiac MR images are typically acquired using end-expiratory breath-holds, which are used to suspend respiration so the bulk motion of the heart is minimized during imaging. DENSE acquisitions are typically performed using end-expiratory breath-holds that are $\sim 15\text{--}20$ s in duration [12, 15, 13, 16, 17, 18, 19]. However, this method's success depends upon the patient's ability to breath-hold, which is limited in young subjects and many stages of advanced heart disease.

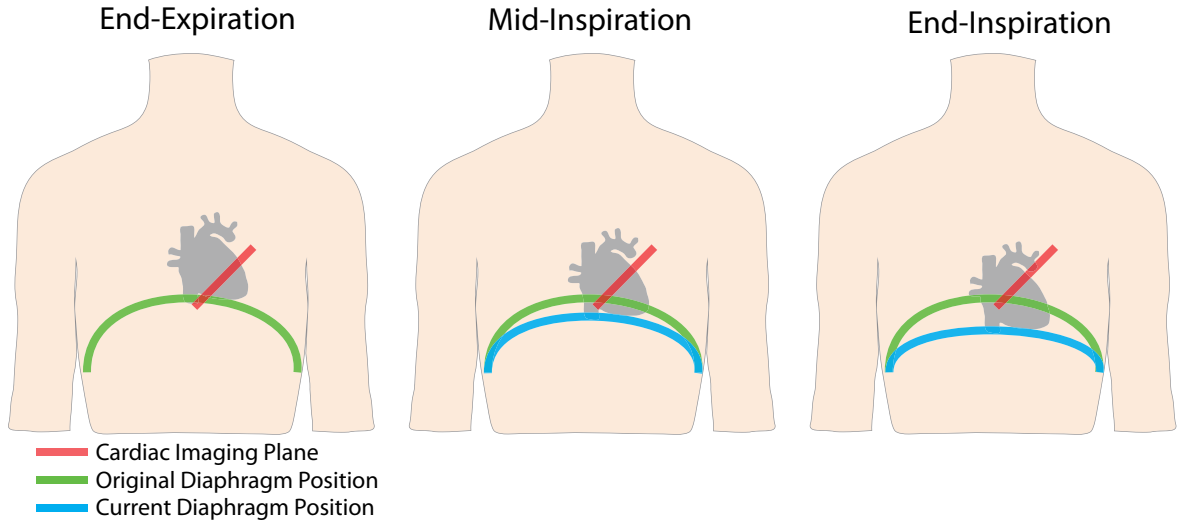


Figure 1.3: During respiration, diaphragm motion causes the heart to translate a significant distance while the imaging plane remains fixed.

1.6 Inconsistent Breath-holds

Unfortunately, patients typically struggle to achieve a consistent diaphragm position between successive breath-holds and variations of 4–13 mm are normal [20, 21, 22, 23, 24]. Inconsistent breath-holds can impact the position of the heart with respect to the imaging plane (Figure 1.3). Peak strains vary along the longitudinal axis of the heart [25, 26, 27, 28, 29, 30, 31] and torsion is typically computed from two images acquired during *separate* end-expiratory breath-holds [30]. In both cases, quantification of mechanics is performed assuming images were acquired at the same, consistent diaphragm position. Thus, we expect that translation of the heart with respect to the imaging plane (due to inconsistent end-expiratory positions) will result in differences and/or variability in measured strains and torsion. Thus, ***Aim 1*** of this project was to determine if this variability could be reduced by using a respiratory navigator to improve the consistency of the diaphragm position between breath-holds.

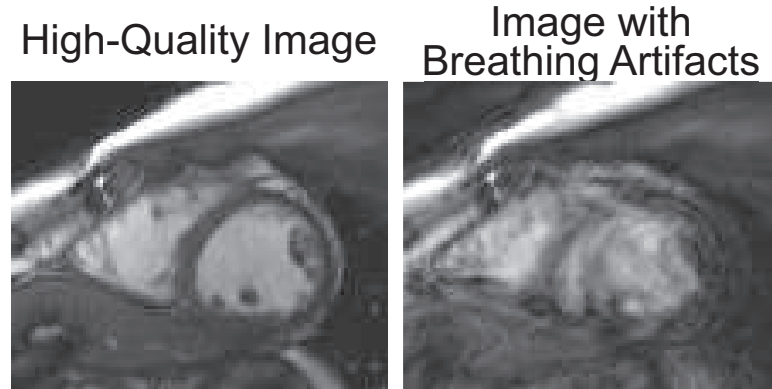


Figure 1.4: High-quality image vs image with breathing artifacts that results in unusable data.

1.7 Respiratory Navigator Gating

Respiratory navigator gating works by measuring the diaphragm position during normal breathing and only acquiring data when the diaphragm is within a pre-defined acceptance window (Figure 1.5). Respiratory navigator gating is also used to overcome the limitations of short acquisitions (end-expiratory breath-holds), which limit the ability to acquire more robust data, such as high-resolution [32] or three-dimensional (3D) DENSE imaging [16, 33, 34]. However, dissimilar to other cardiac MRI techniques, the navigator echo in the DENSE cardiac MRI sequence cannot happen at the beginning of the cardiac cycle as it would disrupt the displacement encoding. Instead, the navigator echo follows immediately after data acquisition, at the end of the cardiac cycle; this creates several configurations (prospective, retrospective, and dual) as to how the navigator can be used to either accept or reject acquired DENSE data. Previous studies have reported using the prospective single navigator configuration [16, 34]. Each configuration has distinct advantages and disadvantages that can directly affect image quality and scan duration, but no formal comparison of the configurations has been performed. Moreover, the accuracy of derived cardiac mechanics and overall image quality for these navigator configurations compared with breath-hold acquisitions as a reference

standard are unknown. Therefore, ***Aim 2** of this project was to determine the optimal navigator configuration compared to the "gold-standard" (breath-holds).*

1.8 Navigator Efficiency

Navigator efficiency is defined as the ratio of the time for which image data are accepted to the total time required to complete the image acquisition. Unfortunately, due to poor navigator efficiency, respiratory navigator gating results in significantly increased scan duration. For example, previous CMR studies have reported respiratory navigator efficiencies of 20 to 45% in adults [35, 36, 37, 38]. This poor navigator efficiency lengthens the duration of currently used clinical imaging and limits clinical feasibility of emerging advanced imaging techniques.

In general, navigator efficiency is poor due to inconsistent breathing patterns [20, 21, 22] (Figure 1.6), as commonly seen in children, and due to the patient being generally unaware of the desired acceptance window location. The use of visual feedback of the diaphragm position during CMR has been shown to improve breathing consistency and efficiency in adults up to 29% compared to traditional acquisitions without feedback [36, 37]. Therefore, it's important to investigate whether similar benefits can be achieved using visual feedback with pediatric participants, which could have substantial clinical benefit. Therefore, ***Aim 3** of this project was to develop and engage pediatric participants with a navigator-controlled videogame to help control breathing patterns, which would improve navigator efficiency.*

1.9 Dissertation Outline

The overall goal of this project was to optimize respiratory navigator gating, which would improve the clinical utility of DENSE. To accomplish this goal, we set out to accomplish 3 aims: 1) understand how respiratory navigator gating could improve the reproducibility of measures of cardiac mechanics, 2) determine the optimal respiratory navigator configuration, and 3) improve navigator efficiency,

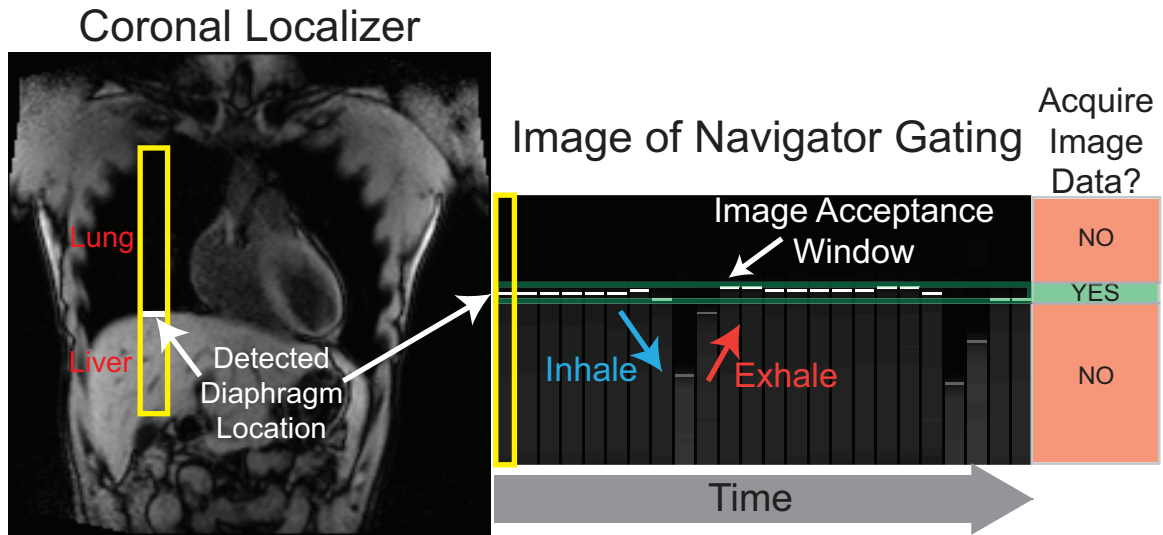


Figure 1.5: Respiratory navigator gating. (Left) The diaphragm is detected at the high-contrast interface between the lung (dark) and the liver (bright). (Right) The diaphragm location determined for multiple cardiac cycles with a narrow acceptance window defining when image data was acquired.

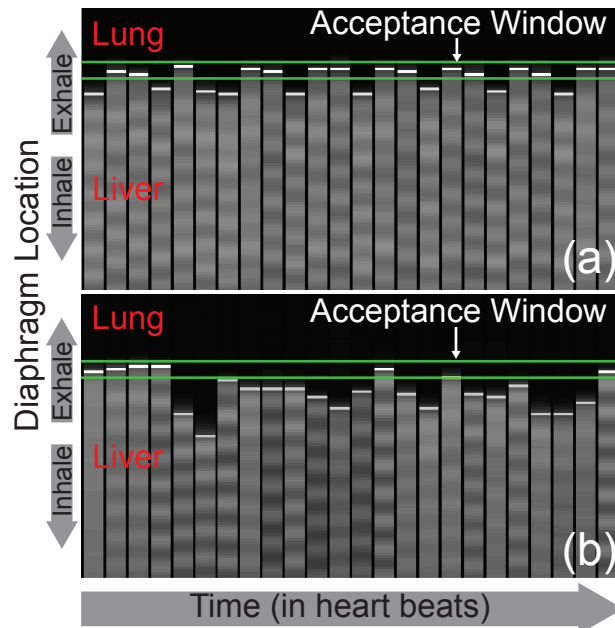


Figure 1.6: Navigator window of consistent breathing (a) resulting in a high (82%) navigator efficiency compared to inconsistent breathing (b) resulting in a very low (26%) navigator efficiency.

which reduces scan duration, by developing an interactive breathing-controlled videogame during cardiac MRI.

In Chapters 2 and 3, we address Aim 1 and the effects of inconsistent end-expiratory diaphragm position between breath-holds and respiratory navigator gating on DENSE-derived cardiac mechanics, such as left ventricular strain and torsion. In Chapter 2, we learn that cardiac strain is insensitive to normal changes in end-expiratory position between breath-hold DENSE acquisitions. In Chapter 3, we discover that use of a respiratory navigator significantly reduces the variability of cardiac torsion and thus the sample size needed to detect small changes in torsion. The conclusions of the studies performed for Chapters 2 and 3 discuss the importance of employing a respiratory navigator or some form of consistent respiratory compensation for future studies.

In Chapter 4, we address Aim 2 and determine the optimal navigator configuration compared to the breath-hold "gold-standard". We learn that left ventricular peak strains were not different between breath-held and navigator-gated DENSE acquisitions and image quality (as measured by signal-to-noise ratio) was reduced with single navigator configurations (prospective and retrospective), but not the dual configuration, compared to breath-held acquisitions. Unfortunately, use of the dual configuration resulted in a trade off with navigator efficiency, which was the poorest compared to the other navigator configurations. The conclusion of chapter 4 discusses that some form of visual feedback of the diaphragm was helpful in improving the poor navigator efficiency of the dual navigator.

In Chapter 5, we address Aim 3 by developing and testing an interactive breathing-controlled videogame for improving navigator efficiency during cardiac MRI. Fifty children participated in using the videogame during navigator-gated DENSE cardiac MRI. Analysis was performed to assess the videogame's effects on navigator efficiency, heart rate, and derived strain compared to normal free-breathing. We discovered that

using the videogame during navigator-gated cardiac MRI resulted in a substantial (76%) improvement in navigator efficiency, which leads to a 43% reduction in scan duration, and a slight (5%) improvement in image quality. Importantly, we also learn that these results can be achieved without lengthy pre-scan training on how to use the videogame. The conclusion of this chapter discusses that these findings should be generalizable to all cardiac MRI that employ the use of a respiratory navigator.

In Chapter 6, we discuss a summary of the results of all studies, their clinical implications, and future directions.

CHAPTER 2

EFFECTS OF PATIENT-SPECIFIC VARIABILITY IN INCONSISTENT END-EXPIRATORY DIAPHRAGM POSITION ON THE QUANTIFICATION OF LEFT VENTRICULAR CARDIAC STRAINS

2.1 Background

Cardiac strains describe the deformation of myocardial tissue during contraction and relaxation. Measures of cardiac strains have been shown to be superior predictors of outcomes, such as mortality, compared to traditional measures of cardiac function or traditional clinical risk factors alone [3]. Imaging can non-invasively assess cardiac strains using echocardiographic techniques such as speckle tracking [5] and cardiovascular magnetic resonance (MR) techniques such as myocardial feature tracking [39], myocardial tissue tagging [40, 41], phase velocity mapping [42], strain encoding [43], and displacement encoding with stimulated echoes (DENSE) [8, 11].

Peak strains vary longitudinally throughout the left ventricle [25, 26, 27, 28, 29, 30, 31]. For example, previous studies have shown that left ventricular radial, circumferential, and longitudinal strains vary between the base and apex by up to 14%, 5%, and 5% (absolute), respectively [25, 26, 27, 28, 29, 30, 31]. Cardiac MR images are often acquired during end-expiratory breath-holds to minimize respiratory motion artifacts. However, it is difficult to achieve consistency in end-expiratory diaphragm position between successive breath holds, and variations of 4 to 13 mm are normal [20, 21, 22, 23, 24]. Inconsistent end-expiratory positions will impact the position of the heart with respect to the imaging plane (Figure 2.1). For example, previous studies have

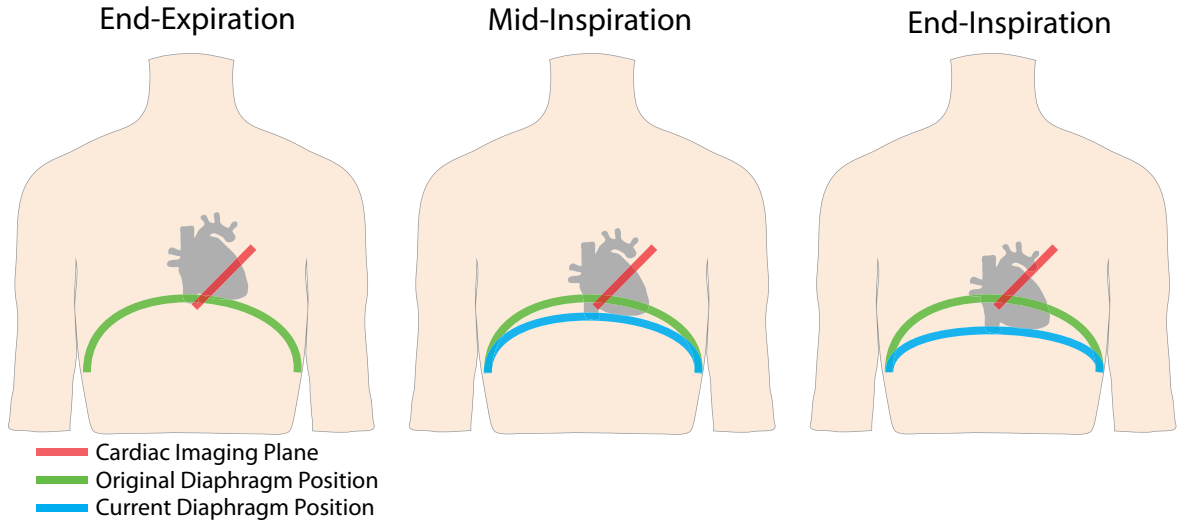


Figure 2.1: During respiration, diaphragm motion causes the heart to translate a significant distance while the imaging plane remains fixed.

reported short-axis and long-axis through-plane displacements of up to 14 mm due to displacement of diaphragm position between breath-holds [44, 45], and other studies have reported that the superior/inferior position of the heart can displace 55-92% of the displacement of the diaphragm position [46, 47]. Because peak strains vary throughout the left ventricle, we hypothesized that translation of the heart with respect to the imaging plane would result in differences and variability in measured strains.

To our knowledge, no study has evaluated the sensitivity of cardiac strains to natural end-expiratory position variability. This is an important knowledge gap, especially since the use of cardiac strains is increasing dramatically both in research and clinical practice. The purpose of this study was to determine if normal inconsistency in end-expiratory position significantly affects the quantification of cardiac strains and therefore results in higher variability in measured cardiac strains compared to strains measured at a consistent end-expiratory position by using a respiratory navigator.

2.2 Methods

2.2.1 Subjects

The study protocol was approved by the local Institutional Review Board. Ten healthy volunteers without known cardiovascular disease or chronic illnesses and 7 patients with a history of heart disease (known diagnosis of heart failure, cardiomyopathy, or myocardial infarction) provided written informed consent. Image acquisitions were performed on a 3T Siemens Tim Trio (Siemens Healthcare, Erlangen, Germany) scanner with a 6-element chest coil and a 24-element spine coil.

2.2.2 Quantification of Inconsistent End-Expiratory Positions

To determine the inconsistency in end-expiratory positions for each subject, a respiratory navigator sequence measured the diaphragm position (Figure 2.2) during 10 consecutive breath-holds. During each breath-hold, the diaphragm position was imaged three times per second over a period of 10 seconds for 30 total measurements. No cardiac image data were collected during these acquisitions. The mode of the 30 diaphragm positions defined the measured end-expiratory position of that breath-hold. The patient-specific minimum, middle, and maximum end-expiratory positions were defined from the series of 10 breath-holds (Figure 2.3).

2.2.3 DENSE Acquisition

For each subject, navigator-gated 2D spiral cine DENSE in 2-chamber and 4-chamber long-axis and basal, mid-ventricular, and apical short-axis orientations of the left ventricle were acquired four times. Specifically, all image orientations were acquired with the navigator acceptance window prescribed at the patient-specific maximum and minimum end-expiratory positions, and twice in the middle position to quantify variability in strain independent of end-expiratory position variability (Figure 2.3). A navigator feedback system, which used an angled mirror and

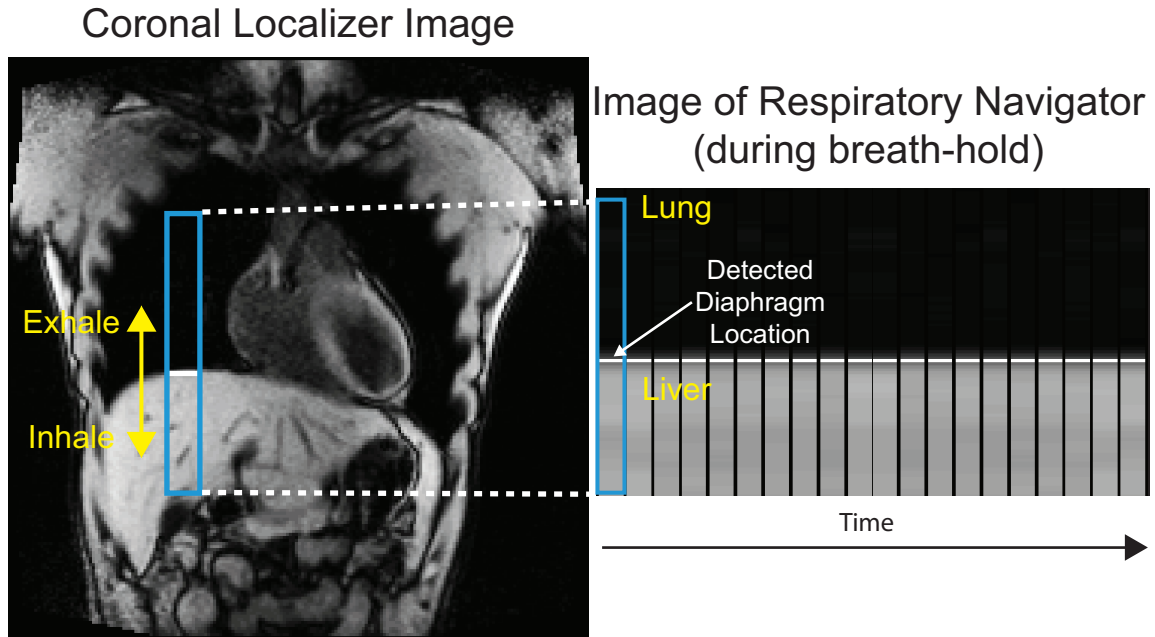


Figure 2.2: Respiratory navigator gating. (Left) The diaphragm position was measured at the high-contrast interface between the lung (dark) and the liver (bright). (Right) Image of a measured diaphragm position over time during a breath-hold.

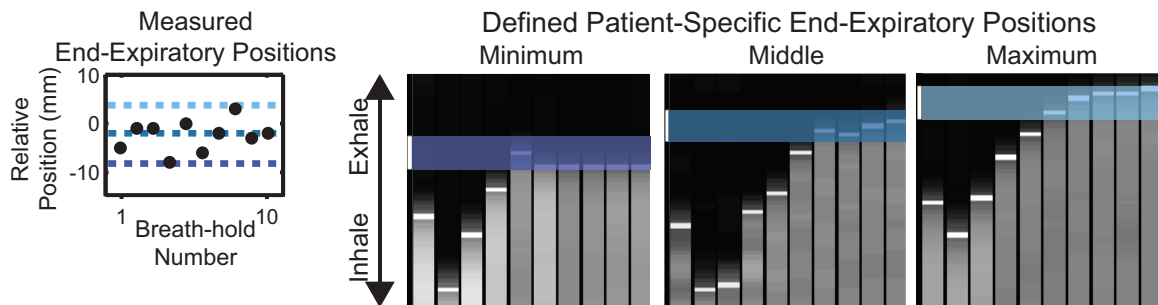


Figure 2.3: A respiratory navigator was used to measure end-expiratory positions to define the patient-specific minimum, middle, and maximum end-expiratory positions. The minimum position was defined as being closer to the end-inspiratory position while the maximum position was defined as being closer to the end-expiratory position.

projector screen placed at the back of the scanner bore, was used to facilitate quicker acquisitions by enabling subjects to view the navigator acceptance window position in real-time during image acquisition [48]. For each end-expiratory position, all image orientations were acquired within a single navigator-gated scan.

Prospective ECG gating was used during DENSE acquisitions. The number of cardiac phases ranged from 31 to 49 and varied based on subject heart rate. Additional DENSE imaging parameters included: spiral interleaves = 6, FOV = 360x360 mm², pixel spacing = 2.8x2.8 mm², slice thickness = 8 mm, TE = 1.1 ms, TR = 17 ms, variable flip angle = 20°, displacement encoding = 0.06 cyc/mm [10], through-plane dephasing = 0.08 cyc/mm [15], CSPAMM echo suppression [12], and view sharing. A dual-navigator strategy was used, requiring the diaphragm to be within the navigator acceptance window (± 3 mm) both before and after the data acquisition during each R-R interval [49].

2.2.4 DENSE Post-Processing

DENSE image data were analyzed using the open-source software, *DENSEanalysis* [50]. For each image orientation, the left ventricular myocardium was manually delineated using epicardial and endocardial contours and an end-diastolic and end-systolic cardiac phase [51]. Post-processing and segmentation were performed as described by Suever et al. [51]. Seed points indicating unwrapped phase data were manually selected, and a path-following algorithm was used to unwrap the displacement-encoded phase data. The resulting displacement trajectories were further processed by applying spatial smoothing and temporal fitting as previously described [18].

Two-dimensional Lagrangian strains were computed from the smoothed trajectories over the entire cardiac cycle. Radial and circumferential strains were computed from the short-axis images and longitudinal strain was computed from the long-axis images. Global peak strains were calculated by averaging the mean strain

curves of all the myocardial segments and identifying the peak of the global mean curve. Regional peak strains were computed by averaging the strain curves from all the myocardial segments for a given region and identifying the peak of the regional curve. Segmental peak strains were computed by identifying the peak of the strain curve for each myocardial segment. For peak longitudinal strain computation, pixels within 10% of left ventricular longitudinal length from the most basal and apical regions were excluded because of the increased noise which is typically observed in the strain curves in those regions. Peak strain was defined as positive for thickening (radial) and negative for shortening (circumferential and longitudinal).

2.2.5 Statistics

Statistical analyses were performed using R version 3.2.2 (R Foundation for Statistical Computing, Vienna, Austria). All continuous variables were expressed as mean \pm standard deviation or range. Cardiac strains were tested for normality using a Shapiro-Wilk test.

To quantify mean differences in cardiac strains due to inconsistent end-expiratory positions (minimum, middle, and maximum positions), cardiac strains were compared between the patient-specific acceptance window positions using a two-way analysis of variance (ANOVA) with repeated measures with group (healthy vs patient) and acceptance window position as the independent factors. A Scheirer-Ray-Hare test was used for data determined to be non-normally distributed [52]. Using the results of the two-way ANOVA or Scheirer-Ray-Hare test, the interaction between group and acceptance window position on cardiac strains was determined. If there was no interaction between group and acceptance window position, the groups were combined and mean differences due to inconsistent end-expiratory positions were quantified by comparing cardiac strains between acceptance window positions using a one-way ANOVA with repeated measures with acceptance window position as the independent factor. A Friedman test was used for data determined to be non-normally distributed

[52].

To quantify variability due to inconsistent end-expiratory positions, the standard deviations of strains were compared between the inconsistent positions (maximum, middle, and minimum) and consistent positions (two acquisitions at the middle position) using a Students t-test. For all statistical tests, significance was defined as $p < 0.05$. Bland-Altman analysis [53] was used to assess the reproducibility of each measurement using inter-test 95% limits of agreement defined using the two measurements from the middle position. Inconsistency in end-expiratory position across ten separate breath-holds for each subject was reported using both ranges and standard deviations from the ten breath-holds, and these values were compared between patients and healthy controls.

Power analyses were performed to quantify the ability of this study to detect meaningful differences in strain between the different end-expiratory positions. Because repeated-measures ANOVAs were used to detect differences, and because equations for power are not readily available for repeated-measures ANOVA, simulations were performed to estimate power. Specifically, for each strain, 10,000 iterations were performed. For each iteration, strain values for the minimum end-expiratory position were randomly drawn from a normal distribution using the mean and standard deviation across the subjects measured in this study. The number of strain values drawn corresponded with the number of subjects (healthy and patients combined). For a given difference to detect, δ , values at the two other end-expiratory positions were calculated by adding $\delta/2$ and δ to the values at the minimum position. Measurement variability was then added to those two end-expiratory positions by drawing random values from a normal distribution with zero mean and a standard deviation equal to the measured average standard deviation of the differences between any two positions. In this manner, each iteration simulated a mean difference of δ between the minimum and maximum

breath-hold positions and included typical inter-test measurement variability. The percentage of iterations for which a repeated-measures ANOVA yielded a significant result ($p < 0.05$) was the estimate of power. The 95% confidence interval of that estimate was calculated from the normal approximation to the binomial distribution with $N = 10,000$. The values of δ that yielded at least 80% power were reported separately for global and regional strains.

2.3 Results

Ten healthy volunteers (Age: 22 ± 6 years, 60% female) along with 7 patient volunteers (Age: 57 ± 8 years, 43% female) were recruited. One healthy subject was excluded due to movement during imaging, so data from the remaining 9 healthy subjects are reported.

2.3.1 *Inconsistent End-Expiratory Positions*

The average range of end-expiratory positions were not significantly different ($p = 0.94$) between the healthy (10.1 ± 4.8 mm) and patient (10.3 ± 4.2 mm) groups (total range of 4-19 mm). Since range is sensitive to outliers, the standard deviation of end-expiratory position was also compared between groups, and similarly there were no significant differences (3.1 ± 1.3 mm vs 3.4 ± 1.7 mm, $p = 0.70$) [54].

2.3.2 *Differences and Variability in Peak Strains*

There was no interaction between group (healthy vs patient) and navigator acceptance window position for peak strains (Table 2.1), thus the remaining analyses were performed with all subjects combined. Neither global, regional, nor segmental peak strains were significantly different as a function of acceptance window position (Tables 2.1, 2.2, and 2.3). Moreover, the differences in mean strain between any two acceptance window positions were each smaller than their

corresponding inter-test 95% limits of agreement (Table 2.1). For example, mean global circumferential strain across acceptance window positions ranged from -16% to -17%; the difference was 1%, which is smaller than the corresponding inter-test 95% limits of agreement of $\pm 1.7\%$ (Table 2.1). Finally, the standard deviations in peak strains were not significantly different between inconsistent (minimum, middle, and maximum) and consistent (repeated measurements at middle position) acceptance window positions for all subjects combined (Table 2.4). With at least 80% power, this study had the ability to detect strain differences of 4.7%, 1.0%, and 1.7% (absolute) between end-expiratory positions for global radial, circumferential, and longitudinal strain, respectively (Table 2.5). Additionally, this study had at least 80% power to detect differences of 8.9%, 2.2% and 2.6% for regional radial, circumferential, and longitudinal strain, respectively (Table 2.5). For both global and regional strains, detectable strain differences were smaller than the corresponding inter-test 95% limits of agreement (Table 2.5).

Table 2.1: Global and regional peak strains (mean standard deviation) from the three acceptance window positions (minimum, middle, and maximum) for all subjects combined.

Measurement	Acceptance Window Position			p-value [†]	95% LoA	p-value [‡]
	Minimum	Middle	Maximum			
Radial Strain (%)						
Global	29 ± 12	29 ± 12	30 ± 13	0.95	±7.9	0.99
Base	37 ± 15	35 ± 14	37 ± 14	0.95	±13.1	0.89
Mid-Ventricle	28 ± 11	29 ± 14	28 ± 13	0.77	±10.4	0.51
Apex	26 ± 12	27 ± 10	29 ± 16	0.78	±15.8	0.79
Circum. Strain (%)						
Global	-16 ± 4	-17 ± 4	-17 ± 5	0.57	±1.7	0.65
Base	-15 ± 4	-15 ± 4	-15 ± 4	0.83	±3.6	0.71
Mid-Ventricle	-16 ± 4	-17 ± 4	-17 ± 4	0.17	±2.1	0.78
Apex	-19 ± 5	-19 ± 5	-19 ± 5	0.98	±4.6	0.93
Long. Strain (%)						
Global	-12 ± 4	-12 ± 3	-13 ± 4	0.44	±3.2	0.48
2ch	-13 ± 3	-12 ± 3	-13 ± 4	0.94	±6.2	0.75
4ch	-12 ± 4	-13 ± 4	-13 ± 4	0.84	±4.1	0.38

[†]Results from test comparing acceptance window positions

[‡]Results from test comparing interaction between group (healthy vs patient) and acceptance window position

Table 2.2: Segmental circumferential strain (% , mean \pm standard deviation) from the three acceptance window positions (minimum, middle, and maximum) for all subjects combined.

Acceptance Window Position	Anterior		Anteroseptal		Inferoseptal		Inferior		Inferolateral		Anterolateral	
	Strain	P	Strain	P	Strain	P	Strain	P	Strain	P	Strain	P
Basal												
Max	-16 \pm 5		-14 \pm 5		-14 \pm 5		-15 \pm 5		-19 \pm 6		-19 \pm 5	
Mid	-16 \pm 3	0.99	-13 \pm 5	1.0	-15 \pm 5	0.95	-15 \pm 5	0.91	-18 \pm 5	0.88	-19 \pm 5	0.76
Min	-15 \pm 4		-13 \pm 5		-15 \pm 4		-15 \pm 5		-19 \pm 6		-18 \pm 4	
Mid-Ventricular												
Max	-17 \pm 5		-14 \pm 5		-13 \pm 5		-17 \pm 5		-22 \pm 6		-20 \pm 6	
Mid	-17 \pm 5	0.93	-14 \pm 4	0.83	-14 \pm 4	0.87	-18 \pm 5	0.93	-21 \pm 4	1.0	-21 \pm 6	0.81
Min	-17 \pm 6		-14 \pm 4		-13 \pm 4		-17 \pm 3		-20 \pm 5		-21 \pm 6	
Apical												
Max	-18 \pm 5		-15 \pm 6		-17 \pm 6		-20 \pm 6		-23 \pm 7		-22 \pm 6	
Mid	-18 \pm 5	0.66	-15 \pm 5	0.99	-17 \pm 6	0.79	-20 \pm 6	0.98	-23 \pm 6	0.84	-22 \pm 7	0.99
Min	-18 \pm 6		-15 \pm 5		-16 \pm 6		-21 \pm 6		-24 \pm 6		-21 \pm 7	

P-values indicate results from test comparing acceptance window positions.

Table 2.3: Segmental radial strain (% , mean \pm standard deviation) from the three acceptance window positions (minimum, middle, and maximum) for all subjects combined.

Acceptance Window Position	Anterior		Anteroseptal		Inferoseptal		Inferior		Inferolateral		Anterolateral	
	Strain	P	Strain	P	Strain	P	Strain	P	Strain	P	Strain	P
Basal												
Max	37 \pm 20		36 \pm 16		40 \pm 20		43 \pm 23		47 \pm 29		41 \pm 21	
Mid	40 \pm 21	0.78	41 \pm 18	0.61	37 \pm 14	0.53	36 \pm 21	0.77	47 \pm 31	0.94	44 \pm 24	0.64
Min	38 \pm 18		38 \pm 17		37 \pm 18		40 \pm 22		51 \pm 29		46 \pm 28	
Mid-Ventricular												
Max	28 \pm 17		33 \pm 24		34 \pm 15		32 \pm 15		36 \pm 32		32 \pm 17	
Mid	31 \pm 19	0.94	35 \pm 19	0.44	31 \pm 13	0.88	33 \pm 24	0.96	38 \pm 29	0.83	33 \pm 18	0.49
Min	30 \pm 19		36 \pm 14		36 \pm 16		31 \pm 21		35 \pm 24		28 \pm 17	
Apical												
Max	28 \pm 24		36 \pm 37		41 \pm 21		41 \pm 37		31 \pm 23		27 \pm 16	
Mid	23 \pm 12	0.72	31 \pm 13	0.87	39 \pm 20	0.83	40 \pm 20	0.20	27 \pm 17	0.84	26 \pm 15	0.69
Min	25 \pm 15		35 \pm 24		40 \pm 27		34 \pm 24		29 \pm 20		33 \pm 16	

P-values indicate results from test comparing acceptance window positions.

2.4 Discussion

Quantification of cardiac strains typically requires a series of image acquisitions performed during end-expiratory breath-holds. This study explored the effects of inconsistent end-expiratory positions on the quantification of left ventricular cardiac strains. The results of the study showed that 1) inconsistent end-expiratory positions had minimal effect on the quantification of global and regional peak strains compared to inter-test variability for a given imaging location; and 2) the variability of global and regional peak strains was similar between inconsistent and consistent end-expiratory positions. Importantly, these findings provide assurance that the measurement of cardiac strains is relatively robust with respect to inconsistent end-expiratory positions.

Peak strains vary throughout the left ventricle. For example, we found that the magnitude of circumferential strain was 2% (absolute) higher in the apical region than the base—in agreement with previous studies [25, 26, 27, 28, 29, 30]—and radial strain was 9% (absolute) higher in the basal region than the apex. Due to these strain gradients, we hypothesized that the displacement of the heart due to motion of the diaphragm with respect to the imaging plane would create differences in measured strains. For example, we might expect that radial strains for the maximum end-expiratory position (i.e., maximal exhalation) would be lower in magnitude compared to the minimum end-expiratory position due to the heart being imaged more apically. We also might expect this to manifest as higher variability in strains across different end-expiratory positions compared to consistent end-expiratory positions. The likely explanation for finding that there is no difference in strains between end-expiratory positions is that, because the longitudinal axis of the heart (base to apex) is not necessarily perpendicular to the diaphragm plane, a 10 mm translation in the diaphragm position does not directly correspond with a 10 mm translation of the heart through the imaging plane. Thus,

Table 2.4: Standard deviation of global and regional peak strains across inconsistent (maximum, middle, minimum) and consistent (middle and repeated middle) acceptance window positions. Values reported as mean \pm standard deviation.

Measurement	Acceptance Window Positioning		p-value
	Inconsistent	Consistent	
Radial Strain (%)			
Global	3.2 \pm 1.7	2.3 \pm 1.8	0.17
Base	4.9 \pm 2.5	3.5 \pm 3.3	0.18
Mid-Ventricle	4.3 \pm 2.5	2.5 \pm 2.8	0.10
Apex	5.7 \pm 4.1	4.3 \pm 3.9	0.16
Circumferential Strain (%)			
Global	0.7 \pm 0.4	0.5 \pm 0.3	0.10
Base	1.0 \pm 0.5	1.1 \pm 0.7	0.41
Mid-Ventricle	0.7 \pm 0.3	0.6 \pm 0.5	0.55
Apex	1.4 \pm 0.9	1.4 \pm 0.9	0.95
Longitudinal Strain (%)			
Global	1.1 \pm 0.7	0.8 \pm 0.9	0.27
2ch	1.4 \pm 1.1	1.5 \pm 1.6	0.89
4ch	1.4 \pm 1.6	1.2 \pm 0.9	0.72

Table 2.5: Power analyses for the ability to detect a difference in global and regional strain between different end-expiratory positions. Inter-test 95% limits of agreement are shown for reference comparison.

Measurement	Power (%)	Difference To Detect (absolute, %)	Inter-test Limits (%)
Radial Strain (%)			
Global	80.9 \pm 0.8	4.7	\pm 7.9
Base	96.1 \pm 0.4		\pm 13.1
Mid-Ventricle	98.4 \pm 0.2	8.9	\pm 10.4
Apex	80.2 \pm 0.8		\pm 15.8
Circumferential Strain (%)			
Global	80.5 \pm 0.8	1.0	\pm 1.7
Base	99.6 \pm 0.1		\pm 3.6
Mid-Ventricle	100 \pm 0.0	2.2	\pm 2.1
Apex	80.6 \pm 0.8		\pm 4.6
Longitudinal Strain (%)			
Global	80.0 \pm 0.8	1.7	\pm 3.2
2ch	95.0 \pm 0.4		\pm 6.2
4ch	80.5 \pm 0.8	2.6	\pm 4.1

the minimal translation of the heart does not lead to a significant difference in the measured cardiac strains.

Previous studies suggest that regions of the heart could displace at least 3 and possibly up to 14 mm through the fixed imaging plane between breath-holds [44, 45, 46, 47]. Our study had an average range of end-expiratory diaphragm position between breath-holds of approximately 10 mm, which is consistent with previous studies. Since the imaging slice thickness is 8 mm, even with a 14 mm through-plane displacement, there is likely not much difference in the acquired data from the imaged heart locations compared to the imaging plane location. Overall, since there were no significant differences in peak global, regional, and segmental strains between end-expiratory positions, patient end-expiratory diaphragm position does not have to be monitored when performing breath-hold DENSE acquisition for single image analyses.

The goal of this study was to quantify the effects of inconsistent end-expiratory positions on cardiac strains by computing the differences in strain between different end-expiratory positions. Thus, it was important for this study to detect meaningful strain differences between different patient-specific end-expiratory positions. The study had 80% power to detect global strain differences of 4.7%, 1.0%, and 1.7% and regional strain differences of 8.9%, 2.2%, and 2.6%, between different end-expiratory positions for radial, circumferential, and longitudinal strain, respectively. Importantly, these detectable differences were similar to or smaller than this study's reported inter-test 95% limits of agreement (Table 2.5) and previously reported values of inter-test limits of agreement for circumferential strain (± 2.0 %) and radial strain (± 13.0 %) [10]. Notably, in some regions, the power to detect a meaningful difference was much higher (close to 100%) indicating that, in those regions, this study may have had the ability to detect even smaller than reported detectable differences.

We used DENSE to investigate our hypothesis that a patient's normal variability

in end-expiratory position between image acquisitions significantly affects the quantification of cardiac strains. DENSE was chosen to test our hypothesis because it has been previously shown to have good reproducibility [9], can be acquired with high spatial resolution [8, 11], and enables straightforward computation of cardiac strains. However, our findings should generalize to other image acquisitions that are used to derive measures of cardiac strains such as echocardiography, tagged MRI, etc.

2.4.1 Limitations

We used respiratory navigator gating to acquire the DENSE cardiac images, which reduces respiratory artifacts during image acquisition, so we could not measure the effect of inconsistent end-expiratory position *during* breath-holds on the derived strains. It would be beneficial to quantify the amount of end-expiratory position variability during breath-hold cardiac MR image acquisition to determine whether the magnitude of inconsistent end-expiratory positions correlates with changes in strain values. An example would be to explore whether inconsistent end-expiratory positions during a breath-hold DENSE scan causes blurring due to motion and results in lower strain magnitudes.

This study examined the effects of inconsistent end-expiratory positions on cardiac strains in a small patient sample. It would be beneficial to investigate this effect in a larger patient sample who have heterogeneous contraction patterns, for example, due to myocardial infarction. These patients may have steeper gradients in strain across infarcted to non-infarcted tissue regions [55]. Therefore, we cannot definitively say that the effects of inconsistent end-expiratory positions in that setting are similarly small and negligible. Future studies should investigate strain variability due to inconsistent end-expiratory positions in patients who have infarcted tissue in specific regions (e.g. anterior vs inferior).

2.5 Conclusion

The quantification of peak left ventricular cardiac strains is relatively insensitive to normal variations in end-expiratory positions between image acquisitions. Since there were no differences in peak strain between end-expiratory positions, patient end-expiratory diaphragm position does not have to be monitored when performing breath-hold DENSE acquisition for single image analyses. These findings should generalize to other image acquisitions that are used to derive measures of cardiac strains.

CHAPTER 3

USING A RESPIRATORY NAVIGATOR REDUCES VARIABILITY WHEN QUANTIFYING LEFT VENTRICULAR TORSION

Adapted from Hamlet SM, Haggerty CM, Suever JD, Wehner GJ, Andres KN, Powell DK, Charnigo RJ, Fornwalt BK. Using a Respiratory Navigator Significantly Reduces Variability when Quantifying Left Ventricular Torsion with Cardiovascular Magnetic Resonance. Journal of Cardiovascular Magnetic Resonance. 2017, 19:25.

[54]

3.1 Background

The purpose of this work was to determine the effects of using a respiratory navigator on the variability of left ventricular torsion derived from spiral cine displacement encoding with stimulated echoes (DENSE) MRI. In this chapter, we discuss the two separate experimental protocols (using 1. *enforced* and 2. *natural* variability in end-expiratory position) used to test the hypothesis that high inter-test variability in left ventricular torsion is partly due to inconsistent breath-hold positions during serial image acquisitions, which could be significantly improved by using a respiratory navigator for cardiac MRI-based quantification of left ventricular torsion.

Left ventricular (LV) torsion is an important indicator of cardiac function [56, 4]; however, the quantification of torsion is limited by poor inter-test reproducibility. For example, a previous study with myocardial tagging demonstrated that the inter-test variability of torsion represented nearly 50% of the mean value [30]. This substantial variability reduces prognostic value for individual patients and leads to larger required sample sizes for research studies to detect meaningful differences or changes. Previous studies have reported that sample sizes ranging from 80-107 are required to detect

a 10% relative difference in torsion with 90% power [30, 7, 57]. Reducing variability and lowering required sample sizes is important to improve the clinical and research utility of torsion.

LV torsion is typically quantified as the gradient of twist along the longitudinal axis of the heart. This gradient is computed using twist derived from two short axis images (basal and apical) of the LV and the longitudinal distance between the images [30] (Figure 3.1). End-expiratory breath-holds are used to minimize respiratory motion artifacts, and the basal and apical short axis images are typically acquired during separate breath-holds. When post processing the image data to compute LV torsion, the longitudinal distance between the short axis images is calculated from either A) assumptions derived from an additional longitudinal image (echocardiography) or B) information specifying the location of the imaging planes in 3D space taken from the Digital Imaging and Communications in Medicine (DICOM) image header (cardiac magnetic resonance [MR]). A confounding factor that is not considered is that the exact end-expiratory position may differ by up to 13 mm between separate breath-holds [20, 21, 22, 23, 24], which creates differences in heart position between the basal and apical image acquisitions (Figure 3.2). We hypothesized that inconsistent end-expiratory diaphragm positions during serial breath-holds accounts for a significant portion of the variability in measured LV torsion and that this variability could be reduced by using cardiac MR based quantification of LV torsion with a respiratory navigator.

3.2 Methods

Respiratory related variability in measured LV torsion was assessed with two distinct experimental protocols: 1) using *enforced* variability in end-expiratory position between acquisitions and 2) allowing for *natural* variability in end-expiratory position between acquisitions. The former experiment was performed to establish an upper bound on respiratory related variability in torsion, while the

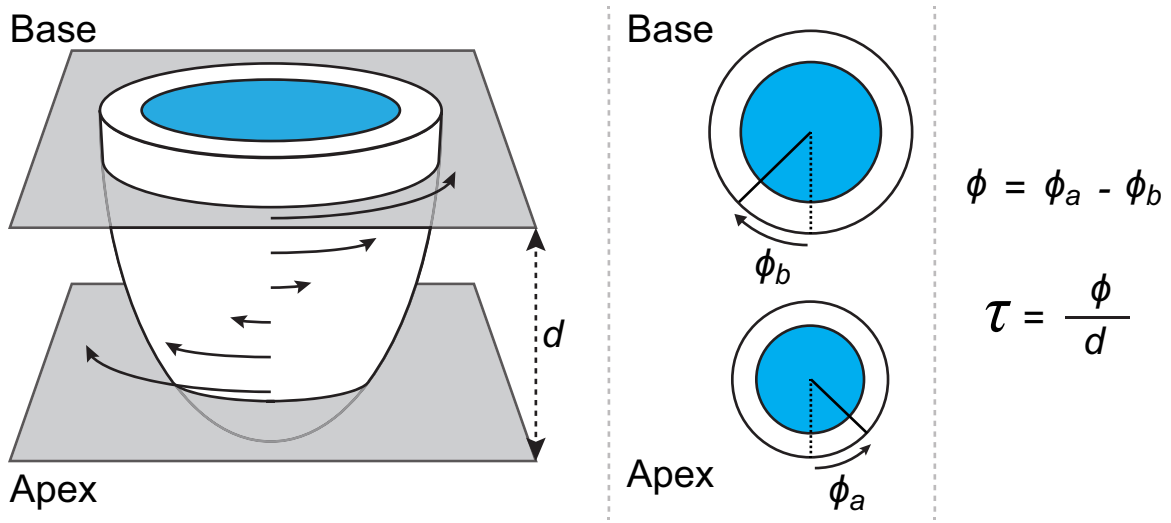


Figure 3.1: Computation of LV torsion from basal and apical images. The curved arrows represent the relative twist along the longitudinal axis of the left ventricle. LV twist (ϕ) was measured as the difference in rotation between the apex (ϕ_a) and base (ϕ_b) (twist direction shown as viewed from foot to head). Torsion τ was computed as LV twist divided by the distance (d) between basal and apical image locations.

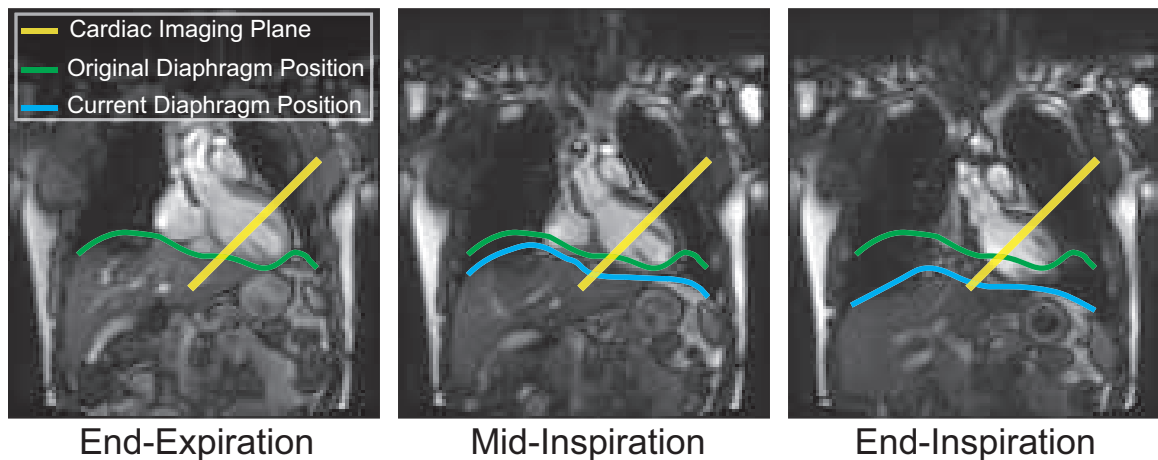


Figure 3.2: Real time images of the diaphragm as it translates during a respiratory cycle. During respiration, diaphragm motion causes the heart to translate a substantial distance through the fixed imaging plane.

latter mimics a more relevant clinical setting. In both experiments, the effect of using a respiratory navigator to ensure a consistent end-expiratory position on torsion variability was also quantified. The local Institutional Review Board approved the study protocols, and all subjects provided written informed consent.

3.2.1 LV Motion Quantification

Imaging was performed on a 3T Siemens Tim Trio (Siemens Healthcare, Erlangen, Germany) with a 6 element chest coil and a 24 element spine coil. LV twist was measured at basal and apical short axis locations in both experiments using 2D spiral cine Displacement Encoding with Stimulated Echoes (DENSE) cardiac MR [16, 58].

The basal and apical short axis locations were defined as follows: On a four chamber image, five short axis slices were planned equidistant across the end systolic endocardial ventricular long axis length. The slices were planned such that the outermost slices did not extend beyond the mitral valve plane and endocardial apex, respectively. The second and fourth slices of this stack were defined as the basal and apical short axis locations. Imaging parameters were: spiral interleaves = 6, interleaves per frame = 2, FOV = 360x360 mm², pixel spacing = 2.8x2.8 mm², slice thickness = 8 mm, TE/TR = 1.1/17 ms, temporal resolution = 34 ms, variable flip angle = 20°, displacement encoding = 0.06 cyc/mm [10], through plane dephasing = 0.08 cyc/mm [15], CSPAMM echo suppression [12], view sharing, prospective ECG gating, and a dual-navigator strategy [48] with an acceptance window of ± 3 mm. For each cardiac cycle, the navigator echo occurred immediately after data acquisition. The dual-navigator strategy required the diaphragm position to be within the acceptance window for both the preceding *and* current cardiac cycles in order for data to be accepted.

DENSEanalysis [50] was used to derive LV twist from the DENSE images. Epicardial and endocardial contours were manually delineated on the DENSE magnitude images at end-diastolic and end-systolic cardiac phases [51]. Post

processing was performed as previously described [51]. A semi-automatic path following algorithm was used to unwrap the displacement encoded phase data. The resulting displacement trajectories were further processed by applying spatial smoothing and temporal fitting [18].

LV twist was computed over the cardiac cycle relative to the centroid of the endocardial boundary at end-diastole. The distance between the basal and apical image locations was calculated from the DICOM headers. LV torsion was computed as the difference in rotation between the apex and base (ϕ) divided by the distance (d) between the basal and apical image locations [30, 59, 60] (Figure 3.1).

3.2.2 Experiment 1: Enforced End-Expiratory Variability

Ten healthy volunteers with no known cardiovascular disease or chronic illnesses and seven patients with a history of heart disease (known diagnosis of heart failure, cardiomyopathy, or myocardial infarction) were recruited; these are the same volunteers from Chapter 2. We first quantified the end-expiratory variability for each subject by acquiring respiratory navigator measurements (90-180 cross pair configuration; Figure 3.3) of 10 consecutive, 10 second breath-holds. No cardiac image data were acquired, but the mode position of each breath-hold was retained to identify subject specific minimum, middle and maximum end-expiratory positions of the diaphragm across the 10 breath-holds (Figure 3.4). These subject specific positions were then used to define the locations of the navigator acceptance windows for subsequent acquisitions of respiratory navigator-gated DENSE. Specifically, the basal and apical slices were both acquired with the navigator acceptance window at each of the three positions. Moreover, the acquisitions at the middle acceptance window location were repeated to define inter-test variability when ensuring a consistent position with a respiratory navigator. For all scans, the image of the respiratory navigator was projected to the subjects in real time during DENSE acquisition, which helped to ensure consistent efficiency [49] across scans

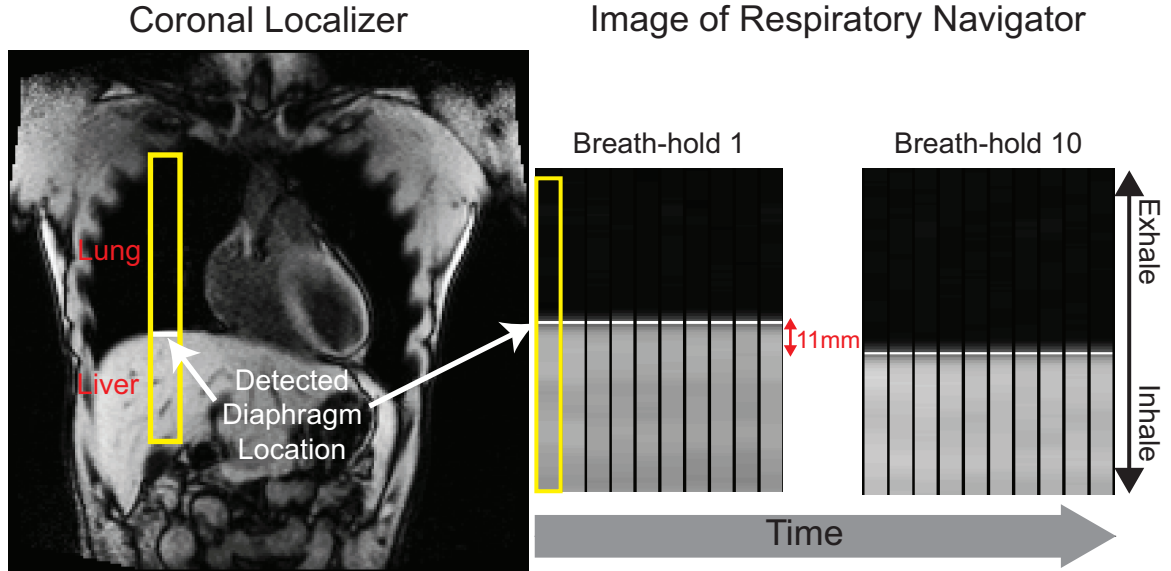


Figure 3.3: Respiratory navigator gating. (Left) The diaphragm position is at the high contrast interface between the lung (dark) and the liver (bright). (Right) Image of a measured diaphragm position over time for separate breath-holds. For this subject, there was an 11 mm difference in end-expiratory position between breath-hold 1 and breath-hold 10.

despite varying acceptance locations.

With three independent measurements at both LV locations, nine permutations of torsion were calculated from the possible combinations (Figure 3.5), providing an estimate of torsion variability due to inconsistent end-expiratory positions. This variability in torsion was compared to the inter-test variability (i.e., comparing the two torsion measures acquired at the middle navigator acceptance position, Figure 3.5) to isolate respiratory position effects.

3.2.3 Experiment 2: Natural End-Expiratory Variability

We next sought to quantify the effects of natural end-expiratory variability. Twenty new healthy volunteers were recruited. In these subjects, 10 basal and apical images were each acquired with two protocols: 1) during consecutive breath-holds, and 2) during consecutive navigator-gated acquisitions with a single acceptance window location. In each case, the 10 image pairs were used to derive 20

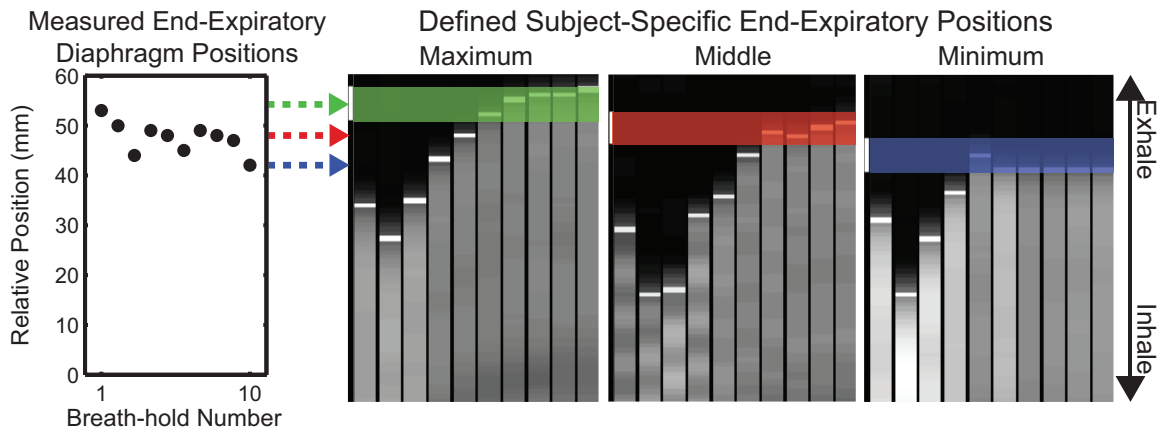


Figure 3.4: Measured end-expiratory diaphragm positions were used to define subject specific maximum, middle, and minimum end-expiratory positions. The maximum diaphragm position was defined as being closer to the end-expiratory position while the minimum diaphragm position was defined as being closer to the end-inspiratory position.

		Torsion Permutations									For Inter-test Comparison
		1	2	3	4	5	6	7	8	9	Repeat 5
Base		Maximum	Maximum	Maximum	Middle	Middle	Middle	Minimum	Minimum	Minimum	Middle
Apex		Maximum	Middle	Minimum	Maximum	Middle	Minimum	Maximum	Middle	Minimum	Middle

Figure 3.5: The nine possible torsion permutations were constructed from three basal and three apical images. One basal and apical image was acquired for each subject specific end-expiratory position (maximum, middle, and minimum). Image acquisitions were repeated at the middle position to assess inter-test variability (far right).

measurements of LV torsion, by combining each basal twist measurement with the two closest apical twist measurements in the temporal sequence. The torsion variability between these protocols was then quantified to compare the differences as a result of consistent (navigator-gated) and inconsistent (breath-hold) end-expiratory positions. Importantly, to monitor the end-expiratory position of the breath-hold acquisitions, the scans were acquired with the respiratory navigator enabled, but with a wide (± 50 mm) acceptance window width that never resulted in the exclusion of acquired image data.

3.2.4 Statistics

Statistical analyses were performed using R version 3.2.2 (R Foundation for Statistical Computing, Vienna, Austria). All continuous variables were expressed as mean \pm standard deviation and group means were compared using Student's t tests. Pearson correlation was used to observe associations between continuous variables.

For experiment 1, the inter-test variability of torsion was quantified using 95% inter-test limits of agreement of the two middle navigator acceptance window scans. To test for an overall difference in variability between inconsistent and consistent end-expiratory positions, the LV torsion permutations from the variable end-expiratory positions were compared to the 95% inter-test limits of agreement using a binomial test to evaluate whether values fell within the 95% limits significantly less than 95% of the time. The root mean squared error (RMSE) was then computed to quantify the differences in variability. Specifically, the RMSE for the consistent end-expiratory position was derived by computing the mean squared error (MSE) of the two middle acceptance window scans and taking the square root. The RMSE for the LV torsion permutations was derived by separately computing the MSE of the permutations with respect to each of the two middle acceptance window scans, averaging the MSEs, and taking the square root.

For experiment 2, breath-hold and navigator-gated acquisitions were compared

by computing the standard deviations of the 20 respective measurements and performing a Student’s t test. Variability in torsion was also quantified using 95% inter-test limits of agreement, which were computed using the standard deviation of the difference between consecutive pairs of torsion measurements. For all statistical tests, significance was defined as $p < 0.05$.

3.2.5 Theoretical Sample Size Calculation

To quantify the effects of the differences in torsion measurement variability, we computed theoretical sample sizes required to detect a clinically meaningful change in LV torsion for each experimental condition. Study sample sizes required to detect a 10% relative difference in LV torsion with a power of 90% and a significance level of 0.05 were computed using the standard deviation of the inter-test differences in torsion (α) and the equation:

$$n = f(\alpha, P) \cdot \sigma^2 \cdot \frac{2}{\delta^2} \quad (3.1)$$

where n is the sample size per group, α is the significance level, P is the power, f is the value of the factor for different values of α and P ($f = 10.5$ for $\alpha = 0.05$ and $P = 0.90$), and δ is the magnitude of the difference to be detected [61]. To determine the improvement in sample size compared to other modalities, sample sizes calculated by this formula were compared to those calculated based on data from previous studies that quantified LV torsion.

3.3 Results

For experiment 1, ten healthy volunteers (Age: 22 ± 6 years, Range: 19–38 years, 60% female) and seven patients (Age: 57 ± 8 years, Range: 45–67 years, 43% female) were enrolled. One healthy volunteer was excluded due to movement during imaging, so data from the remaining nine healthy volunteers are reported. For experiment 2,

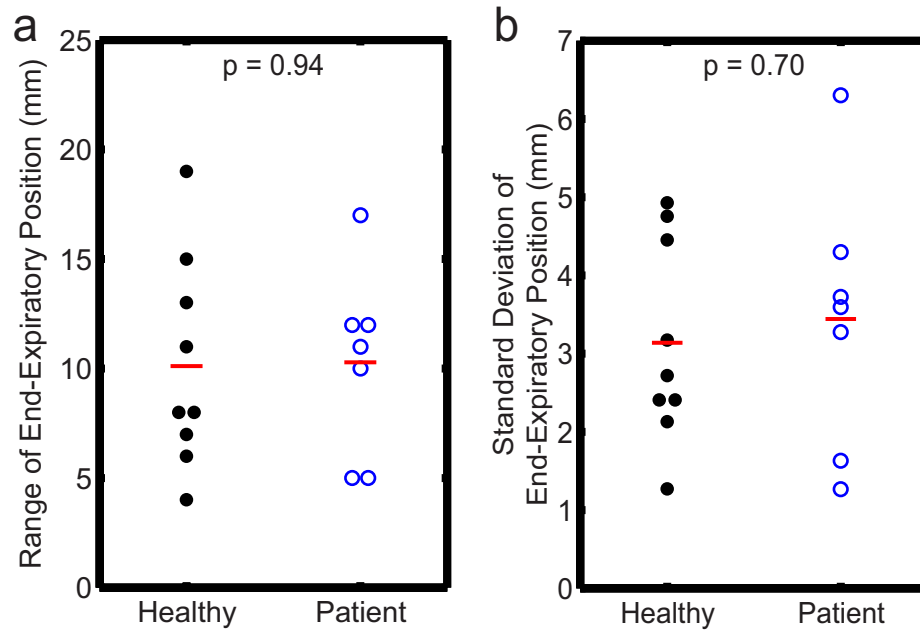


Figure 3.6: Inconsistent end-expiratory positions across ten consecutive breath holds in patients and healthy controls. There were no significant differences in either the range (a) or standard deviation (b) of end-expiratory position between the healthy and patient groups. Solid red lines denote the mean for each group.

20 healthy volunteers (Age: 25 ± 4 years, Range: 20–34 years, 60% female) were enrolled.

3.3.1 Inconsistent End-Expiratory Positions

From experiment 1, the intra-subject range and standard deviation of end-expiratory positions were 10.2 ± 4.4 mm and 3.3 ± 1.4 mm, respectively. There was no significant difference in the range or standard deviation of end-expiratory position between healthy and patient groups ($p = 0.94$ and $p = 0.70$, respectively; Figure 3.6). From experiment 2, the intra-subject range and standard deviation of end-expiratory positions over 20 breath-holds were 13.9 ± 10.5 mm and 3.8 ± 3.1 mm, respectively.

3.3.2 Torsion

DENSE images and displacements from a representative subject show the relative twist differences between the base and apex at end-systole (Figure 3.7). Table 3.1 summarizes the LV torsion results for each protocol. From experiment 1, the inter-test limits of agreement at a consistent position were ± 0.6 °/cm, and the binomial test indicated that the variability in LV torsion due to enforced variability in end-expiratory position was significantly higher than the variability at a consistent end-expiratory position ($p < 0.001$). Specifically, the RMSE of LV torsion permutations across end-expiratory positions was 0.56 ± 0.24 °/cm (range: 0.2–1.3 °/cm), while the RMSE from a consistent end-expiratory position was 57% lower (0.24 ± 0.16 °/cm). Moreover, there was a moderate correlation across subjects between the torsion RMSE and the range of end-expiratory positions ($r = 0.50$, $p = 0.049$, Figure 3.8). Finally, the mean LV torsion for consistent end-expiratory positions was not significantly different between the healthy (3.6 ± 1.2 °/cm) and patient (3.2 ± 1.3 °/cm) groups ($p = 0.30$).

For experiment 2, consecutive breath-holds yielded a significantly larger standard deviation of LV torsion compared to consecutive navigator scans (0.24 ± 0.10 °/cm vs 0.18 ± 0.06 °/cm, $p = 0.02$). There was a moderate correlation across subjects between the standard deviation of torsion and the standard deviation of end-expiratory position ($r = 0.34$, $p = 0.03$, Figure 3.9). The 95% limits of agreement from the consecutive breath-hold scans and consecutive navigator-gated acquisitions were ± 0.74 °/cm and ± 0.56 °/cm, respectively.

3.3.3 Theoretical Sample Sizes

The theoretical sample sizes required to detect a 10% relative difference in peak torsion ($\delta = 0.34$ °/cm) from each experimental protocol are shown in Table 3.2. From both experiments, using a respiratory navigator with DENSE produced

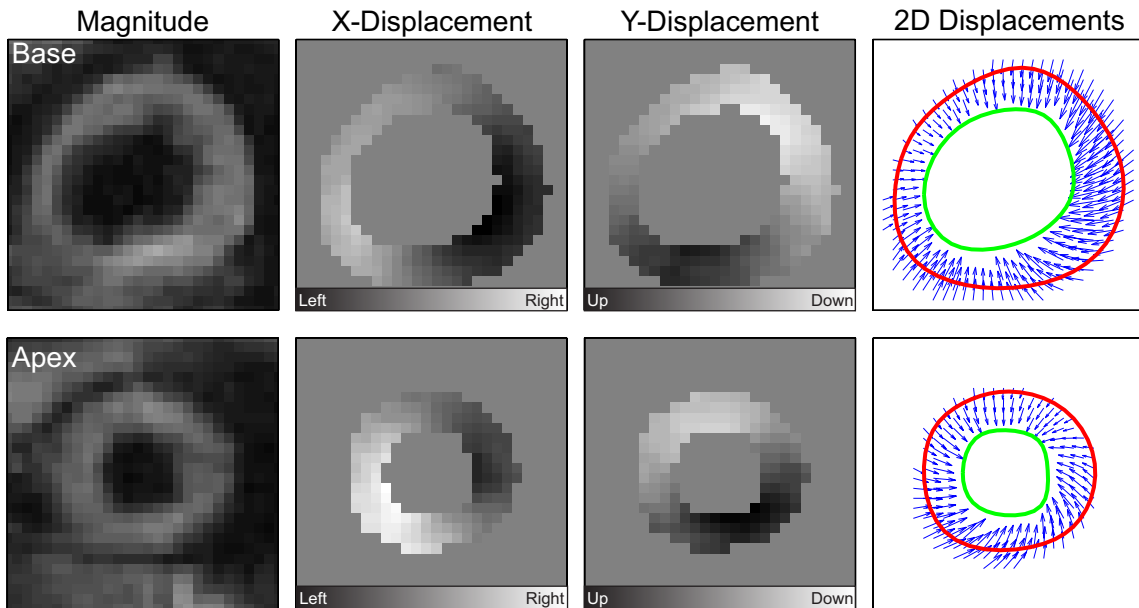


Figure 3.7: DENSE images from a representative subject show the relative twist differences between the basal and apical images at end systole. Twist in the basal region is predominantly in the clockwise direction, while the apex is predominantly counter clockwise.

Table 3.1: Mean (\pm standard deviation) of torsion across the volunteers within each experiment.

Method (experiment)	Torsion ($^{\circ}/\text{cm}$)	p-value
<i>Experiment 1*</i>		
Enforced inconsistent positions	3.4 ± 0.4	0.85
Consistent positions with navigator	3.4 ± 0.2	
<i>Experiment 2</i>		
Enforced inconsistent positions	3.6 ± 0.3	0.32
Consistent positions with navigator	3.5 ± 0.2	

*Reported values are from combined group of healthy and patient volunteers

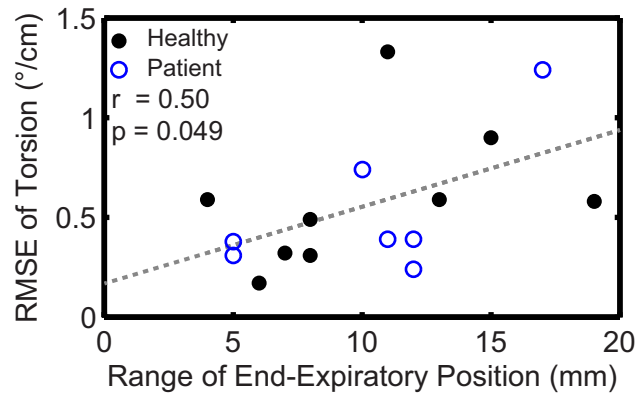


Figure 3.8: Variability of torsion due to enforced inconsistent end-expiratory positions versus the subject specific range of end-expiratory position. There was a moderate positive correlation between RMSE of LV torsion due to inconsistent expiratory positions and the range of end-expiratory position ($r = 0.50$, $p = 0.049$). The dashed grey line illustrates the linear best fit.

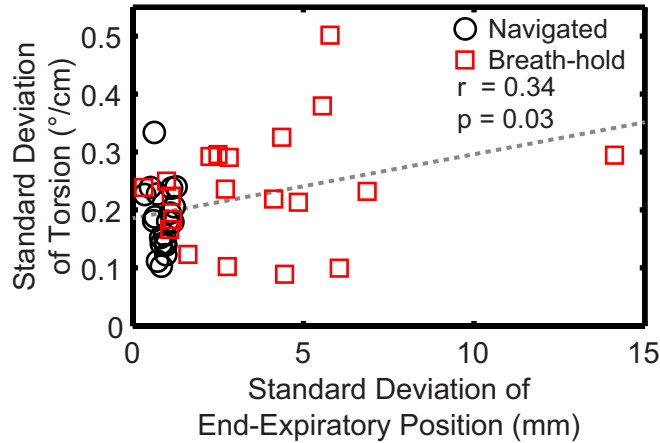


Figure 3.9: Variability of torsion due to naturally inconsistent end-expiratory positions versus the standard deviation of end-expiratory position. There was a moderate positive correlation between the standard deviation of LV torsion and the standard deviation of end-expiratory position ($r = 0.34$, $p = 0.03$). The dashed grey line illustrates the linear best fit.

Table 3.2: Sample sizes required to detect a 10% relative change in LV torsion calculated using data in this and previous studies.

Method (experiment)	Sample Size (n)
<i>Experiment 1</i>	
Enforced inconsistent positions	66
Consistent positions with navigator	16
<i>Experiment 2</i>	
Enforced inconsistent positions	26
Consistent positions with navigator	15
<i>Previous Studies</i>	
Cardiac MR Tagging [30]	107
Cardiac MR Feature Tracking [7]	81
3D Speckle Tracking [57]	80

similar sample size estimates ($n = 16$ and 15). By comparison, sample sizes based on measurements with variable end-expiratory positions were up to 313% higher. Additionally, compared to other modalities, using a respiratory navigator with DENSE provided an 80 to 86% reduction in the required sample size compared to cardiac MR tagging [30], cardiac MR feature tracking [7], and 3D speckle tracking echocardiography [57] (Table 3.2).

3.4 Discussion

This study explored the effects of inconsistent end-expiratory diaphragm positions on the quantification of LV torsion and showed that enforcing a consistent end-expiratory position with a respiratory navigator can significantly reduce inter-test variability of measured LV torsion. Our primary findings include 1) using a respiratory navigator with DENSE to enforce a consistent end-expiratory position reduced the variability in measuring torsion by 2257%; 2) this decreased variability reduced the required sample sizes to detect a 10% relative difference in torsion from $n = 66$ to $n = 16$ (from enforced variability to consistent) and $n = 26$ to $n = 15$ (from natural variability to consistent); 3) the variability of LV torsion due to inconsistent end-expiratory positions had a modest correlation with the variability

in end-expiratory positions, such that greater inconsistency in end-expiratory positions was associated with larger errors in measured LV torsion. Regarding inconsistency in end-expiratory positions, within each subject, substantial inconsistency existed with a mean range of 10 ± 4 mm and 14 ± 10 mm in experiment 1 and 2, respectively, which was similar to that reported previously (7 to 13 mm) [20, 21, 22, 23, 24].

LV torsion is an important indicator of cardiac function because it integrates the three dimensional deformation of the complex myocardial fiber architecture into a single metric [56, 4]. In many disease states, small disruptions in normal cardiac geometry—and thus torsion—may precede appreciable changes in global cardiac function. For example, previous studies in mice and canines have reported that changes in torsion precede changes in ejection fraction and volumes in obese animals compared to healthy controls [62, 63]. Previous human studies have reported that LV torsion differs between younger and older populations, and is also reduced in patients with hypertrophic cardiomyopathy, valvular heart disease, myocardial infarction, and dilated cardiomyopathy compared to healthy controls [4, 59, 64, 27, 65, 66]. Therefore, accurate and reproducible quantification of LV torsion may provide a robust, clinically relevant marker of cardiac health and function.

For LV torsion to be a useful clinical measurement, minimizing the magnitudes and sources of measurement error is important. A previous cardiac MR tagging study reported mean torsion values of 3.4 °/cm with inter study 95% limits of agreement of ± 1.6 °/cm, representing a large percentage of the mean [30]. Previous cardiac MR feature tracking studies have reported inter-test limits of agreement of ± 0.9 °/cm [7, 6]. Using DENSE cardiac MR, we observed a similar mean LV torsion of 3.4 °/cm for all subjects combined in experiment 1 and 3.5 °/cm in experiment 2, and smaller inter-test 95% limits of agreement from the breath hold scans in experiment

2 (± 0.74 °/cm). However, the observed inter-test 95% limits of agreement were considerably smaller when using a respiratory navigator (± 0.6 °/cm and ± 0.56 °/cm for experiments 1 and 2, respectively). An important distinction between the present study and previous studies, apart from cardiac MR sequence differences, is control of the end-expiratory position when quantifying the inter-test variability.

From experiment 1, by comparing the variability of LV torsion inclusive of enforced, *inconsistent* end-expiratory positions (0.56 ± 0.34 °/cm) to the variability without this inconsistency (0.24 ± 0.16 °/cm), we determined that using a respiratory navigator to ensure a consistent end-expiratory position reduced the variability in measured LV torsion by 57%. In experiment 2, using a respiratory navigator reduced the variability in measured LV torsion by 22% compared to the variability in LV torsion inclusive of naturally inconsistent end-expiratory positions.

In this study, we examined variability in measured LV torsion. A previous cardiac MR study examined the bias in LV twist and circumferential longitudinal (CL) shear angle between different acquisition techniques, including breath holds and free breathing [67]. In agreement with that previous study [67], we did not observe a bias in torsion between breath hold and navigator gated scans (Table 3.1).

To detect a 10% relative difference in peak LV torsion, experiment 1 found that using DENSE with a respiratory navigator required a sample size of only $n = 16$ subjects, which is about 76% lower than the sample size required when using DENSE without a respiratory navigator ($n = 66$). In experiment 2, we found similar results where using DENSE with natural respiratory variability required a sample size of 26 compared to using DENSE with a respiratory navigator ($n = 15$). Using a respiratory navigator with DENSE provided an 80 to 86% reduction in the required sample size compared to cardiac MR tagging [30], cardiac MR feature tracking [7], and 3D speckle tracking echocardiography [57].

These findings have meaningful implications for future cardiac MR based

quantification of LV torsion in the clinical and research settings. First, acquisition of LV torsion data using a respiratory navigator should be employed, where feasible, to minimize variability. This approach is not typical in the majority of published papers reporting torsion and may reduce clinical feasibility of such data acquisition; however, the additional effort appears justified by the considerable reduction in variance. If inconsistency in end-expiratory position is not addressed with the data acquisition, then it is important to incorporate effects of inconsistent end-expiratory position into the assessment of the standard error of measurement for LV torsion, which will substantially increase needed sample sizes for research trials or reduce prognostic value for individual subjects.

These results also have important implications for echocardiography. While operators may be able to correct for inconsistency in end-expiratory position by adjusting the position of the probe, it is unlikely that the operator can recreate the exact distance between each short axis image that was measured from the long axis image. Because inconsistent end-expiratory positions are a source of measurement variability in measured LV torsion in cardiac MR, the discrepancy in distances may be a source of substantial variability in measured LV torsion in echocardiography.

We used spiral cine DENSE to investigate our hypothesis that inconsistent end-expiratory positions accounts for a significant portion of the variability in measured torsion and that inter-test reproducibility could be improved by using a respiratory navigator. We chose to use spiral cine DENSE to investigate our hypothesis since it allows for simple quantification of mechanics, has good spatial resolution, has good reproducibility, and includes a respiratory navigator, which allows control of the end-expiratory position during image acquisition [16, 9, 8, 11]. However, our findings should generalize to all other imaging modalities that use short axis images to quantify torsion.

3.4.1 Limitations and Future Directions

We examined the effects of variable end-expiratory position on LV torsion in a small patient sample. It may be beneficial to examine these results in a larger, more heterogeneous patient sample to determine whether specific diseases affect the results more than others, especially conditions that affect a patient’s ability to repeatedly hold his or her breath reproducibly (for example, pulmonary diseases).

The breath-hold acquisition protocol was not performed in patients due to their limited breath-holding ability and lengthy duration of DENSE breath holds (20 seconds). Based on these factors, we expect that patients would demonstrate higher variability in LV torsion with the breath-hold measures compared to the healthy volunteers we studied. Hence, the potential reduction in mean variability when using the respiratory navigator may in fact be higher in patients than the 22% we report from the healthy volunteers in experiment 2. Nevertheless, the reduction in LV torsion variability patients will achieve by using a respiratory navigator will likely fall between the study’s reported values of 22 and 57%.

3.5 Conclusion

Using a respiratory navigator to enforce a consistent end-expiratory position during image acquisition can reduce the variability in measured LV torsion by 22–57%. Accounting for inconsistent end-expiratory positions results in favorable inter-test variability and reduces required sample sizes by 80 to 86% compared to previous studies. Future efforts to measure LV torsion should use a respiratory navigator or similar form of consistent respiratory compensation.

CHAPTER 4

OPTIMAL RESPIRATORY NAVIGATOR CONFIGURATION

Adapted from Hamlet SM, Haggerty CM, Suever JD, Wehner GJ, Andres KN, Powell DK, Zhong X, Fornwalt BK. Optimal Configuration of Respiratory Navigator Gating for the Quantification of Left Ventricular Strain Using Spiral Cine Displacement Encoding with Stimulated Echoes (DENSE) MRI. Journal of Magnetic Resonance Imaging. 2017. 45(3):796-794 [49]

4.1 Introduction

The purpose of this work was to determine the optimal respiratory navigator gating configuration for the quantification of left ventricular strain using spiral cine displacement encoding with stimulating echoes (DENSE) MRI. In this chapter, we detail the different respiratory navigator configurations, their advantages and disadvantages, and the experimental protocol used to compare them against a reference standard breath-hold acquisition. The results of this study identify the optimal respiratory navigator configuration in adults and children.

Magnetic resonance (MR) can be used to non-invasively assess cardiac function. Displacement encoding with stimulated echoes (DENSE) is an advanced cardiac MR imaging technique that directly measures tissue displacements and can be used to quantify cardiac mechanics, such as myocardial strains and torsion [8, 11]. When combined with clinical risk factors, these measures of cardiac mechanics have been shown to be better predictors of mortality than traditional measures of cardiac function, such as ejection fraction [3].

Compensation for respiratory motion is an important consideration for all cardiac MR techniques, particularly quantitative imaging sequences like spiral cine DENSE. DENSE acquisitions are generally performed using end-expiratory

breath-holds (~ 15 -20 seconds in duration) [12, 15, 13, 16, 17, 18, 19]; however, this approach is constrained by the patient’s ability to breath-hold, which is limited in young subjects and many stages of advanced heart disease. Furthermore, short acquisitions preclude the ability to capture more robust data, such as three-dimensional (3D) DENSE [16, 33, 34], or high resolution imaging [32].

As with many other cardiac MR sequences, a respiratory navigator has been used to overcome this time limitation by allowing the subject to breathe freely but restricting data acquisition based on the position of the diaphragm within a prescribed ‘acceptance’ window [16]. However, unlike some other MR sequences, the navigator echo in the DENSE sequence cannot occur at the beginning of the cardiac cycle, since this would lead to interference with displacement encoding. Instead, the navigator echo must occur at the end of the cardiac cycle, immediately after data acquisition. This creates several options for how the navigator can then be used to either accept or reject the acquired DENSE data (Figure 4.1). For example, a single echo can be used retrospectively or prospectively to define acceptance of DENSE data from the current or preceding cardiac cycle, respectively. Alternatively, a dual-navigator configuration can be used, which requires an echo from the current and preceding cardiac cycle to define acceptance of DENSE data (Figure 4.1). Each configuration has distinct advantages and disadvantages. For example, compared to the single navigator configurations, the dual-navigator configuration has more rigorous criteria for correctly accepting data (Figure 4.2). However, these strict criteria likely lead to worse navigator efficiency compared to the single navigator configurations (Figure 4.2).

Previous studies using navigator-gated DENSE have reported using a prospective single navigator configuration [16, 34]. However, there has been no formal comparison of the available navigator configurations. Moreover, the accuracy of derived cardiac mechanics and overall image quality for these navigator configurations compared with

breath-hold acquisitions as a reference standard are largely unknown. The purpose of this study was to determine the optimal configuration of respiratory navigator gating for the quantification of left ventricular strain using spiral cine DENSE MRI.

4.2 Methods

4.2.1 Subjects

Ten healthy adults and 20 healthy children without known history of cardiovascular disease or chronic illnesses and with a normal 12-lead electrocardiogram were prospectively enrolled. The protocol was approved by the local Institutional Review Board and all subjects provided written informed consent (or assent/parental consent, as appropriate).

4.2.2 Image Acquisition

Image acquisition was performed on a 3T Siemens Tim Trio (Siemens Healthcare, Erlangen, Germany) with a 6-element chest coil and a 24-element spine coil. 2D spiral cine DENSE [16, 58] in mid-ventricular short-axis and four-chamber long-axis orientations were separately acquired using breath-holds and retrospective, prospective, and dual navigator gating. Due to the lengthy breath-hold duration (~ 20 seconds), breath-hold acquisitions were not performed in children. The order of acquisition of the navigator gating configurations was randomized. Prospective ECG gating was used and the number of cardiac phases was selected to allow 100-150 ms at the end of the cardiac cycle for heart rate variability. Acquisition parameters for all scans were: spiral type: uniform density, interleaves = 6, interleaves per beat = 2, FOV = 360×360 mm², pixel spacing = 2.8×2.8 mm², slice thickness = 8 mm, TE = 1.1 ms, TR = 17 ms, variable flip angle = 20° [58, 68], displacement encoding = 0.06 cyc/mm [10], through-plane dephasing = 0.08 cyc/mm [15] CSPAMM echo suppression [12], and view sharing. The temporal resolution was 34 ms, however sliding window view sharing yielded a 17 ms

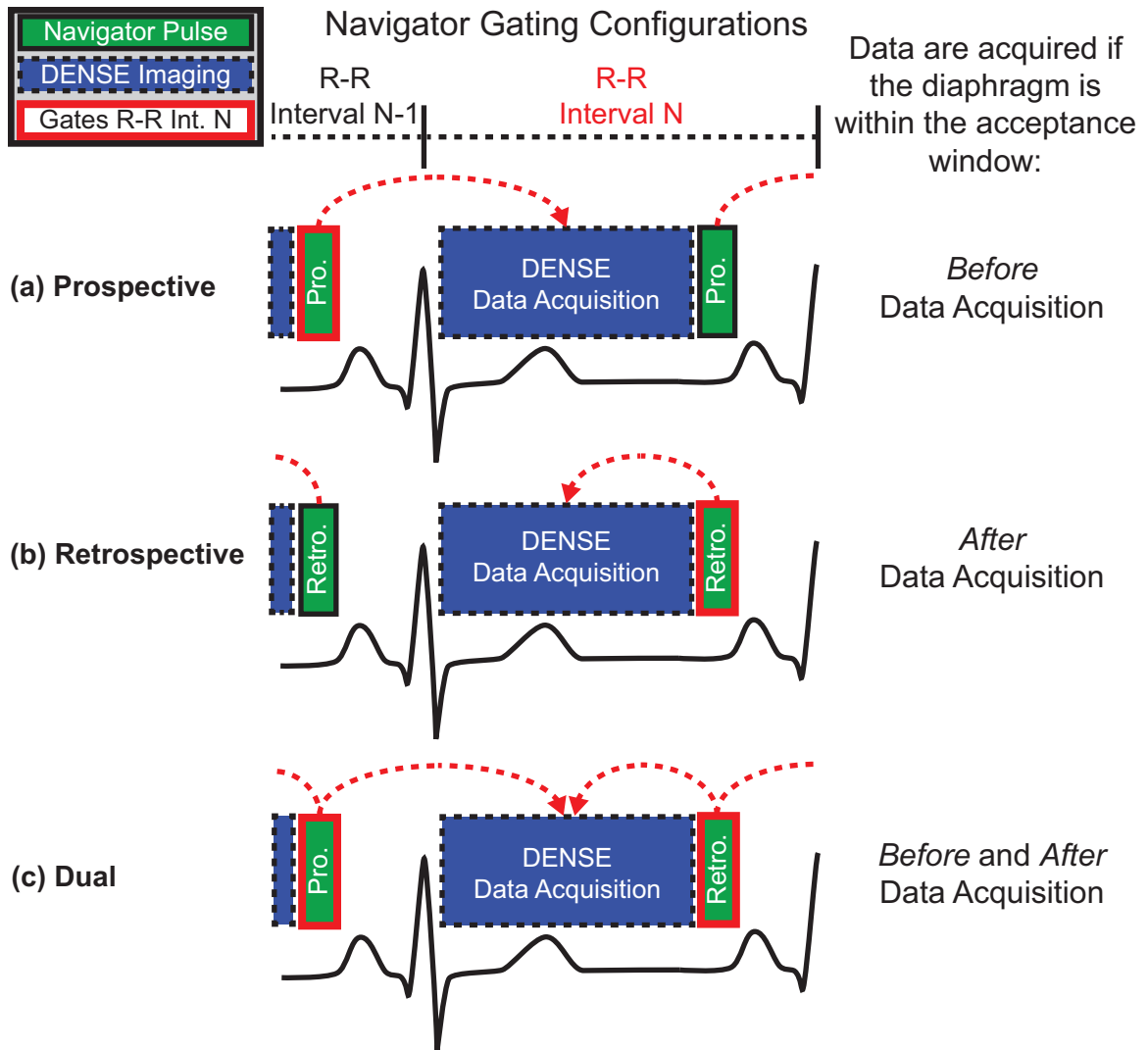


Figure 4.1: Different navigator gating configurations used to acquire DENSE image data. The single navigator configurations: (A) prospective and (B) retrospective; and the (C) dual navigator configuration. The red outlines and arrows indicate which navigator pulse(s) is/are gating the DENSE data acquisition.

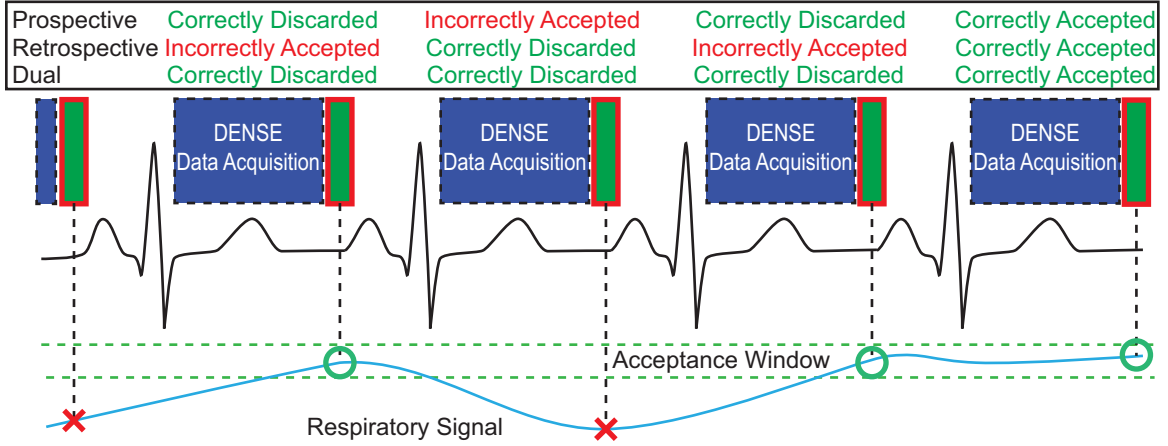


Figure 4.2: Theoretical example to demonstrate the disadvantages of single- and dual-navigator gating configurations. The red colored text identifies the incorrectly accepted DENSE data from single-navigator gating configurations (i.e. the diaphragm is not within the acceptance window for the entirety of DENSE data acquisition, but the data are still accepted). The number of Accepted/Discarded data in the example above illustrate how a dual navigator gating configuration will discard more data compared to single navigator gating configurations (retrospective and prospective) and lead to lower navigator efficiency. The red 'x' or green 'o' represents the detected diaphragm location being outside or inside the acceptance window, respectively.

temporal resolution between reconstructed cardiac frames. Based on the DENSE parameters, acquisition duration for each orientation was 20 heartbeats.

The respiratory navigator was placed over the dome of the liver. Subjects were asked to breathe comfortably and a scout navigator was used to track the diaphragm. The navigator acceptance window was placed so that the maximum acceptance window position was located 1-2 millimeters above the subject's maximum expiration position. A navigator acceptance window of ± 3 mm (total range of 7 mm) was used for all navigator gated scans. Navigator efficiency was measured as the number of cardiac cycles from which data were acquired and accepted over the total number of cardiac cycles required to complete a scan.

4.2.3 Navigator Feedback

Because the dual-navigator configuration was expected to decrease navigator efficiency, we developed and tested a feedback system, which allowed the subject to view their diaphragm position in real-time during image acquisition. The goal was to compensate for reduced navigator efficiency in order to preserve the clinical feasibility of DENSE imaging using a dual-navigator configuration.

The feedback system consisted of an angled mirror placed above the patient’s head so that an image of the diaphragm location was viewable on a screen located at the back of the scanner bore. The image of the diaphragm location (respiratory navigator display) was projected from the scanner console’s video feed onto the screen with an MRI-compatible projector. After all other scans were completed, subjects used this feedback system, with the dual-navigator gating configuration, to acquire the same short-axis and long-axis images.

This feedback system was also used prior to the breath-hold scan to ensure a consistent end-expiratory diaphragm location between the navigator-gated acquisitions and the breath-hold acquisitions. With instruction, the subject exhaled and breath-held in the acceptance window, at which point the navigated scan was halted and the breath-hold acquisition was immediately performed. Breath-hold acquisitions were always performed after the navigator-gated acquisitions that did not involve navigator feedback in order to minimize the potential effect of navigator feedback on respiratory patterns.

4.2.4 DENSE Post-Processing

All DENSE images were analyzed using custom, open-source MATLAB (The Mathworks Inc, Natick, MA) software, *DENSEanalysis* [50]. For each set of DENSE images, endocardial and epicardial boundaries were drawn on the magnitude image from an end-diastolic and end-systolic frame. A simplified analysis technique was

used to reconstruct the motion field [51]. The displacement-encoded phase images were unwrapped using a path-following algorithm with manual selection of seed points. The resulting Lagrangian displacements underwent spatial smoothing and temporal fitting as previously described [18].

Segmental two-dimensional Lagrangian strains were computed over the cardiac cycle for 6 segments in the short-axis images (radial and circumferential strain) and from the long-axis images (longitudinal strain). Cardiac segments were defined using the American Heart Association 17-segment model. For segmental strain, peak strain was computed for each segment and reported using mean and standard deviation of all segments. Average peak strains were computed by averaging the strain curves of all the myocardial segments together and finding the peak of this average strain curve. When computing peak longitudinal strain, pixels within 10% of left ventricular longitudinal length from the most basal and apical regions were excluded in order to remove the noise which is typically observed in the strain curves in those regions. Thickening was defined by convention as positive strain, whereas shortening was defined as negative.

4.2.5 Analysis

Mean modified coefficient of variation (CoV) [10, 9, 58] was used to measure agreement in strain between different navigator configurations and breath-holds. The calculation of the CoV is shown below where N is the number of subjects and x_1 and x_2 are the strain measurements.

$$CoV = \frac{\sum_{i=1}^N [St.Dev(x_1[i], x_2[i])]/N}{|\sum_{i=1}^N [(x_1[i] + x_2[i])/2]/N|} \quad (4.1)$$

Consistent with previous studies reporting CoVs [9, 69, 70, 6, 7], results less than or equal to 20% were considered acceptable.

To compare image quality, signal-to-noise ratio (SNR) was computed using the

DENSE magnitude images at end-systole. SNR was quantified from the average myocardial signal and the standard deviation of the noise within an area free from tissue or imaging artifacts [10, 58, 71]. Because the MR signal has a Rician distribution, corrections were applied to calculate the true SNR [72]. The measured standard deviation, σ_M , was used to compute the true standard deviation, σ , by

$$\sigma = \sqrt{\frac{2}{4 - \pi}} * \sigma_M \approx 1.526 * \sigma_M \quad (4.2)$$

The measured myocardial signal, M , was used to compute the true myocardial signal, S , by

$$S = \sqrt{M^2 - \sigma^2} \quad (4.3)$$

SNR was defined as the ratio of the true myocardial signal (S) to the true standard deviation (σ).

4.2.6 Comparison of Acquisition Configurations

We compared peak global and segmental strains (circumferential, radial, and longitudinal) and SNR of the end-systolic DENSE magnitude images between each acquisition technique (breath-hold and navigator gating) in adults. Bland-Altman analyses [53], CoV [9], and 95% confidence intervals (CI) were used to measure agreement in strain between the separate navigator configurations and breath-holds. A paired Student's t-test was used to compare strains between navigator configurations and breath-holds. We also compared SNR and navigator efficiency between all navigator configurations (dual, retrospective, and prospective) in adults and children using a one-way repeated measures ANOVA with post-hoc analyses and Bonferroni correction. All data are presented as mean \pm one standard deviation. Significance was defined as $p < 0.05$.

4.3 Results

Ten healthy adults (Age: 23 ± 3 years, 40% female) and 20 healthy children (Age: 13 ± 3 years, 45% female) were enrolled in the study. DENSE data were successfully acquired in all subjects except for one child who could not complete the study protocol due to an erratic respiratory pattern.

4.3.1 Average Peak Strains

Average peak left ventricular strains are shown in Table 4.1. There were no significant mean differences in circumferential, radial, and longitudinal strain between the dual, retrospective, and prospective navigator configurations and breath-holds in adults (Figure 4.3). Compared to breath-holds, all navigator configurations had a CoV of less than 20% for circumferential, radial, and longitudinal strain in adults (Figure 4.3). The differences in strain are listed as confidence intervals in Table 4.4. Peak segmental left ventricular strains are shown in Table 4.2). There were no significant differences in segmental strain between the navigator configurations and breath-holds except for radial strain from the prospective configuration ($p = 0.002$, Table 4.3). Compared to breath-holds, all navigator configurations had CoVs of less than 20% except for radial segmental strain (19-28%) (Table 4.3).

4.3.2 Signal-to-Noise Ratio

In adults, single navigator configurations had a 17-28% reduction in SNR compared to breath-hold DENSE (Table 4.5). There was no difference in SNR between the dual navigator configuration and breath-hold DENSE ($p = 0.06$). Among navigator configurations, dual and retrospective navigator configurations were comparable and both had better SNR (23% and 15%, respectively) compared to the prospective configuration ($p = 0.02$, $p = 0.004$, respectively).

Table 4.1: Average strains for different acquisition techniques.

	Mean \pm Std. Dev.	
	Adults	Children
Circumferential Strain (%)		
Breath-hold	-17 \pm 2	-
Retrospective	-18 \pm 2	-19 \pm 2
Prospective	-17 \pm 3	-18 \pm 2
Dual	-18 \pm 3	-20 \pm 2
Radial Strain (%)		
Breath-hold	30 \pm 10	-
Retrospective	26 \pm 9	30 \pm 9
Prospective	31 \pm 7	26 \pm 12
Dual	27 \pm 9	27 \pm 12
Longitudinal Strain (%)		
Breath-hold	-14 \pm 2	-
Retrospective	-14 \pm 2	-14 \pm 2
Prospective	-13 \pm 2	-14 \pm 2
Dual	-14 \pm 2	-14 \pm 2

Table 4.2: Segmental strain results for navigator gating and breath-holds in adults.

	Mean \pm Std. Dev.
Circumferential Strain (%)	
Breath-hold	-18 \pm 5
Retrospective	-18 \pm 5
Prospective	-18 \pm 5
Dual	-18 \pm 4
Radial Strain (%)	
Breath-hold	35 \pm 16
Retrospective	34 \pm 16
Prospective	42 \pm 17
Dual	34 \pm 16
Longitudinal Strain (%)	
Breath-hold	-13 \pm 4
Retrospective	-14 \pm 3
Prospective	-13 \pm 3
Dual	-14 \pm 4

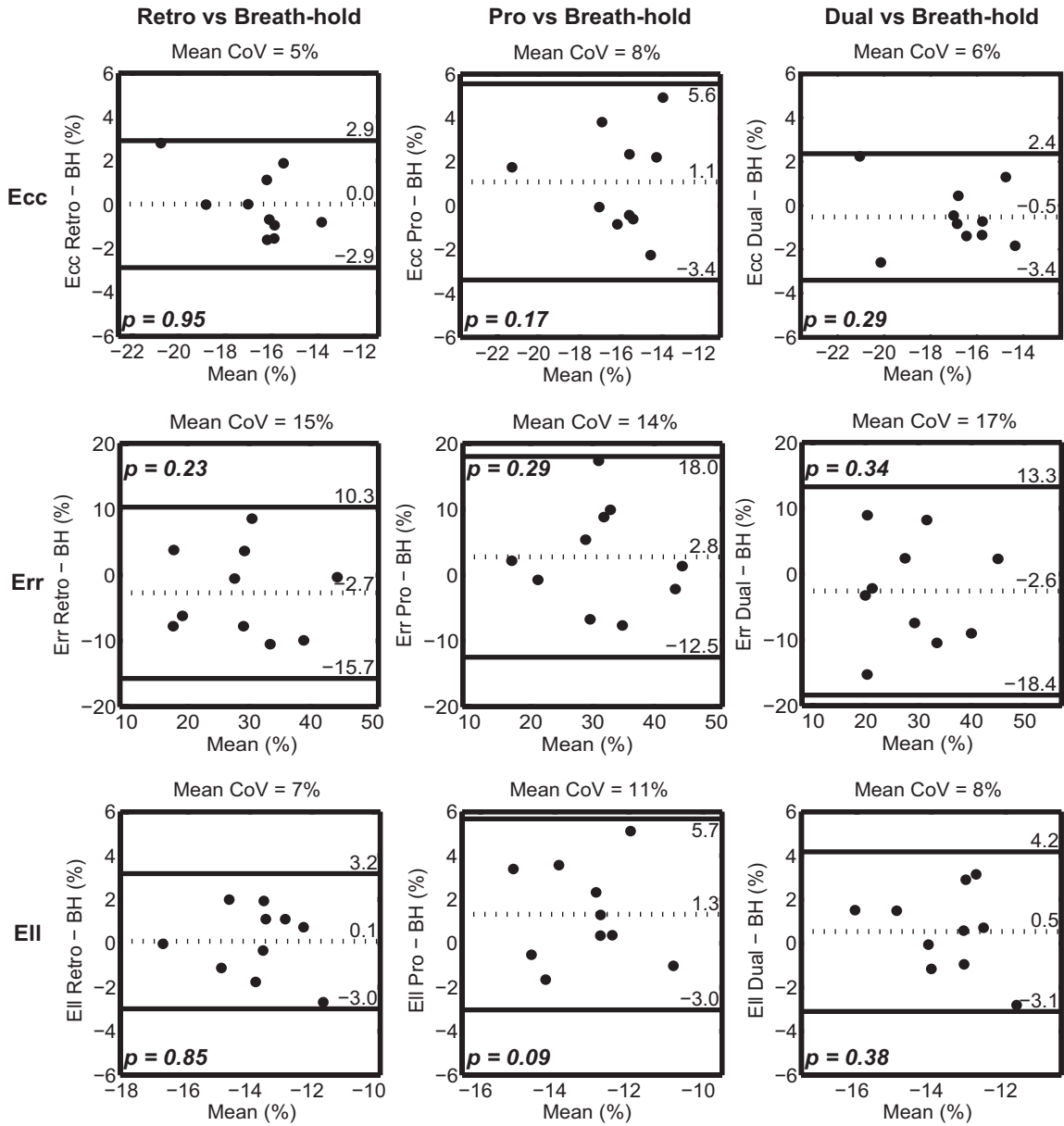


Figure 4.3: Bland-Altman plots of average peak circumferential (Ecc), radial (Err), and longitudinal (Ell) strains for retrospective, prospective, and dual navigator gating vs breath-hold.

Table 4.3: Segmental strain agreement between navigator gating and breath-holds from spiral cine DENSE.

	Bias	95% LoA	CoV (%)	p-value
Circumferential Strain (%)				
Retrospective–Breath-hold	0	± 5	8	0.94
Prospective–Breath-hold	0	± 8	13	0.78
Dual–Breath-hold	-1	± 5	8	0.11
Radial Strain (%)				
Retrospective–Breath-hold	0	± 25	19	0.79
Prospective–Breath-hold	8	± 36	28	0.002*
Dual–Breath-hold	-1	± 29	23	0.61
Longitudinal Strain (%)				
Retrospective–Breath-hold	-1	± 7	13	0.17
Prospective–Breath-hold	0	± 9	17	0.75
Dual–Breath-hold	-1	± 8	13	0.19

* indicates $p < 0.05$

Table 4.4: CI Results for Differences in Strain Between Navigator Gating and Breathhold DENSE.

	95% LoA	p-value
Circumferential Strain (%)		
Retrospective–Breath-hold	[-1.0–1.1]	0.95
Prospective–Breath-hold	[-0.6–2.7]	0.17
Dual–Breath-hold	[-1.6–0.5]	0.29
Radial Strain (%)		
Retrospective–Breath-hold	[-7.4–2.0]	0.23
Prospective–Breath-hold	[-2.8–8.3]	0.29
Dual–Breath-hold	[-8.3–3.2]	0.34
Longitudinal Strain (%)		
Retrospective–Breath-hold	[-1.0–2.0]	0.85
Prospective–Breath-hold	[-0.3–2.9]	0.09
Dual–Breath-hold	[-0.8–1.9]	0.38

Table 4.5: Signal-to-noise ratios for different navigator gating configurations in adults and children.

	Adults	p-value	Children	p-value
Breath-hold	18 ± 8		–	
Retrospective	15 ± 6*†	< 0.001	22 ± 6‡	< 0.001
Prospective	13 ± 5*		20 ± 8‡	
Dual	16 ± 7		27 ± 9	

* p < 0.05 vs. breath-hold; † p < 0.05 vs. prospective; ‡ p < 0.05 vs. dual

In children, SNR also differed based on navigator gating configuration (Table 4.5). The dual navigator configuration had the highest SNR compared to the retrospective (23% higher, p < 0.001) and prospective (35% higher, p < 0.001) configurations. There was no difference in SNR between the retrospective and prospective navigator configurations (p = 0.15).

4.3.3 Navigator Efficiency

For adults and children combined, there were significant differences in navigator efficiency between navigator configurations (p < 0.001, Table 4.6). The retrospective and prospective navigator configurations had higher navigator efficiencies than the dual navigator configuration by an average of 54% (p < 0.001) and 60% (p < 0.001), respectively. Using visual feedback with the dual navigator configuration improved navigator efficiency by 57% (p < 0.001) compared to the dual configuration without feedback and resulted in comparable efficiency to the single navigator configurations. The scan times mirrored the navigator efficiency results. For example, scan times for adults were, on average, 64, 37, 37, and 25 seconds for the dual, retrospective, prospective configurations, and the dual navigator configuration with feedback, respectively.

Table 4.6: Navigator efficiencies for different navigator gating configurations in adults and children.

	Pooled	p-value	Adults	Children
Retrospective	54 ± 15*	< 0.001	48 ± 15*	57 ± 16*
Prospective	56 ± 15*		52 ± 17*	58 ± 14*
Dual	35 ± 13		31 ± 16	37 ± 11
Dual Feedback	55 ± 16*		67 ± 11*	48 ± 15*

* p < 0.05 vs. dual (without feedback)

4.4 Discussion

The use of respiratory navigated acquisitions for spiral cine DENSE extends the potential utility of the technique by removing restrictions on patient breath-holding abilities and allowing for high resolution [32] and/or three dimensional [16, 33] data collection. While previous studies have used a respiratory navigator with DENSE, the optimal configuration for gating and how it might differ among subjects has not been explored. This study addressed these knowledge gaps by showing that: 1) left ventricular peak strains were not different between breath-held and navigator-gated DENSE acquisitions; 2) SNR was reduced with single navigator configurations, but not the dual configuration, compared to breath-held acquisitions; 3) the SNR benefit of the dual navigator configuration was offset by reduced navigator efficiency compared to single navigator configurations, but visual navigator feedback maintained clinically acceptable efficiencies for the dual navigator acquisition. The following paragraphs explore each of these findings in greater detail.

There were no significant mean differences and good paired agreement of all peak strains between retrospective, prospective, and dual navigator configurations and breath-holds in adults. This finding agrees with the prior work by Zhong et al., which compared segmental strains from navigator-gated 3D DENSE to breath-hold 2D DENSE [16] and similarly reported acceptable agreement. Our study extends this work by demonstrating that the agreement exists not only for prospective

navigator-gating used by Zhong et al., but for retrospective and dual navigator-gating configurations as well. Demonstrating this agreement of strain values—a primary endpoint for most DENSE acquisitions—has pragmatic value by ensuring that data from acquisitions with differing respiratory compensation can be readily compared.

Our results demonstrate that using a single navigator configuration resulted in significantly lower SNR compared to breath-hold DENSE acquisitions. While this result was only demonstrated in adults because of the prohibitively long breath-hold duration in children, it is reasonable to assume that a similar trend holds in children as well. Among the navigator configurations, the dual configurations provided the best SNR as it was superior to prospective navigator gating in both adults and children, had better SNR than retrospective gating in children, and resulted in comparable SNR to breath-hold DENSE.

Differences in SNR among the different acquisitions are likely attributable to heart rate and respiratory variability. The breath-hold acquisitions had the shortest acquisition time, with presumably less physiologic variability. Also, the dual navigator configuration had the most stringent acceptance criteria, which likely minimized the effects of respiratory variability during acquisition compared to the other configurations. This reasoning is supported by previous studies, which have reported associations between consistent diaphragm position during navigator-gated acquisitions and improved SNR [36, 37]. In both adults and children, the prospective navigator configuration had the lowest SNR of all navigator configurations. The observed difference in SNR between the single navigator configurations was perhaps unexpected given the theoretical similarities in their design and function. However, these differences are similarly attributable to the effects of variability: for the retrospective navigator, the interval between the R wave and the navigator echo is fixed, whereas heart rate changes during the scan

will affect the interval between the navigator echo and the succeeding R wave in prospective gating, increasing the likelihood of respiratory variability during that interval. Based on these findings, the use of prospective navigator gating for DENSE should be avoided.

Notably, a previous study compared SNR of a 2D steady-state free precession sequence between dual navigator-gated and breath-hold acquisitions and found that end-systolic myocardial SNR for breath-hold acquisitions was 23% lower than the dual navigator configuration in adults [73]. This finding contrasts with our data in which the dual navigator configuration was statistically comparable to breath-hold. However, the previous study had substantially different imaging parameters between their dual navigator-gated acquisition and the breath-hold acquisition, which likely accounted for the observed SNR differences [73].

Although the purpose of this study was to determine the optimal navigator gating strategy, it is worth noting that SNR was higher for children than it was for adults. The difference in SNR between adults and children is likely related to the smaller body habitus of children, which results in a shorter distance between the MRI coils and the heart. Moreover, adults likely have more adipose tissue, which could also lead to lower SNR. Ultimately, these SNR differences may lead to differences in inter-test reproducibility between adults and children.

As expected, single navigator gating configurations resulted in better navigator efficiency compared to dual navigator gating, due to the additional acceptance criteria constraints of the dual navigator. Simply put, more data are discarded with dual navigator gating, leading to prolonged scan time. Previous studies using a single-navigator configuration with the same size acceptance window (± 3 mm) reported navigator gating efficiencies ranging from 20 to 48% [16, 36, 35]. Compared to these studies, we observed slightly better single-navigator efficiencies of 48 to 52% in adults and 57 to 58% in children. The dual navigator efficiency was comparable to results

from previous studies [73].

To potentially offset this reduced efficiency, we evaluated the effect of providing the subject with visual feedback of the diaphragm position, which has been shown to considerably improve navigator efficiency compared to traditional free-breathing acquisitions [36]. We found that using visual feedback during dual navigator gated acquisitions improved navigator efficiency compared to the dual configuration without feedback and resulted in comparable efficiency to the single navigator configurations. The improvement with feedback was not uniform across adults and children (i.e., the improvement in kids was not as substantial), perhaps reflecting the superior ability of the adults to hold their breath within the acceptance window. Alternatively, the difference may be indicative of the non-intuitive nature of the respiratory navigator display and the differential abilities of adults and kids to quickly learn and use it. This provides motivation for the work in Chapter 5, where we developed and transformed the navigator image to a more kid-friendly video game design to improve usability and navigator efficiency [48].

The increased scan time associated with the dual navigator configuration presents an obvious trade-off with improved SNR for its utility in a clinical setting where time is a critical consideration. In adults, given the minimal difference in SNR between the dual and retrospective navigator configurations, the substantial drop in efficiency with the dual navigator may not be justified. In children, however, the SNR benefit with dual navigator gating is more substantial and warrants consideration to optimize data quality. Hence the demonstrated improvement in navigator efficiency by providing the subject with visual feedback is an important finding because it provides one option for compromise: achieving improved SNR while approximately maintaining scan time compared to other navigator configurations.

This study was performed using 2D cine DENSE. However, given the similarity in the fundamental sequence designs of 2D and 3D DENSE, the results are applicable to

3D cine DENSE acquisitions as well. In fact, given the longer time generally required for 3D data acquisition, respiratory compensation/navigation is essential, so these results are highly relevant. Specifically, our navigator efficiency findings agree with reported efficiencies from a previous study using 3D DENSE [16]. Also, while absolute magnitudes of SNR may differ with more data acquired, there is no reason to suspect that the relative differences in SNR would change between different navigator gating strategies when applying these results to 3D DENSE.

4.4.1 Limitations and Future Directions

A limitation of this study is the potentially limited power for detecting small strain differences between navigator configurations and breath-hold DENSE. However, our study had 80% power to detect a difference of 1.5% between the retrospective navigator configuration and breath-holds. This 1.5% difference is smaller than the typical inter-test limits of agreement of circumferential strain [10]. Moreover, even if the strains from the prospective navigator configuration, which had the worst agreement, are in fact different from the breath-hold technique, the conclusions of the study would not change as the prospective navigator configuration was separately found to be sub-optimal based on SNR.

Another limitation was the lack of breath-hold data for the pediatric subjects. The DENSE acquisition required 20 heartbeats. The required breath-hold time was further extended by using a navigator-gated pre-scan to ensure that breath-holds were performed at the same diaphragm position as the navigator-gated scans. This duration was viewed to be prohibitively long for pediatric subjects, and so no breath-hold DENSE data were acquired in these cases. The equivalence of DENSE-derived strains between breath-hold and navigator sequences was demonstrated in adults. Since children did not undergo breath-hold DENSE, we must caution future studies regarding these strain results as they apply to children. However, since the relative SNR and navigator efficiency results from navigator gating were similar to those in

adults, we would expect potential differences to be small. Furthermore, the primary objective of the study was to identify optimal navigator configurations for DENSE, so the lack of breath-hold data in children is a minor limitation.

A third limitation of this study is the lack of assessment of clinical patients. Cardiac patients, who routinely undergo MR imaging and who may have limited ability to hold their breath, may not be able to perform the lengthy breath-hold scan and may not achieve as high navigator efficiency when performing a dual navigator scan with feedback. However, since this population is more likely to undergo DENSE MR imaging than this study's volunteer subjects, it would be beneficial to determine whether the results remain the same. For example, it may be important to use dual navigator gating, even at the expense of navigator efficiency, to achieve higher SNR, since SNR is commonly lower in the clinical patient population compared to healthy volunteers.

4.5 Conclusion

For spiral cine DENSE acquisitions, respiratory navigator gating and breath-hold acquisitions yield comparable values of left ventricular peak strains. However, differences in signal-to-noise ratios and navigator efficiencies were observed among the different navigator gating configurations, which warrant consideration in clinical and research protocol design. In adult subjects, the dual navigator configuration produced the best SNR, although only slightly better than the single retrospective navigator, which produced acceptable SNR and therefore may be used to maintain good efficiency. For children, the benefit of a dual navigator configuration for improved SNR was even more apparent, but resulted in a considerable drop in scan efficiency. The prospective navigator resulted in the poorest SNR and should be avoided. The use of visual navigator feedback represents an effective option to maintain navigator efficiency while using the dual navigator in children (and adults).

CHAPTER 5

INTERACTIVE FEEDBACK GAME DESIGNED TO IMPROVE NAVIGATOR EFFICIENCY

Adapted from Hamlet SM, Haggerty CM, Suever JD, Wehner GJ, Grabau JD, Andres KN, Vandsburger MH, Powell DK, Sorrell VL, Fornwalt BK. An interactive videogame designed to improve respiratory navigator efficiency in children undergoing cardiovascular magnetic resonance. Journal of Cardiovascular Magnetic Resonance. 2016. 18:54 [48]

5.1 Background

Advanced cardiac magnetic resonance (MR) acquisitions, which often require respiratory navigator gating, have poor scan efficiency or long scan times, especially in children. Importantly, in Chapter 4, the *dual* navigator configuration was shown to have the best SNR, but worst navigator efficiency. Thus, it is important to improve the efficiency as this currently limits the clinical feasibility of advanced imaging techniques. The purpose of this study was to develop and have children use an interactive, breathing-controlled feedback videogame during DENSE cardiac MR to improve navigator efficiency and maintain image quality compared to no feedback.

Cardiac magnetic resonance (MR) can be used to non-invasively assess heart function. In the clinical setting, cardiac MR techniques play an important role in the diagnosis and monitoring of the complex anatomy and physiology of congenital and acquired heart diseases. Moreover, there is considerable pre-clinical research devoted to the development and evaluation of new, advanced imaging techniques, such as 3D displacement encoding with stimulated echoes (DENSE) [16], 3D steady state free precession [74], and 4D flow imaging [75]. These new techniques have

demonstrated promise in distinguishing normal and pathological tissue deformation and blood flow and may become beneficial tools in the diagnosis and management of heart disease. Many of these clinical and pre-clinical techniques require scan durations that exceed patients' ability to hold their breath.

End-expiratory breath-holds are used by many cardiac MR sequences to minimize respiratory-motion artifacts. However, requiring subjects to hold their breath introduces significant limitations on the duration of data acquisition or the quality of the acquired images, particularly for young children or patients with advanced disease. A common alternative is respiratory navigator gating, which works by measuring the diaphragm position during normal breathing and only acquiring data when the diaphragm is within a pre-defined acceptance window (Figure 5.1a). The trade-off of respiratory navigator gating is significantly increased scan duration because of poor navigator efficiency. For example, previous cardiac MR studies have reported respiratory navigator efficiencies of 20 to 45% in adults [35, 36, 37, 38]. This poor navigator efficiency lengthens the duration of currently used clinical imaging and limits clinical feasibility of emerging advanced imaging techniques.

Navigator efficiency is typically poor because breathing patterns can be erratic [20, 21, 22], and the patient is generally unaware of the desired acceptance window location. Providing the patient with visual feedback of the diaphragm position during cardiac MR ("navigator feedback") has been shown to improve breathing consistency and scan efficiency in adults [36, 20]. For example, studies have shown efficiency improvements up to 29% (absolute) compared to traditional acquisitions without feedback [36, 37]. Importantly, these previous studies have demonstrated that image quality from navigator feedback acquisitions is similar to acquisitions without feedback [36, 37]. The potential to achieve similar benefits using navigator feedback with pediatric participants has not been explored. Given the challenge of

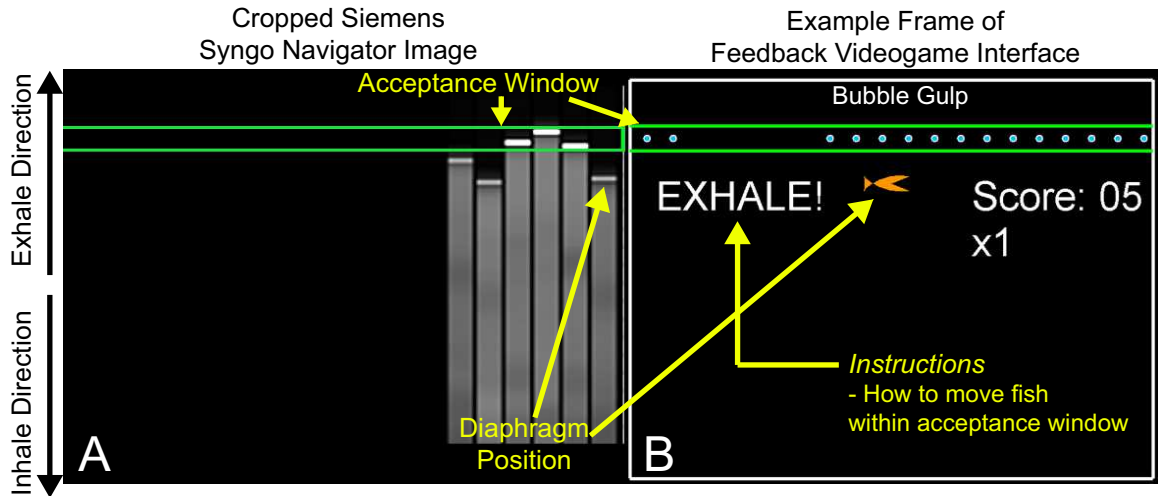


Figure 5.1: Feedback videogame. (A) Cropped version of the Siemens Syngo navigator image that was processed in real-time during cardiac MR acquisition to yield the feedback videogame. (B) Example frame of the navigator feedback videogame interface, which was shown to the child during cardiac MR (yellow overlay text was not shown to the child).

keeping these participants still and motionless for long periods of time, this improved efficiency could have substantial clinical benefit.

Most previous studies involving navigator feedback simply utilized the built-in navigator display. One previous study evaluated a custom videogame interface in a study of adults for increasing navigator efficiency [37]. Such an interface theoretically combines the benefits of visual feedback with an intuitive and engaging design for the user—attributes that are highly desirable for scanning children. Thus, the present study sought to extend and tailor this paradigm specifically for children by providing navigator feedback in the form of an interactive, kid-friendly videogame. Moreover, this study sought to test this design using DENSE, an imaging technique that can be used to quantify advanced measures of heart function such as cardiac strains. We hypothesized that navigator feedback using an interactive videogame (that we would develop) during cardiac MR would improve navigator efficiency and maintain image quality and strains in children.

5.2 Methods

5.2.1 Feedback videogame overview

A navigator feedback videogame (FG), called "Bubble Gulp", was developed using MATLAB (The Mathworks Inc, Natick, MA). Each frame of the navigator image provided within the Siemens Syngo user-interface (Siemens Healthcare, Erlangen, Germany) (Figure 5.1a) was captured using an Epiphan DVI2USB 3.0 (Epiphan Systems Inc., Palo Alto, California) frame grabber and processed in real-time during cardiac MR to yield a kid-friendly representation of the diaphragm position (Figure 5.1b). Navigator image processing was performed using an externally connected laptop running Windows 7 with an Intel Core i7 processor and 16 GB of RAM. The FG interface was then projected to the participant in the scanner using an angled mirror and a magnetic resonance compatible projector (Figure 5.2).

The diaphragm position relative to the acceptance window (Figure 5.1a) was represented by the vertical position of a fish character relative to parallel green lines containing scrolling dots, representing bubbles (Figure 5.1b). The objective of the game was to control the fish's vertical position, which was updated with each navigator pulse, so it would "gulp" bubbles and acquire points. To incentivize slow, stable breathing, point values increased as the fish spent more time within the green lines, instead of frequent short-duration breath-holds. However, prior to any use of the FG, children were instructed *not* to hold their breath for an uncomfortable amount of time and to breathe when needed. Finally, the FG interface displayed text to instruct children how to adjust their breathing to place the fish in between the green lines (Figure 5.1b).

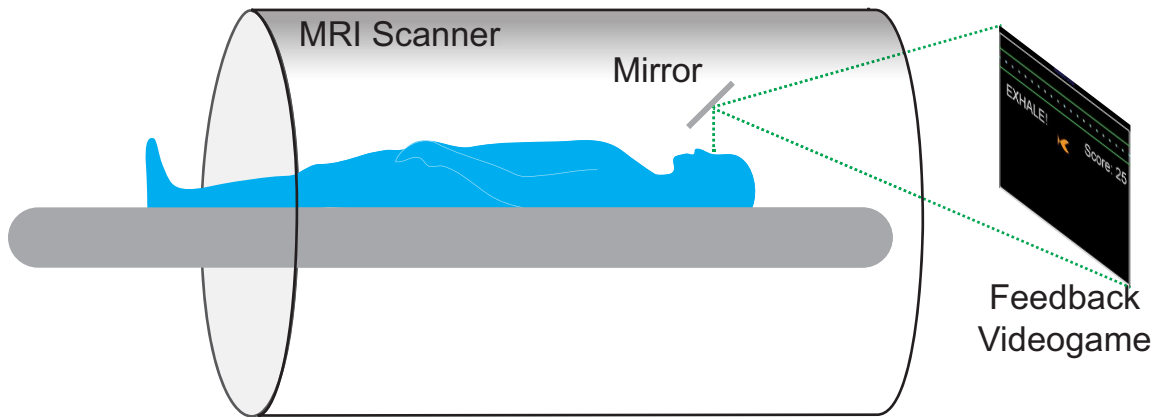


Figure 5.2: MRI Feedback Setup Feedback videogame was shown to children during cardiac MR with an angled mirror and MR-compatible projector.

5.2.2 Motivation for Design

Bubble Gulp’s overall design was based on three concepts: *portability*, *compatibility*, and *independence*. First, Bubble Gulp needed to have the ability to be transferred easily from one MRI machine site to another so that the system can be easily relocated to collaborators or within research groups. Second, Bubble Gulp needed to be compatible with multiple MRI machine vendors (and their corresponding navigator image designs) so that its use was not restricted to one vendor. Third, Bubble Gulp needed to work independently from the MRI machine and to not directly integrate with the MR machine’s software so that its use does not affect the delicate controls.

5.2.3 Hardware Design

The hardware design begins with the MRI computer itself, which has the ability to independently display the navigator image on one of its video outputs. The overall block diagram is shown in Figure 5.3. The second video signal only displayed the navigator image. This signal was split so that one signal was connected to a monitor in the control room (for viewing the navigator image in real time) and the second signal was connected to the Epiphan DVI2USB 3.0 (Epiphan Systems Inc., Palo

Alto, California) frame grabber, so that the navigator image could be captured and processed into the videogame.

This DVI frame grabber allowed for high resolution (up to 1920x1200) capturing at up to 60 frames per second (fps), which allowed for simpler image processing due to more accurate image capturing. Most importantly, this frame grabber had a Java interface for Windows, Linux, and Mac OS X. Thus, we wrote a small Matlab "wrapper" program to interface and connect with the frame grabber so that the entirety of the Bubble Gulp code was written using Matlab.

The frame grabber was connected directly to the laptop via USB. Once the navigator image was captured, the Matlab code on the laptop processed the image into Bubble Gulp which was displayed as an independent Matlab figure window on the laptop's secondary display through the VGA port. This VGA port was then connected to an MRI-compatible projector within the MRI room, which displayed Bubble Gulp to the child on a screen at the back of the scanner bore (Figure 5.2). Not shown in the block diagram is a VGA splitter that allowed Bubble Gulp to also be seen by the operator in the MR control room.

Regarding the overall design, the hardware design allowed for *portability* and *independence*, since the interface simply connected to the video output on the scanner and did not integrate with the scanner software, and *compatibility*, since multiple machine vendors have some form of video output that can be used to capture the navigator image with a frame grabber.

5.2.4 Overall Software Design

The overall software design is shown in Figure 5.4 and was written using Matlab (Mathworks, Natick, MA). The input to the software was a navigator image, which was captured using the DVI framegrabber and the Matlab wrapper class for the Java interface, which contained a method that allowed simple capture of the frame. Since the navigator image was updated with new data with every patient heartbeat

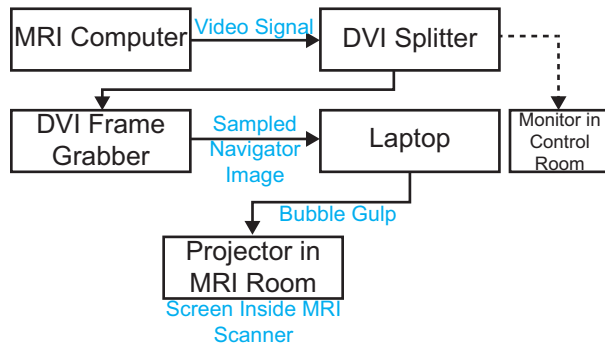


Figure 5.3: Overall hardware block diagram for Bubble Gulp (Feedback Game).

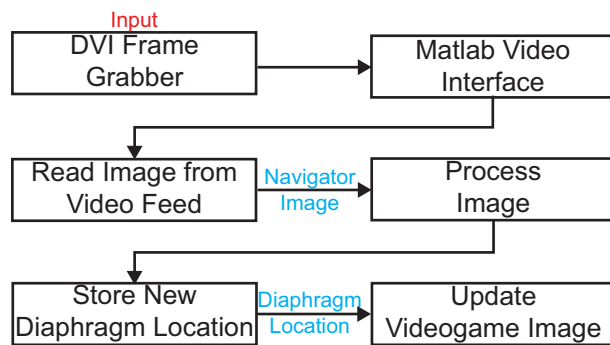


Figure 5.4: Overall software block diagram for Bubble Gulp (Feedback Game).

(typically lower than 120 heartbeats per minute), a frame sampling rate of 10 fps was sufficient to capture all changes in diaphragm position. The diaphragm location was identified and, if different from the previous position, the new position was used to update the videogame.

5.2.5 Algorithm

The overall goal of the image processing algorithm is to identify the location of the diaphragm position with respect to the acceptance window (Figure 5.5). Once a new navigator image was sampled using the frame grabber, the first step was to identify the Microsoft Windows' window region of interest (ROI). The next step was to identify the Red Search Window ROI (Figure 5.6). The search window ROI was then used to crop the image because the videogame only needed to identify the diaphragm position

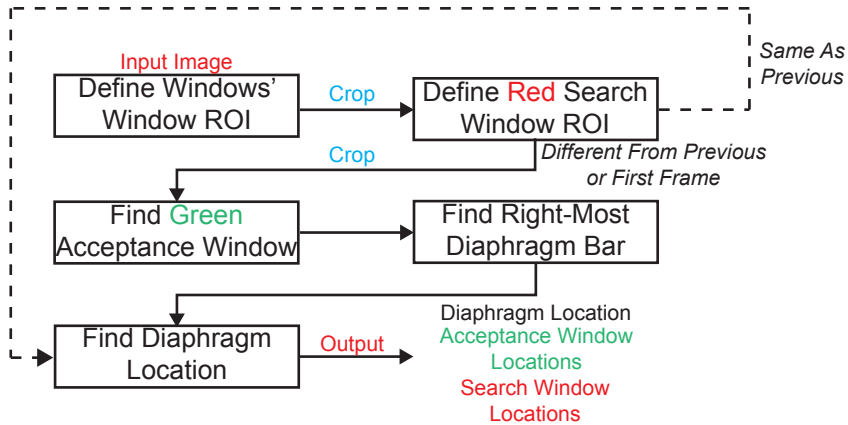


Figure 5.5: Overall image processing algorithm block diagram for Bubble Gulp (Feedback Game).

with respect to the acceptance window, all area outside of the search window ROI was ignored. Within the new cropped image, the green acceptance window borders were identified along with the current diaphragm location (right-most bar). Since the DVI frame grabber captured such high resolution images, the pure color channels were used to identify the red and green ROIs. This entire algorithm (Figure 5.5) only has to be run 1 time (for the first frame) so long as the position of the red search window remain the same (which will occur if the operator does not move the navigator image window during scanning). This is because the previous positions of the red search window, green acceptance window, and diaphragm position are always stored and compared with the new position. For example, if the position of the red search window is the *same as previous*, then the algorithm can use the previously stored positions to identify the current vertical location of the diaphragm position with respect to the acceptance window position. This removes several processing steps and saves time. Specifically, the entire algorithm takes about 200 ms. However, if you remove extra processing steps by having the same red search window positions, then the algorithm takes about 100 to 150ms.

The text feedback instructions requires another simple algorithm to instruct the patient on how to breathe in order to place his or her diaphragm position within the

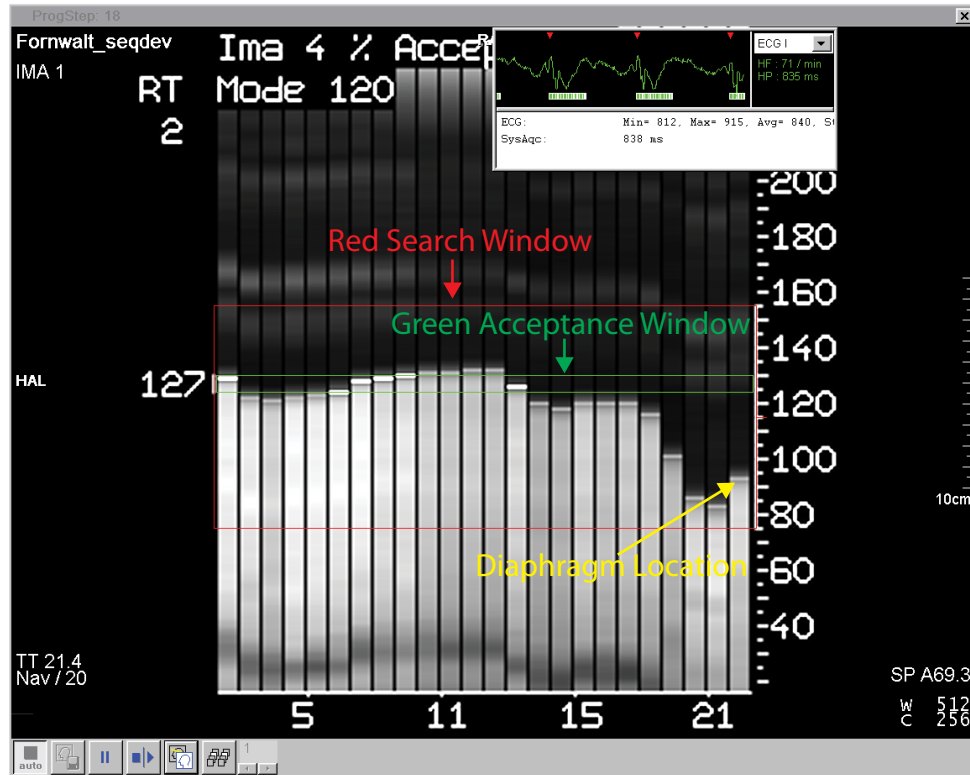


Figure 5.6: Example Navigator Image to be Processed.

acceptance window. This text is displayed underneath the acceptance window on the left side of the videogame (Figure 5.1b). This algorithm is shown in Figure 5.7. The acceptance window locations and diaphragm location were passed as inputs to the "feedback" function that determined if the diaphragm position was within the acceptance window. This function then would output the appropriate response to the subject on whether he or she should "hold", "breathe in", or "breathe out" (Figure 5.7). The subjects were instructed to use this feedback text as a guideline when needed so that they still breathed comfortably.

5.2.6 Participants

Fifty children without significant past medical history were recruited. Participants were recruited from the broader clinical community based out of our university medical center using a wide range of participant recruitment services

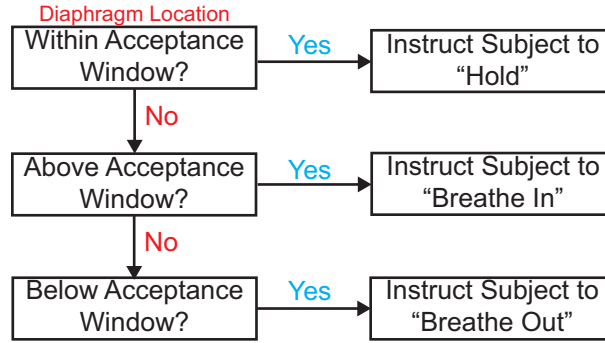


Figure 5.7: Basic text feedback block diagram.

provided by the University of Kentucky Center for Clinical and Translational Science. All participants were screened with a 12-lead ECG prior to imaging to rule out arrhythmias. The local Institutional Review Board at the University of Kentucky approved the study protocol and all participants and legal guardians provided written informed consent or assent.

5.2.7 Imaging

All imaging was performed using a 3T Siemens Tim Trio (Siemens Healthcare, Erlangen, Germany) with a 6-element chest coil and a 24-element spine coil. For each participant, navigator-gated 2D spiral cine DENSE cardiac MR [16, 58] images from mid-ventricular, 4-chamber, basal, and apical image orientations were separately acquired with no feedback (NF) and then while using the FG. No instructions regarding breathing were given for the NF acquisitions, thus participants were allowed to breathe naturally. Between acquisitions with NF and those with the FG, each participant underwent two 30-heartbeat practice scans to familiarize himself or herself with the FG.

DENSE imaging parameters included: number of spiral interleaves = 12, interleaves per beat = 2, FOV= 360 360 mm², pixel spacing = 2.8 2.8 mm², slice thickness = 8 mm, TE = 1.4 ms, TR = 17 ms, variable flip angle = 20°, displacement encoding = 0.06 cyc/mm [10], through-plane dephasing = 0.08

cyc/mm [15], CSPAMM echo suppression [12], view sharing and a dual-navigator strategy [48] with an acceptance window size of ± 3 mm. For each cardiac cycle, the navigator echo occurred immediately after data acquisition. The dual-navigator strategy required the diaphragm position to be within the acceptance window for both the preceding *and* current cardiac cycles for data to be accepted. Prospective ECG gating was performed and 23–51 cardiac phases were acquired depending on participant heart rate. As a result of the imaging parameters, each complete image acquisition required 38 heartbeats that satisfied the navigator gating criteria.

Due to erratic respiratory patterns or participant movement, image acquisition can be difficult to complete in children in a reasonable amount of time with NF. As scan session duration increases, the likelihood of patient movement also increases, so we defined criteria for maintaining a target scan protocol duration of 30 min. We defined image acquisition as incomplete (data not acquired) following 192 heartbeats without a completed image acquisition. Progressing past 192 heartbeats for a 38-heartbeat scan is equivalent to achieving less than 20% navigator efficiency, which is worse than previously reported NF values [35, 36, 37, 38]. Once any NF image acquisition was marked as incomplete, we proceeded to the FG acquisitions. If a participant moved, the number of acquired image orientations was reduced from four (mid, 4ch, base, apex) to two (mid, 4ch) to ensure at least two images were acquired with NF and FG.

5.2.8 Calculation of cardiac strains from DENSE

DENSE images were analyzed using *DENSEanalysis* [50], a custom, open-source MATLAB (the Mathworks Inc, Natick, MA) software. To delineate the myocardium, endocardial and epicardial boundaries were manually drawn on the DENSE magnitude image using an end-systolic and end-diastolic frame. The motion field was reconstructed using a simplified analysis technique [51]. Using manual selection of seed points, which indicated unwrapped phase data, a

path-following algorithm was used to unwrap the displacement-encoded phase data. Temporal fitting and spatial smoothing was applied to the resulting Lagrangian displacements as previously described [18].

Two-dimensional segmental Lagrangian strains were quantified from the smoothed trajectories over the entire cardiac cycle. Radial and circumferential strain was computed for 6 myocardial segments of the short-axis images and longitudinal strain was computed from the long-axis images. The strain curves of all the cardiac segments were averaged into a single mean curve. Global peak strain was quantified by averaging the strain curves from each slice and finding the resulting peak strain of this curve. When computing peak longitudinal strain, pixels within 10% of left ventricular longitudinal length of the most basal and apical regions were excluded due to increased noise typically observed in the strain curves in those regions. Peak strain was defined according to typical convention as a positive for thickening (radial strain) and negative for shortening (circumferential and longitudinal strain).

5.2.9 Analysis

This study measured navigator efficiency and heart rate during image acquisition and used image signal-to-noise ratio (SNR) of the end-systolic DENSE magnitude image as a measure of image quality. Navigator efficiency was defined as the ratio of the number of heartbeats for which image data were accepted to the total number of heart beats required to complete the image acquisition. To compare image quality, signal to noise ratio (SNR) was calculated for each cardiac phase of each DENSE magnitude image. SNR was computed from the average signal of the myocardium and the standard deviation of the signal (noise) within an area without signal (free from tissue and imaging artifacts). Due to the Rician distribution of the MR signal, corrections were applied to the measured standard deviation (σ_M in Equation 5.1) and measured myocardial signal (M in Equation 5.2) to compute the true SNR [58, 10, 72].

The SNR was defined as the ratio of the true myocardial signal to the true standard deviation.

$$\sigma = \sqrt{\frac{2}{4 - \pi}} * \sigma_M \approx 1.526 * \sigma_M \quad (5.1)$$

$$S = \sqrt{M^2 - \sigma^2} \quad (5.2)$$

For incomplete NF image acquisitions (satisfied stoppage criterion), navigator efficiency and heart rate measurements were computed based on the partial data that were acquired.

5.2.10 Training

Off-scanner training has been used by other investigators to ensure participants are comfortable and understand a navigator feedback interface before entering the magnet [36]. We wanted to determine the efficacy of off-scanner training with the FG on navigator efficiency, image quality, and heart rate. Thus, 30 of the 50 enrolled participants were randomized into equal groups to either receive extensive off-scanner training or no off-scanner training prior to scanning; thus, the groups were referred to as 'trained' and 'untrained.' As mentioned above, all subjects (including trained and untrained participants) underwent minimal training in the scanner, which was defined as two 30-heartbeat practice scans prior to FG acquisitions. The remaining 20 participants also received off-scanner training, but they were not included within the trained subgroup for analysis because they were not randomized to this treatment.

Each trained participant was introduced to the FG using an MRI simulator prior to the formal study. The MRI simulator utilized a PrimeSense Carmine 1.09 (PrimeSense, Tel Aviv, Israel) 3D camera to precisely measure the chest wall and abdomen excursion as a proxy for diaphragm translation [76, 77]. Each participant had to complete goal-based training before advancing to cardiac MR scanning. Training

time was recorded for all trained participants.

5.2.11 Training Protocol

The goal-based training protocol was as follows: First, the children were instructed to perform 3 sequential end-expiratory breath-holds to determine the optimal location for the acceptance window. Then the children were instructed to complete 9 levels of the FG, which progressed in difficulty. Difficulty was increased by either 1) decreasing the acceptance window size or 2) increasing the time delay between chest excursion recording and fish location update. Because the navigator gating sequence only measures the diaphragm position during each heartbeat, children with slower heartbeats may experience "delays" between diaphragm movement and fish location update. In order to complete each level, the children had to acquire 100 points. If all bubbles were acquired in a row without breaks, each level could be completed in ~ 33 seconds.

5.2.12 Statistics

Statistical analyses were completed using R version 3.2.2 (R Foundation for Statistical Computing, Vienna, Austria). All continuous measurements were reported as mean \pm standard deviation. Navigator efficiency, SNR, heart rate, and global left ventricular strains were tested for normality using a Shapiro-Wilk test. Average navigator efficiency, SNR, heart rate, and strain were compared between NF and FG acquisitions using a paired student's t-test or Wilcoxon Signed-Rank test when appropriate, and compared between untrained and trained groups using a student's t-test or Mann-Whitney U test when appropriate. To determine whether age influenced navigator efficiency, age was correlated with navigator efficiency for both NF and FG acquisitions.

5.3 Results

Fifty-six children were prospectively enrolled. Six children were excluded from the study due to either being uncomfortable in an MRI scanner, having premature ventricular contractions, having ECG-monitoring equipment fail, or consistently moving during scanning. Thus, this study reported data on 50 children (Age: 14 ± 3 years, 48% female) without significant past medical history, which included a subset of 30 children randomized to either the off-scanner trained ($n = 15$; Age: 15 ± 3 years, 47% female) or untrained ($n = 15$; Age: 13 ± 3 , 66% female) groups. All trained participants successfully completed off-scanner training and the mean goal-based training duration was 11 ± 2 min. The prescribed stoppage criterion for the NF scans was met in 11 cases, resulting in fewer completed NF images for those participants. Additionally, four participants moved during scanning, which included two during NF scans and two during FG scans, resulting in the completion of the abridged imaging protocol, as described in the methods.

5.3.1 Navigator Efficiency

Using the FG significantly improved average navigator efficiency compared to NF ($58 \pm 13\%$ vs $33 \pm 15\%$, $p < 0.001$, Figure 5.8a). Average navigator efficiency was not correlated with age for either NF or FG image acquisitions ($r = 0.07$, $p = 0.63$; $r=0.14$, $p = 0.32$, Figure 5.8b). There was no significant difference in average navigator efficiency between untrained and off-scanner trained groups for FG image acquisitions ($57 \pm 17\%$ vs $57 \pm 11\%$, $p = 0.90$, Figure 5.9).

5.3.2 SNR

Use of the FG significantly improved SNR compared to NF (22 ± 6 vs 21 ± 6 , $p = 0.01$, Figure 5.10). There was no significant difference in SNR between untrained and off-scanner trained groups for FG images (22 ± 6 vs 21 ± 6 , $p = 0.77$).

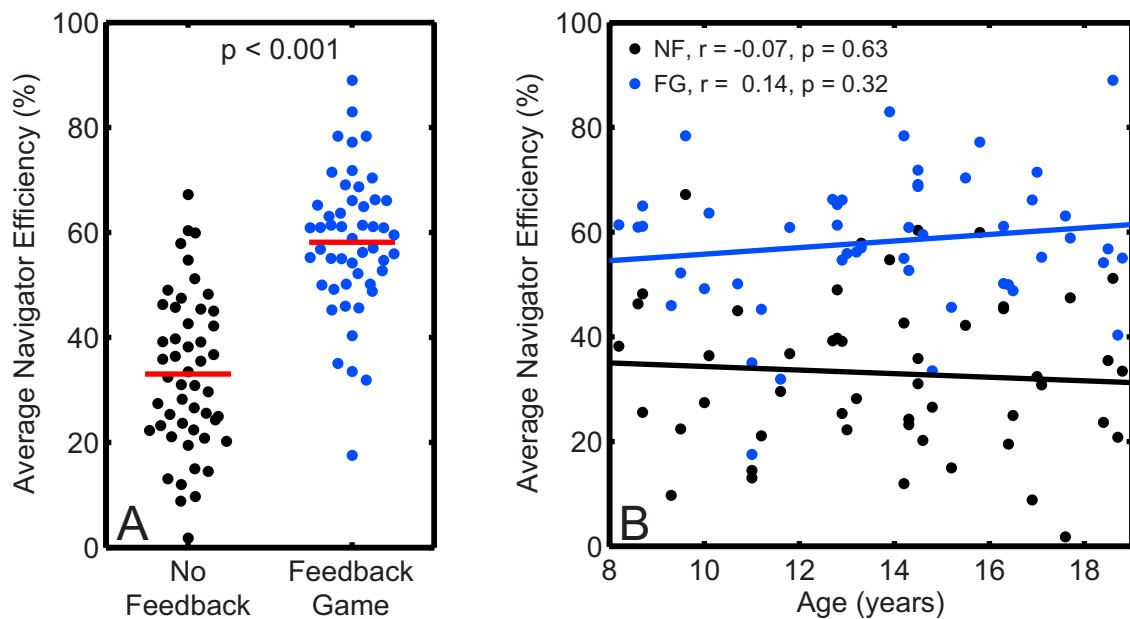


Figure 5.8: (A) Average navigator efficiency for No Feedback and Feedback Game image acquisitions. Use of the feedback game significantly increased navigator efficiency compared to no feedback. The solid red line indicates the mean of each group. **(B) Average navigator efficiency vs age for No Feedback (NF) and Feedback Game (FG) image acquisitions.** There was no correlation between navigator efficiency and age for either no feedback ($r = -0.07$, $p = 0.63$) or feedback game ($r = 0.14$, $p = 0.32$) acquisitions. The solid lines indicate the line of best fit for each group.

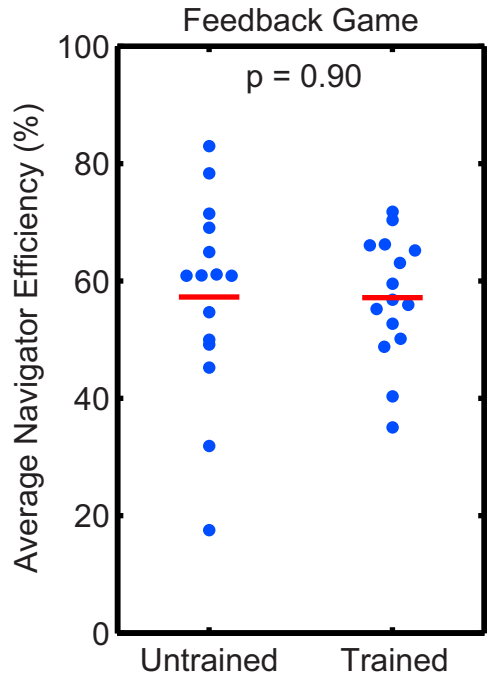


Figure 5.9: Average navigator efficiency for Off-scanner Trained and Untrained groups. There was no significant difference in navigator efficiency between untrained and off-scanner trained groups for feedback game acquisitions. The solid red line indicates the mean of each group.

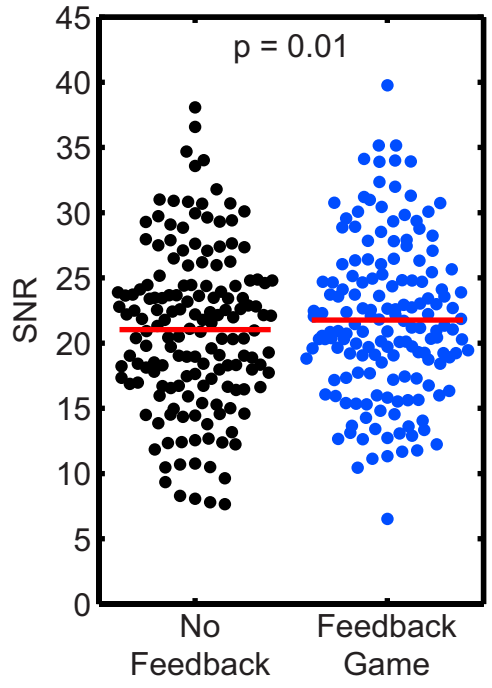


Figure 5.10: SNR for all No Feedback and Feedback Game images. Use of the feedback game resulted in significantly increased SNR compared to no feedback.

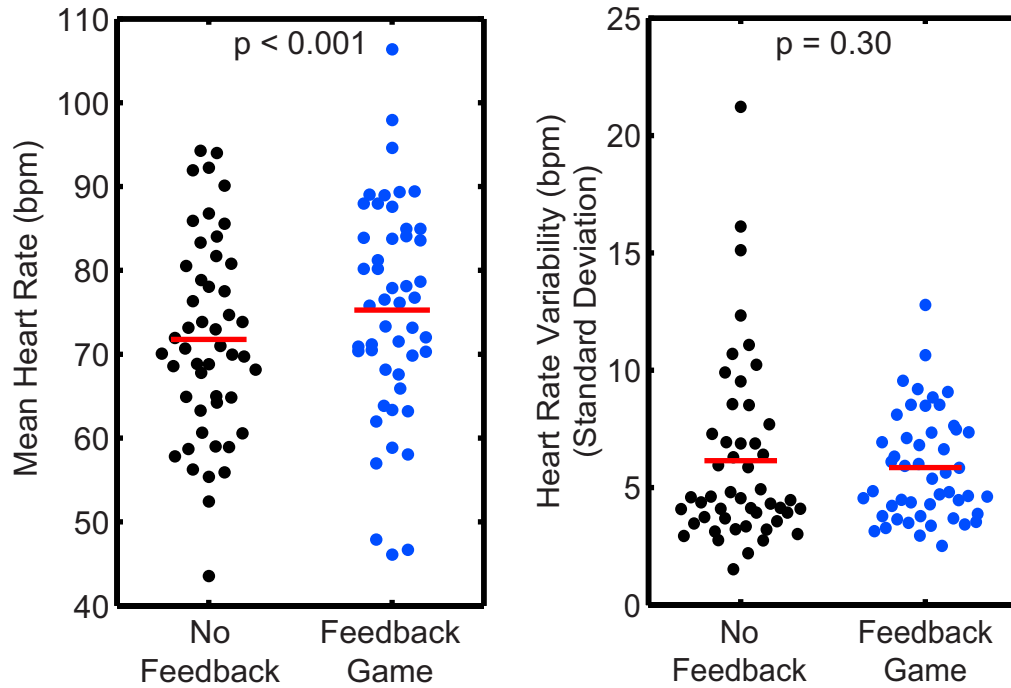


Figure 5.11: Mean and standard deviation of heart rate for No Feedback and Feedback Game acquisitions. Use of the feedback game resulted in significantly higher heart rate compared to no feedback. There was no significant difference in standard deviation of heart rate between no feedback and feedback game acquisitions. The solid red line indicates the mean of each group.

5.3.3 Heart rate

On average, heart rate during FG scans was slightly higher than NF acquisitions (75 ± 13 vs 72 ± 12 bpm, $p < 0.001$, Figure 5.11), but there were no differences in the standard deviation of heart rate (5.9 ± 2.2 vs 6.1 ± 3.9 bpm, $p = 0.30$, Figure 5.11b). Heart rate was similarly elevated during FG acquisitions in both the untrained and off-scanner trained groups compared to NF acquisitions ($p < 0.001$ and $p = 0.03$, respectively, Table 5.1).

Table 5.1: Average Heart Rate for Off-scanner Trained and Untrained groups.

HeartRate (bpm)	Trained			Untrained		
	No Feedback	Feedback Game	p-value	No Feedback	Feedback Game	p-value
Mean	72 ± 13	76 ± 16	0.03	72 ± 9	78 ± 9	< 0.001
Standard Deviation	6.9 ± 5.0	5.7 ± 2.4	0.80	5.3 ± 2.4	6.0 ± 2.0	0.17

Table 5.2: Global peak strain results for NF and FG scans.

	No Feedback	Feedback Game	p-value
Circumferential Strain (%)	-17 ± 2	-16 ± 2	< 0.001
Radial Strain (%)	44 ± 11	40 ± 10	0.005
Longitudinal Strain (%)	-13 ± 2	-13 ± 2	0.38

5.3.4 Strain

Global circumferential and radial strains derived from FG acquisitions were slightly lower in magnitude compared to NF acquisitions ($16 \pm 2\%$ vs $17 \pm 2\%$, $p < 0.001$; $40 \pm 10\%$ vs $44 \pm 11\%$, $p = 0.005$, respectively, Table 5.2). There were no differences in longitudinal strain between NF and FG acquisitions ($13 \pm 2\%$ vs $13 \pm 2\%$, $p = 0.38$).

5.3.5 Survey Responses

In order to formally measure the enjoyment and response of the children playing the Feedback Game, we asked the children to fill out a post-scan survey that consisted of 7 questions. Those questions and responses are listed below. In general, most participants 1) found Bubble Gulp to be easy to play; 2) enjoyed playing Bubble Gulp; 3) thought they were generally getting better as they played; 4) thought training was/would have been somewhat helpful; 5) had no comments on how to improve Bubble Gulp; 6) enjoy playing videogames; and 7) play videogames daily.

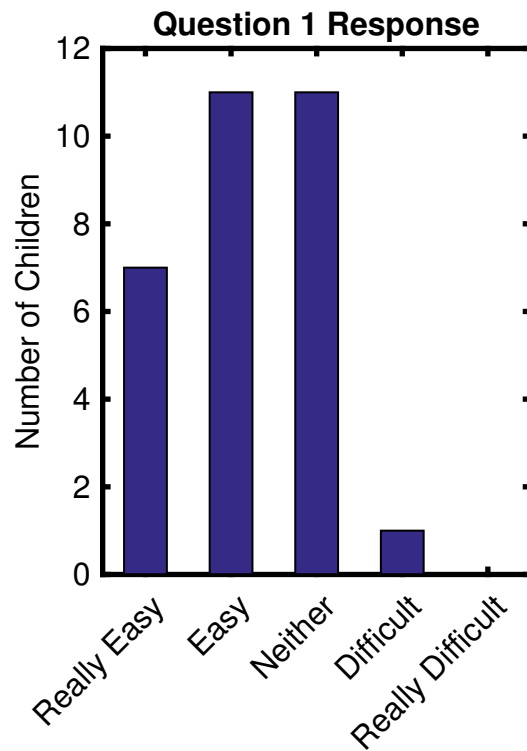


Figure 5.12: Question 1. How easy was playing Bubble Gulp?

- 1: Really easy
- 2: Easy
- 3: Neither easy nor difficult
- 4: Difficult
- 5: Really Difficult

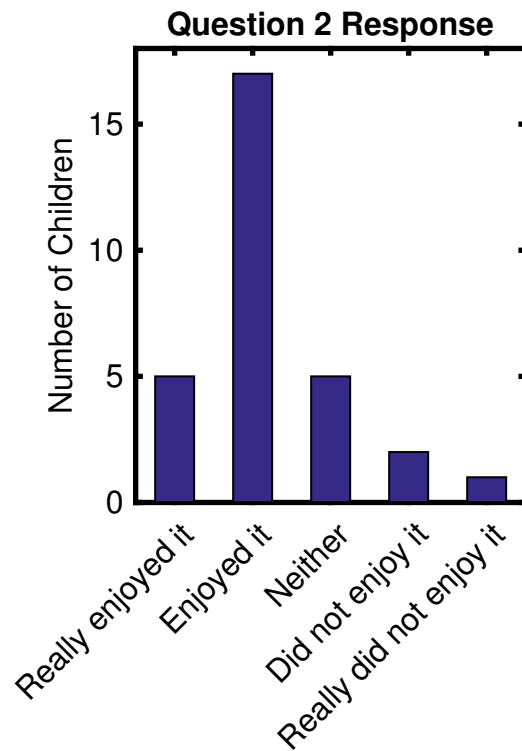


Figure 5.13: Question 2. How much did you enjoy playing Bubble Gulp?

- 1: Really enjoyed it
- 2: Enjoyed it
- 3: Neither
- 4: Did not enjoy it
- 5: Really did not enjoy it

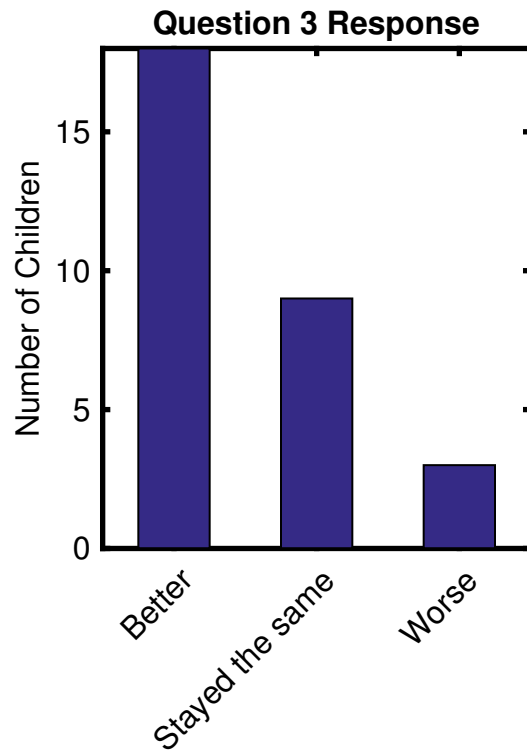


Figure 5.14: Question 3. Did you think you were getting better, stayed the same, or were getting worse as you were playing Bubble Gulp at the end of the study compared to when you first tried it?

- 1: Better
- 2: Stayed the same
- 3: Worse

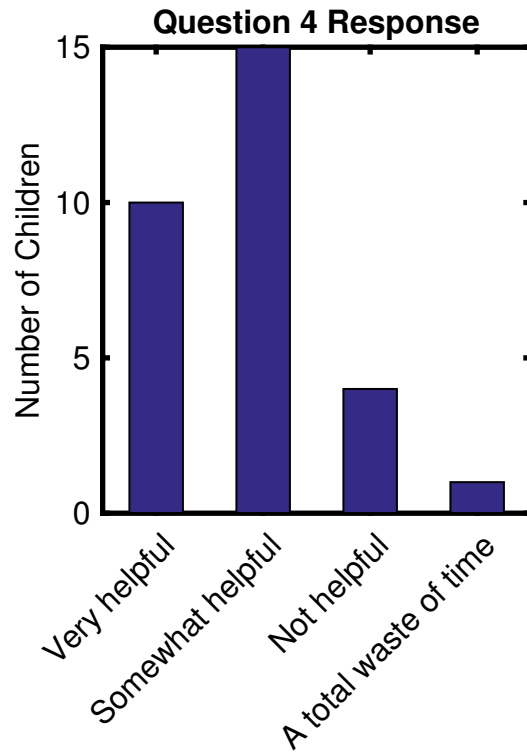


Figure 5.15: Question 4. We have a pretend MRI scanner where you can learn to play Bubble Gulp before getting into the actual MRI scanner. Do you think using this pretend MRI scanner first would have been/was:

- 1: Very helpful
- 2: Somewhat helpful
- 3: Not helpful
- 4: A total waste of time

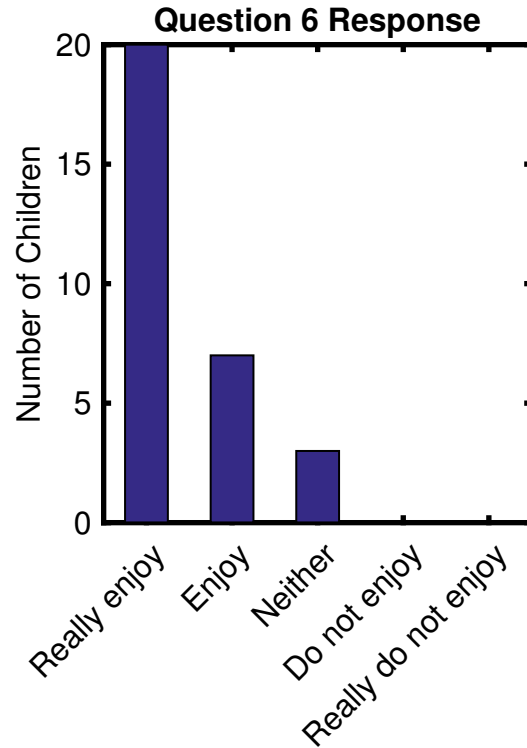


Figure 5.16: Question 6. How much do you enjoy playing videogames?

- 1: Really enjoy
- 2: Enjoy
- 3: Neither
- 4: Do not enjoy
- 5: Really do not enjoy

5. Do you have any comments on how to improve Bubble Gulp?

- Mostly "None"
- "Make the fish pink"
- "Make the lines further a part on the screen"
- "Liked the simple concept and how could control with breathing"
- "Reverse direction of fish movement with breathing"
- "Make not as glitchy, (make smoother)"
- "Make lines move to more comfortable spot to breathe in" (this subject moved)

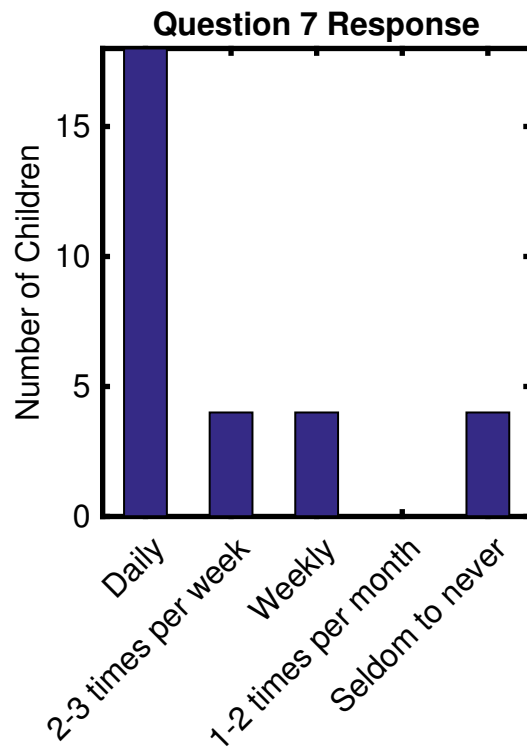


Figure 5.17: Question 7. How often do you play videogames?

- 1: Daily
- 2: 2-3 times per week
- 3: Weekly
- 4: 1-2 times per month
- 5: Seldom to never

5.4 Discussion

Feedback of the diaphragm position during cardiac MR has been shown to improve navigator efficiency in adults [36, 37]. This study explored how the use of a feedback game (FG) affects navigator efficiency compared to traditional no feedback (NF) acquisitions *in children*. The results of the study showed that, compared to NF, using the FG resulted in 1) substantially improved navigator efficiency (from 33 to 58%); 2) slightly improved SNR; 3) slightly higher mean heart rate; and 4) slightly lower global strain magnitudes. Importantly, these results were not affected by using an off-scanner training protocol, which suggests that lengthy, robust training (11 min in our protocol) does not need to be a part of the clinical/imaging workflow to benefit from the use of this interface.

5.4.1 Navigator Efficiency

Navigator efficiency was improved from 33 to 58% by using a FG in children (Figure 5.8a). This increase in navigator efficiency led to a 43% reduction in the number of heartbeats required to complete a scan. Studies have shown that feedback of the diaphragm position during cardiac MR results in a more reproducible breath-hold position [36, 37, 78], which can lead to improved navigator efficiency. Previous cardiac MR studies have reported that NF navigator efficiencies can vary from 20 to 45% in adults [35, 36, 37, 38], and we found a comparable NF navigator efficiency of 33% in children using a conservative dual-navigator acceptance strategy. Visual feedback of the diaphragm position has been shown to improve end-expiratory navigator efficiency from 45 to 56% [37] and from 42 to 71% with the addition of supplemental oxygen [36] leading to a 20% and 41% reduction in the number of required heartbeats, respectively. With the use of the FG, we found a slightly better improvement of navigator efficiency from 33 to 58% in children without the use of supplemental oxygen. Average navigator efficiency was

not correlated with age (Figure 5.8b). Therefore, children ages eight and older should be able to utilize the FG to effectively improve navigator efficiency compared to conventional NF acquisitions.

Off-scanner training using an MRI-simulator was not necessary to achieve the observed improvement in navigator efficiency using the FG. Instead, the subjects with minimal training immediately prior to data acquisition had equivalent efficiency as their extensively-trained counterparts. While this finding might suggest that the chest wall excursion-based training method was ineffective, it is more likely that the intuitive interface design was easy to learn and therefore the children did not require much training. Importantly, the two 30-beat practice scans provided some degree of training in both cases, which is intuitively necessary. Future efforts can optimize that practice time to provide the needed minimal training in the most efficient manner.

5.4.2 SNR

We found that using the FG slightly improved the SNR of the end-systolic magnitude images of our spiral DENSE sequence by 5% compared to NF for all images combined ($p = 0.01$, Figure 5.10). This finding contrasts with previous studies, which reported image quality score using 2 expert reviewers and found that the use of diaphragmatic feedback maintained image quality compared to NF acquisitions [36, 37]. The difference in image quality is likely sequence dependent. The previous studies were performed using steady-state free precession. Additionally, it is likely that quantitative measurement of SNR is more sensitive at detecting small differences in image quality compared to subjective image scoring by expert reviewers.

5.4.3 Heart Rate

A potential negative finding of this study was the slight increase in heart rate observed with the use of the feedback game. To be clear, this difference did not

represent an increase in heart rate variability as evidenced by the comparable standard deviation values but simply a higher baseline value. Such findings are not unprecedented, as a previous cardiac MR study found a mean heart rate increase of 5 beats/min with use of navigator feedback in adults (compared to our 3 beats/min), and similarly no differences in heart rate variability between NF and navigator feedback [36]. A likely reason for this difference is the longer breath-holds performed during the FG, which could have increased the heart rate, compared to relaxed breathing during NF. Another mechanism could be related to stimulation and adrenaline associated with playing the game, compared to the relaxed, passive state associated with NF.

The importance and implications of this potential heart rate difference likely depends on the imaging application. While it may mean very little for purely anatomic evaluations, functional measures, such as strains, may be affected by changing loading conditions and contractility [79]. To counteract such effects, if undesirable, patients could be coached to relax when playing the game and to not be too competitive. The design of the game could be modified to enforce such behavior; for example, by programmatically requiring the participant to inhale/exhale after a fixed period of time, or instructing him/her to periodically take a series of relaxed breaths between cycles of breath-holding.

5.4.4 Strains

We observed small, but statistically significant decreases in global circumferential and radial strains with use of the FG, compared with NF. There was, however, no difference in longitudinal strain. While these findings warrant further study and consideration, the clinical relevance of such small differences (1% for circumferential strain, 4% for radial strain) is likely minimal as they are smaller than previously observed inter-test ($\pm 2.0\%$ for circumferential, $\pm 13\%$ for radial) and inter-observer ($\pm 1.4\%$ for circumferential, $\pm 14\%$ for radial) 95% limits of agreement for DENSE

[58, 10].

5.4.5 Clinical Implications

Importantly, the equipment needed to utilize the FG is minimal and does not directly integrate into an imaging pulse sequence design; it connects externally to the scanner user interface. Due to the minimal equipment needed and non-invasive connection to the MRI scanner, we anticipate that the FG system can be easily adopted at research and clinical sites that perform cardiac MR navigator gating, especially in children. Since navigator efficiency can be increased from 33 to 58%, leading to reduced acquisition times, use of the FG can help improve the clinical feasibility of advanced imaging techniques. While reducing the acquisition time would likely be the most common use of increased navigator efficiency from the FG, the saved time could also be re-allocated to improve image spatial or temporal resolution [36]. Importantly, pre-scan training was not necessary for navigator efficiency improvement with our system, so clinical and research sites would not need to invest in an MRI simulator environment or spend significant time training children. Navigator feedback has been shown to reduce acquisition time in adults [36], thus, the use of the current FG will likely work well in adults also.

Since we only acquired DENSE images for this study, the specific findings are only definitively relevant for DENSE. However, it is reasonable to expect that these findings are generalizable to many other cardiac MR acquisitions that utilize a respiratory navigator. Possible exceptions include higher resolution applications, such as coronary MR angiography, which may be more sensitive to registration issues. Further study is needed to test this technique for these applications.

5.4.6 Comparison with Previous Work

A previous study presented a respiratory biofeedback game and continuously adaptive windowing strategy (CLAWS) to increase navigator efficiency of imaging

the thoracic aorta. The authors reported an increase in efficiency in that study from 45 to 56% in adults [37], which represents a smaller magnitude of improvement (25% vs 11%) but a similar end result (58% vs 56%) compared to our study. Although the two studies are similar, there are distinct differences in design. Most notably, the previous study was in adults; whereas we exclusively focused on children, based on their limited ability to breath-hold and thus potentially greater need for respiratory navigated sequences. Additionally, the previous study modified their pulse sequence to allow acquisition of multiple navigator echoes, likely providing a smoother game experience. We did not modify our cine pulse sequence in our evaluation—we had a single navigator echo per cardiac cycle—to ensure more general clinical applicability. Collectively, these studies demonstrate the potential utility of user-friendly interfaces for improving efficiency and image quality of cardiovascular imaging sequences using a respiratory navigator in a broad array of patients.

5.4.7 Limitations

This study used a dual-navigator strategy when performing image acquisition. Dual-navigator strategies have stricter data acceptance criteria compared to previously used single-navigator strategies [16], and, given the same imaging parameters, will likely result in lower navigator efficiencies. However, a previous study using a single-navigator strategy with navigator feedback reported similar navigator efficiency results compared to our study. Therefore, the use of the FG with a single-navigator strategy will likely have similar results to this study except that both NF and FG acquisitions may have improved navigator efficiency compared to a dual-navigator strategy.

The respiratory navigator gating sequence used in this study only measured the diaphragm position once per cardiac cycle. This low refresh rate can make fine control of the diaphragm position more challenging, especially for participants who may have lower heart rates. Increasing the number of navigator echoes per cardiac cycle could

therefore improve performance, but such modifications may not be possible for all sequences, as is the case for DENSE. Furthermore, even with this limitation, we still found substantial improvement in navigator efficiency when using the FG compared to NF acquisitions.

Due to the randomization of the participants into the trained and untrained groups, there was no attempt to balance age between groups. Therefore, the average trained participant was about 2 years older than the average untrained participant. We found that there was no difference in FG navigator efficiency between trained and untrained participants. Even though there was an age difference between trained and untrained groups, there was no correlation between age and navigator efficiency with the FG (Figure 5.8b); thus, the results of the study apply to all children aged eight to eighteen.

In order to accurately assess the NF navigator efficiency as it would be in the clinical setting, we did not want to influence the children's natural breathing pattern. In particular, we did not want the breathing pattern performed during the FG acquisitions to influence the NF breathing pattern. Therefore, NF acquisitions were always performed before FG acquisitions. Since the order of NF and FG acquisitions was not randomized, this may have affected the results as participants may have become more comfortable as they spent more time in the MRI scanner. However, performing this randomization likely would have resulted in similar conclusions and we felt that it was important to prioritize accurate measurement of the navigator efficiency of the NF acquisitions.

Due to the potential for patient movement or erratic breathing patterns, we utilized a stoppage criterion to attempt to maintain a 30 min protocol length. We observed eleven cases which satisfied stoppage criterion and four cases of patient movement (one which also satisfied stoppage criterion). In these participants, we estimated navigator efficiency, SNR, and heart rate from fewer acquisitions than the

remaining participants. However, since we used all the data that we did acquire for each participant, the computed values are appropriate.

The two 30-heartbeat practice scans were not included in the computation and analysis of navigator efficiency for the FG technique. Their inclusion would only slightly decrease the reported gains in efficiency (for example, if we used the FG to acquire 300 heart beats of actual data, the reduction in scan time would change minimally from 43 to 37% after accounting for the two practice scans); however, it must be noted that the selection of those practice parameters was arbitrary and not optimized. In reality, less training is likely required to familiarize the subject with the interface, so factoring this specific training design into the analysis is not critical.

We performed this study in children without significant past medical history. While we did attempt to recruit from a broad clinical population using recruitment services at our Center for Clinical and Translational Science, the population we ultimately studied may not be entirely representative of a standard pediatric clinical population that would routinely undergo cardiac MRI. For example, approximately 25% of patients with tetralogy of Fallot may have learning and behavioral difficulties [80], which may impair their ability to benefit from the feedback game. It is therefore reasonable to expect that the true benefit of the feedback game in a standard clinical population will be smaller than what was measured in the current study, but still better than what can be expected without the use of feedback. Even if only half of the patients benefit to the extent shown in the current study, the overall navigator efficiency for the clinical population would still increase from 33% efficiency to 46% efficiency (a 38% relative benefit). Future research will seek to evaluate this in further detail as we implement the feedback game during routine clinical workflows.

5.5 Conclusion

Use of a respiratory navigator feedback game designed to engage children during navigator-gated cardiac MRI improved navigator efficiency in children from 33 to 58%. This improved efficiency reduces the number of heartbeats and corresponding scan durations by 43%, and is also associated with a 5% increase in SNR for spiral cine DENSE. Pre-scan training on how to use the feedback game is not necessary to achieve the improvement in navigator efficiency. These findings should generalize to all cardiac MRI acquisitions that utilize a respiratory navigator.

CHAPTER 6

CONCLUSIONS AND FUTURE WORK

6.1 Summary

The overall goal of this project was to optimize respiratory navigator gating to improve the clinical utility of spiral cine DENSE cardiac MRI for the quantification of cardiac mechanics. To accomplish this goal, we completed 3 aims: 1) determined how using a respiratory navigator affects the reproducibility of measures of cardiac mechanics, 2) determined the optimal respiratory navigator gating configuration, and 3) developed and tested an interactive respiratory-controlled videogame to improve navigator efficiency during cardiac MRI.

6.1.1 Aim 1

The purpose of Aim 1 was to understand how using a respiratory navigator during DENSE cardiac MRI can affect the derived cardiac mechanics. Aim 1 was separated into two different studies. In the **first study**, we examined how the measurement of cardiac strain is affected by inconsistent end-expiratory breath-holds and how using a respiratory navigator could reduce differences and variability in strain. Specifically, we wanted to determine if normal inconsistency in end-expiratory diaphragm position between separate image acquisitions significantly affects estimates of cardiac strains. Strain varies longitudinally throughout the heart [25, 26, 27, 28, 29, 30, 31] and patients struggle to hold their breath consistently [20, 21, 22, 23, 24]. Thus, we hypothesized that inconsistent end-expiratory positions during image acquisition affects the quantification of cardiac strains and therefore results in higher variability in measured strain compared to strains measured at a consistent end-expiratory position by using a respiratory navigator.

Analysis was performed in 10 healthy volunteers (Age: 22 ± 6 years, 60%

female) including seven patients with heart disease (Age: 57 ± 8 years, 43% female). To simulate end-expiratory position inconsistency, DENSE images were each acquired at the patient-specific minimum, middle, and maximum end-expiratory positions; a repeated acquisition at the middle position was used to quantify variability independent of end-expiratory differences. The range of end-expiratory positions across 10 breath-holds was 10 ± 4 mm. There were no significant differences in global or regional peak radial, circumferential, or longitudinal strains measured at the different end-expiratory positions ($p = 0.17-0.98$). In general, there were also no differences in variability in global or regional peak strains between inconsistent (minimum, middle, and maximum) and consistent (two acquisitions from middle position) end-expiratory positions ($p = 0.10-0.95$). In summary, Aim 1 Study 1 demonstrated that *measurements of left ventricular peak strains with DENSE cardiac MR are relatively insensitive to normal changes in end-expiratory position between separate image acquisitions*. Importantly, this indicates that using a respiratory navigator to ensure a consistent end-expiratory position is *not* required for acquisitions used to derive cardiac strains.

In the **second study**, we examined how variability in the quantification of left ventricular torsion is affected by using a respiratory navigator. Torsion is computed using a basal and apical image acquired during *separate* end-expiratory breath-holds and the assumption that the distance between the acquired images is precisely known. However, because patients typically struggle to achieve a consistent end-expiratory position for multiple image acquisitions [20, 21, 22, 23, 24], this inconsistency in end-expiratory position could lead to variability in the measurement of torsion. Since torsion has been shown to be limited by high variability [30], we hypothesized that this variability was partly due to inconsistent end-expiratory positions during serial image acquisition, which could be significantly improved by using a respiratory navigator.

We assessed respiratory-related variability in 2 experiments. In experiment 1, 10

healthy volunteers (Age: 22 ± 6 years, 60% female) including seven patients with heart disease (Age: 57 ± 8 years, 43% female) underwent DENSE cardiac MRI to compare inter-test variability between consistent and inconsistent end-expiratory positions due to *enforced* end-expiratory position variability. In experiment 2, twenty new, healthy volunteers (Age: 25 ± 4 years, 60% female) underwent DENSE cardiac MRI to compare inter-test variability between breath-held and navigator-gated acquisitions to assess variability due to *natural* end-expiratory breath-hold position variability. From experiment 1, enforced variability in end-expiratory position translated to considerable variability in measured torsion (0.56 ± 0.34 °/cm), whereas inter-test variability with consistent end-expiratory position was 57% lower (0.24 ± 0.16 °/cm, $p < 0.001$). From the second experiment, natural respiratory variability from consecutive breath-holds translated to a variability in torsion of 0.24 ± 0.10 °/cm, which was significantly higher than the variability from navigator-gated scans (0.18 ± 0.06 °/cm, $p = 0.02$). By using a respiratory navigator with DENSE, theoretical sample sizes to detect a clinically meaningful change in torsion were reduced from 66 to 16 and 26 to 15, by using a respiratory navigator, as calculated from the two experiments. Aim 1 Study 2 demonstrated that *a substantial portion (22-57%) of the inter-test variability of torsion can be reduced by using a respiratory navigator to ensure a consistent breath-hold position between image acquisitions.*

6.1.2 Aim 2

The purpose of Aim 2 was to determine the optimal respiratory navigator gating configuration for the quantification of left ventricular strain using spiral cine DENSE MRI. Two-dimensional spiral cine DENSE was performed using two single-navigator configurations (retrospective, prospective) and a combined dual-navigator configuration in 10 healthy adults (Age: 23 ± 3 years, 40% female) and 20 healthy children (Age: 13 ± 3 years, 45% female). The adults also

underwent breath-hold DENSE as a reference standard for comparisons. Peak left ventricular strains, signal-to-noise ratio (SNR), and navigator efficiency were compared. Subjects also underwent dual-navigator gating with and without visual feedback to determine the effect on navigator efficiency. There were no differences in circumferential, radial, and longitudinal strains between navigator-gated and breath-hold DENSE ($p = 0.09-0.95$). The dual configuration maintained SNR compared with breath-hold acquisitions (16 versus 18, $p = 0.06$). SNR for the prospective configuration was lower than for the dual navigator in adults ($p = 0.004$) and children ($p < 0.001$). Navigator efficiency was higher ($p < 0.001$) for both retrospective (54%) and prospective (56%) configurations compared with the dual configuration (35%). Visual feedback improved the dual configuration navigator efficiency to 55% ($p < 0.001$). Aim 2 demonstrated when quantifying left ventricular strains using spiral cine DENSE MRI, *1) a dual navigator configuration results in the highest SNR in adults and children, 2) in adults, a retrospective configuration has good navigator efficiency without a substantial drop in SNR, 3) prospective gating should be avoided because it has the lowest SNR, and 4) visual feedback represents an effective option to maintain navigator efficiency while using a dual navigator configuration.*

6.1.3 Aim 3

The purpose of Aim 3 was to develop and test an interactive videogame designed to improve navigator efficiency in children undergoing DENSE cardiac MRI. Advanced cardiac MRI acquisitions often require long scan durations that necessitate respiratory navigator gating. The tradeoff of navigator gating is reduced scan efficiency, particularly when the patient's breathing patterns are inconsistent, as is commonly seen in children. We hypothesized that engaging pediatric participants with a navigator-controlled videogame to help control breathing patterns would improve navigator efficiency and maintain image quality. We

developed custom software that processed the Siemens respiratory navigator image in real-time during CMR and represented diaphragm position using a cartoon avatar, which was projected to the participant in the scanner as visual feedback. The game incentivized children to breathe such that the avatar was positioned within the navigator acceptance window (± 3 mm) throughout image acquisition. Fifty children (Age: 14 ± 3 years, 48% female) without significant past medical history underwent a respiratory navigator-gated 2D spiral cine DENSE cardiac MRI acquisition first without feedback and then with the feedback videogame. Thirty of the 50 children were randomized to undergo off-scanner training with the videogame using a MRI simulator, or no off-scanner training. Navigator efficiency, SNR, and global left-ventricular strains were determined for each participant and compared. Using the videogame improved average navigator efficiency from 33 ± 15 to $58 \pm 13\%$ ($p < 0.001$) and improved SNR by 5% ($p = 0.01$) compared to acquisitions without feedback. There was no difference in navigator efficiency ($p = 0.90$) or SNR ($p = 0.77$) between untrained and trained participants for videogame acquisitions. Circumferential and radial strains derived from videogame acquisitions were slightly reduced compared to no feedback acquisitions ($16 \pm 2\%$ vs $17 \pm 2\%$, $p < 0.001$; $40 \pm 10\%$ vs $44 \pm 11\%$, $p = 0.005$, respectively). There were no differences in longitudinal strain ($p = 0.38$). Aim 3 demonstrated that *use of a respiratory navigator feedback videogame during navigator-gated CMR improved navigator efficiency in children from 33 to 58%. This improved efficiency was associated with a 5% increase in SNR for spiral cine DENSE. Off-scanner training was not required to achieve the improvement in navigator efficiency.*

6.2 Clinical Implications

The goal of this project was to optimize respiratory navigator gating for use during DENSE cardiac MRI. From Aim 1 Study 1, it was demonstrated that the quantification of peak left ventricular cardiac strains was relatively insensitive to

normal variations in end-expiratory positions between image acquisitions. In the clinical setting, since there were no differences in peak strain between end-expiratory positions, patient end-expiratory diaphragm position does not have to be monitored when performing breath-hold DENSE acquisition for single image analyses. These findings should generalize to other image acquisitions that are used to derive measures of cardiac strains.

However, Aim 1 Study 2 demonstrated that using a respiratory navigator significantly improves the variability of measured left ventricular torsion. Thus, where possible, a respiratory navigator should be employed for acquisition of left ventricular torsion data to minimize variability. For torsion, if inconsistency in end-expiratory position is not taken care of during scans, then it is important to understand its effects, which will lead to dramatically increased study sample sizes for research and reduce the ability to detect meaningful differences in torsion in individual patients.

From Aim 2, the dual-navigator configuration has been shown to result in the best image quality in both adults and children. It is important to understand the limitations of the dual-navigator before employing it in clinical practice, however, due to its worse navigator efficiency compared to other navigator configurations. Therefore, some form of visual feedback (of the diaphragm position) should be used, where possible, to achieve an adequate scan duration along with the improved image quality.

From Aim 3, it was demonstrated that using an interactive feedback videogame during DENSE cardiac MRI substantially improved navigator efficiency. Importantly, 1) minimal equipment is needed to implement the videogame and 2) the equipment does not directly integrate into an imaging sequence; it connects externally to the scanner user interface. Thus, the videogame can easily be adopted at research and clinical sites that utilize navigator-gated cardiac MRI acquisitions,

especially in children. Since using the videogame results in improved navigator efficiency, which lead to reduced acquisition times, use of the videogame can help improve the clinical feasibility of advanced imaging techniques, such as DENSE. Besides reducing acquisition time, which saves time, increased navigator efficiency can also be used to acquire more data, such as to improve spatial or temporal resolution of images [36].

Notably, off-scanner training was not required to achieve the improved navigator efficiency by using the videogame. Therefore, clinical and research sites would not have to invest in resources for building a simulator or spend significant time training children prior to undergoing navigator-gated cardiac MRI acquisitions. This study was performed only in children, but since previous studies have shown that navigator feedback can improve navigator efficiency in adults [36, 20], the videogame should also work well in adults. The findings of this study are definitely applicable to cardiac DENSE MRI, but it is likely that these findings generalize to several cardiac MRI techniques that use a respiratory navigator. Higher resolution imaging, which may be more sensitive to registration issues, may not result in the same findings. An example would be coronary MR angiography.

6.3 Future Directions

A future direction of the feedback videogame would be to set up the videogame at other research sites, particularly sites that have a high throughput of patients who undergo cardiac MRI acquisitions. Due to its non-invasive connection to the scanner, the videogame can be easily adopted. Recently, the videogame has been implemented on a different MRI acquisition platform (Philips) at Boston Children’s Hospital to test its efficacy in a patient population. Instead of capturing a navigator image and processing it to extract the desired locations, this Philips acquisition platform had a continuously updating text file containing the required locations (acceptance window and diaphragm position). Due to the modular nature of the code, all that was needed

was to write a new input source class that accepted an updating log file instead of a navigator image. If new features are needed in order to adapt the videogame to a different scanner or for patients to better understand or benefit from the videogame, they can be easily added.

Currently, the videogame is written using MATLAB, which requires the purchase of a license. Another possible future direction would be to re-design the videogame using free programming software so that it can be more freely distributed and won't be limiting to people who do not have the MATLAB software license.

Lastly, it would be beneficial to eventually incorporate the videogame as a viewing option within the scanner software itself. This would make the videogame even more adoptable at clinical and research sites. Collaborations with MRI vendors such as Siemens or Philips would be required to achieve this goal, and are currently being investigated.

This project focused on improving respiratory navigator gating for DENSE cardiac MRI. However, there are other respiratory compensation techniques that may be beneficial to improving the clinical utility of DENSE. For example, automated respiratory gating. One technique involves continuously adjusting the navigator acceptance window in order to always have it placed at the optimal position. This is required because patient end-expiratory positions tend to drift over time, so the acceptance window, which is typically placed at a particular location prior to the scan, will not remain in the optimal position for the entirety of the scan. This is especially true for long scans, such as three-dimensional DENSE cardiac MRI which can take upwards of 20 minutes. Fortunately, the continuously updating position of the acceptance window will help improve navigator efficiency compared to a fixed acceptance window.

Another alternative technique for respiratory compensation uses the acquired image data itself to identify adjustments needed to compensate for respiratory

motion. For example, instead of acquiring a separate image to track the diaphragm, the heart image data itself is used to follow the respiratory-related motion of the heart [81]. This technique allows for complete "free-breathing", which is essentially leads to 100% navigator efficiency. Importantly, at least for coronary MR angiography, a previous study showed that this technique led to comparable image data while reducing scan times by about half (14 to 7 minutes) [81].

Using this same concept, along with sparse undersampling and "smart" image reconstruction, there are other techniques that could be used with DENSE to improve clinical utility. Typically, DENSE is acquired by a spiral sampling pattern in frequency space and then, after other processing steps, is inverse Fourier transformed into image space. For spiral cine DENSE in this project, an adequate number of samples were acquired for accurate, non-blurry images. However, by randomly undersampling k-space (or frequency space) and using smart iterative image reconstruction techniques, image acquisition time can be dramatically reduced and still lead to accurate strain and displacement values [82]. As a tradeoff, the time saved during image reconstruction is spent multi-times over on the image reconstruction side due to its iterative nature. For example, a full 3D acquisition may take a few minutes to acquire (undersampled, of course), but may take days to reconstruct depending on the cost function used to converge to a solution.

Another technique that can be used to reduce data acquisition is the use of outer volume suppression or zonal excitation. Typically, with DENSE, the entire heart is encoded before reading out image data. However, with zonal excitation, DENSE acquisitions are performed by selectively exciting a volume of tissue around the heart, which allows for fewer spiral interleaves to be acquired and shorter acquisitions [83]. Overall, these new techniques will need to be tested for their robustness and reproducibility to ensure research and clinical utility.

Bibliography

- [1] CDC. “Underlying Cause of Death 1999-2013 on CDC WONDER Online Database.”, 2015.
- [2] Rosamond W, Flegal K, Friday G, Furie K, Go A, Greenlund K, Haase N, Ho M, Howard V, Kissela B, Kittner S, Lloyd-Jones D, McDermott M, Meigs J, Moy C, Nichol G, O’Donnell CJ, Roger V, Rumsfeld J, Sorlie P, Steinberger J, Thom T, Wasserthiel-Smoller S, Hong Y, American Heart Association Statistics C, and Stroke Statistics S. “Heart disease and stroke statistics–2007 update: a report from the American Heart Association Statistics Committee and Stroke Statistics Subcommittee.” *Circulation*, 2007. **115**(5):e69–171. doi:10.1161/CIRCULATIONAHA.106.179918.
- [3] Stanton T, Leano R, and Marwick TH. “Prediction of all-cause mortality from global longitudinal speckle strain: comparison with ejection fraction and wall motion scoring.” *Circulation Cardiovascular imaging*, 2009. **2**(5):356–64. ISSN 1942-0080. doi:10.1161/CIRCIMAGING.109.862334.
- [4] Götte MJW, Germans T, Rüssel IK, Zwanenburg JJM, Marcus JT, van Rossum AC, and van Veldhuisen DJ. “Myocardial Strain and Torsion Quantified by Cardiovascular Magnetic Resonance Tissue Tagging. Studies in Normal and Impaired Left Ventricular Function.” *Journal of the American College of Cardiology*, 2006. **48**(10):2002–2011. ISSN 07351097. doi:10.1016/j.jacc.2006.07.048.
- [5] Amundsen BH, Helle-Valle T, Edvardsen T, Torp H, Crosby J, Lyseggen E, Støylen A, Ihlen H, Lima J, Smiseth Oa, and Slørdahl Sa. “Noninvasive Myocardial Strain Measurement by Speckle Tracking Echocardiography.” *Journal of the American College of Cardiology*, 2006. **47**(4):789–793. ISSN 07351097. doi:10.1016/j.jacc.2005.10.040.
- [6] Kowallick JT, Lamata P, Hussain ST, Kutty S, Steinmetz M, Sohns JM, Fasshauer M, Staab W, Unterberg-Buchwald C, Bigalke B, Lotz J, Hasenfuß G, and Schuster A. “Quantification of left ventricular torsion and diastolic recoil using cardiovascular magnetic resonance myocardial feature tracking.” *PloS one*, 2014. **9**(10):e109164. ISSN 1932-6203. doi:10.1371/journal.pone.0109164.
- [7] Kowallick JT, Morton G, Lamata P, Jogiya R, Kutty S, Lotz J, Hasenfuß G, Nagel E, Chiribiri A, and Schuster A. “Inter-study reproducibility of left ventricular torsion and torsion rate quantification using MR myocardial feature tracking.” *Journal of magnetic resonance imaging : JMRI*, 2016. **43**:128–137. ISSN 1522-2586. doi:10.1002/jmri.24979.
- [8] Aletras AH, Ding S, Balaban RS, and Wen H. “DENSE: displacement encoding with stimulated echoes in cardiac functional MRI.” *J Magn Reson*, 1999. **137**(1):247–252. doi:10.1006/jmre.1998.1676.

- [9] Haggerty CM, Kramer SP, Binkley CM, Powell DK, Mattingly AC, Charnigo R, Epstein FH, and Fornwalt BK. “Reproducibility of cine displacement encoding with stimulated echoes (DENSE) cardiovascular magnetic resonance for measuring left ventricular strains, torsion, and synchrony in mice.” *Journal of cardiovascular magnetic resonance : official journal of the Society for Cardiovascular Magnetic Resonance*, 2013. **15**(1):71. ISSN 1532-429X. doi:10.1186/1532-429X-15-71.
- [10] Wehner GJ, Grabau JD, Suever JD, Haggerty CM, Jing L, Powell DK, Hamlet SM, Vandsburger MH, Zhong X, and Fornwalt BK. “2D cine DENSE with low encoding frequencies accurately quantifies cardiac mechanics with improved image characteristics.” *Journal of cardiovascular magnetic resonance : official journal of the Society for Cardiovascular Magnetic Resonance*, 2015. **17**(1):93. ISSN 1532-429X. doi:10.1186/s12968-015-0196-z.
- [11] Aletras AH, Balaban RS, and Wen H. “High-resolution strain analysis of the human heart with fast-DENSE.” *Journal of magnetic resonance (San Diego, Calif : 1997)*, 1999. **140**(1):41–57. ISSN 1090-7807. doi:10.1006/jmre.1999.1821.
- [12] Kim D, Gilson WD, Kramer CM, and Epstein FH. “Myocardial tissue tracking with two-dimensional cine displacement-encoded MR imaging: development and initial evaluation.” *Radiology*, 2004. **230**(3):862–871. doi:10.1148/radiol.2303021213.
- [13] Ernande L, Thibault H, Bergerot C, Moulin P, Wen H, Derumeaux G, and Croisille P. “Systolic Myocardial Dysfunction in Patients with Type 2 Diabetes Mellitus : Identification at MR Imaging with Cine Displacement.” *Radiology*, 2012. **265**(2):402–409. doi:10.1148/radiol.12112571/-/DC1.
- [14] Axel L, Summers RM, Kressel HY, and Charles C. “Respiratory effects in two-dimensional Fourier transform MR imaging.” *Radiology*, 1986. **160**(3):795–801. doi:10.1148/radiology.160.3.3737920.
- [15] Zhong X, Spottiswoode BS, Cowart Ea, Gilson WD, and Epstein FH. “Selective suppression of artifact-generating echoes in cine DENSE using through-plane dephasing.” *Magnetic resonance in medicine : official journal of the Society of Magnetic Resonance in Medicine / Society of Magnetic Resonance in Medicine*, 2006. **56**(5):1126–31. ISSN 0740-3194. doi:10.1002/mrm.21058.
- [16] Zhong X, Spottiswoode BS, Meyer CH, Kramer CM, and Epstein FH. “Imaging three-dimensional myocardial mechanics using navigator-gated volumetric spiral cine DENSE MRI.” *Magn Reson Med*, 2010. **64**(4):1089–1097. doi:10.1002/mrm.22503.
- [17] Aletras AH, Ingkanisorn WP, Mancini C, and Arai AE. “DENSE with SENSE.” *Journal of magnetic resonance (San Diego, Calif : 1997)*, 2005. **176**(1):99–106. ISSN 1090-7807. doi:10.1016/j.jmr.2005.05.010.

- [18] Spottiswoode BS, Zhong X, Hess aT, Kramer CM, Meintjes EM, Mayosi BM, and Epstein FH. “Tracking myocardial motion from cine DENSE images using spatiotemporal phase unwrapping and temporal fitting.” *IEEE transactions on medical imaging*, 2007. **26**(1):15–30. ISSN 0278-0062. doi:10.1109/TMI.2006.884215.
- [19] Young Aa, Li B, Kirton RS, and Cowan BR. “Generalized spatiotemporal myocardial strain analysis for DENSE and SPAMM imaging.” *Magnetic resonance in medicine*, 2012. **67**(6):1590–9. ISSN 1522-2594. doi:10.1002/mrm.23142.
- [20] Liu YL, Riederer SJ, Rossman PJ, Grimm RC, Debbins JP, and Ehman RL. “A Monitoring, Feedback, and Triggering System for Reproducible Breath-Hold MR Imaging.” *Magnetic Resonance in Medicine*, 1993. **30**:507–511.
- [21] Wang Y, Christy PS, Korosec FR, Alley MT, Grist TM, Polzin JA, and Mistretta CA. “Coronary MRI with a Respiratory Feedback Monitor: The 2D Imaging Case.” *Magnetic Resonance in Medicine*, 1995. **33**:116–121.
- [22] Taylor aM, Jhooti P, Wiesmann F, Keegan J, Firmin DN, and Pennell DJ. “MR navigator-echo monitoring of temporal changes in diaphragm position: implications for MR coronary angiography.” *Journal of magnetic resonance imaging : JMRI*, 1997. **7**(4):629–36. ISSN 1053-1807.
- [23] Holland AE, Goldfarb JW, and Edelman RR. “Diaphragmatic and Cardiac Motion during Suspended Breathing: Preliminary Experience and Implications for Breath-hold MR Imaging.” *Radiology*, 1998. **209**(2):483–489.
- [24] Fischer RW, Botnar RM, Nehrke K, Boesiger P, Manning WJ, and Peters DC. “Analysis of residual coronary artery motion for breath hold and navigator approaches using real-time coronary MRI.” *Magnetic resonance in medicine : official journal of the Society of Magnetic Resonance in Medicine / Society of Magnetic Resonance in Medicine*, 2006. **55**(3):612–8. ISSN 0740-3194. doi:10.1002/mrm.20809.
- [25] Kuijjer JPa, Marcus JT, Götte MJW, van Rossum AC, and Heethaar RM. “Three-dimensional myocardial strains at end-systole and during diastole in the left ventricle of normal humans.” *Journal of cardiovascular magnetic resonance : official journal of the Society for Cardiovascular Magnetic Resonance*, 2002. **4**(3):341–351. ISSN 1097-6647. doi:Doi10.1081/Jcmr-120013299.
- [26] Moore C, Lugo-Olivieri C, McVeigh E, and Zerhouni E. “Three-dimensional systolic strain patterns in the normal human left ventricle: characterization with tagged MR imaging.” *Radiology*, 2000. **214**(2):453–466. ISSN 0033-8419. doi:10.1148/radiology.214.2.r00fe17453.

- [27] Young aa, Kramer CM, Ferrari Va, Axel L, and Reichek N. “Three-dimensional left ventricular deformation in hypertrophic cardiomyopathy.” *Circulation*, 1994. **90**(2):854–867. ISSN 0009-7322. doi:10.1161/01.CIR.90.2.854.
- [28] Feng L, Donnino R, Babb J, Axel L, and Kim D. “Numerical and in vivo validation of fast cine displacement-encoded with stimulated echoes (DENSE) MRI for quantification of regional cardiac function.” *Magnetic resonance in medicine*, 2009. **62**(3):682–90. ISSN 1522-2594. doi:10.1002/mrm.22045.
- [29] Nasiraei Moghaddam A, Saber NR, Wen H, Finn JP, Ennis DB, and Gharib M. “Analytical method to measure three-dimensional strain patterns in the left ventricle from single slice displacement data.” *Journal of cardiovascular magnetic resonance : official journal of the Society for Cardiovascular Magnetic Resonance*, 2010. **12**:33. ISSN 1532-429X. doi:10.1186/1532-429X-12-33.
- [30] Donekal S, Ambale-Venkatesh B, Berkowitz S, Wu CO, Choi EY, Fernandes V, Yan R, Harouni Aa, Bluemke Da, and Lima Ja. “Inter-study reproducibility of cardiovascular magnetic resonance tagging.” *Journal of cardiovascular magnetic resonance : official journal of the Society for Cardiovascular Magnetic Resonance*, 2013. **15**(1):37. ISSN 1532-429X. doi:10.1186/1532-429X-15-37.
- [31] Suever J, Wehner G, Jing L, Powell D, Hamlet S, Grabau J, Mojsejenko D, Andres K, Haggerty C, and Fornwalt B. “Right Ventricular Strain, Torsion, and Dyssynchrony in Healthy Subjects using 3D Spiral Cine DENSE Magnetic Resonance Imaging.” *IEEE Transactions on Medical Imaging*, 2017. 1–1. ISSN 0278-0062. doi:10.1109/TMI.2016.2646321.
- [32] Wehner GJ, Suever JD, Haggerty CM, Jing L, Powell D, Zhong X, Epstein FH, and Fornwalt BK. “High resolution cine displacement encoding with stimulated echoes (DENSE) at 3T with navigator feedback for quantification of cardiac mechanics.” *Journal of Cardiovascular Magnetic Resonance*, 2014. **16**(Suppl 1):P48. ISSN 1532-429X. doi:10.1186/1532-429X-16-S1-P48.
- [33] Kar J, Knutsen AK, Cupps BP, Zhong X, and Pasque MK. “Three-dimensional regional strain computation method with displacement encoding with stimulated echoes (DENSE) in non-ischemic, non-valvular dilated cardiomyopathy patients and healthy subjects validated by tagged MRI.” *Journal of magnetic resonance imaging : JMRI*, 2014. **00**:1–11. ISSN 1522-2586. doi:10.1002/jmri.24576.
- [34] Auger DA, Zhong X, Epstein FH, and Spottiswoode BS. “Mapping right ventricular myocardial mechanics using 3D cine DENSE cardiovascular magnetic resonance.” *J Cardiovasc Magn Reson*, 2012. **14**:4. doi:10.1186/1532-429X-14-4.
- [35] Abd-Elmoniem KZ, Obele CC, Sibley CT, Matta JR, Pettigrew RI, and Gharib AM. “Free-breathing single navigator gated cine cardiac magnetic resonance at 3 T: feasibility study in patients.” *J Comput Assist Tomogr*, 2011. **35**(3):382–386. doi:10.1097/RCT.0b013e31821b0ade.

- [36] Feuerlein S, Klass O, Pasquarelli A, Brambs HJ, Wunderlich A, Duerk JL, Aschoff AJ, and Hoffmann MHK. “Coronary MR Imaging: Navigator Echo Biofeedback Increases Navigator Efficiency-Initial Experience.” *Acad Radiol*, 2009. **16**(3):374–379. doi:DOI10.1016/j.acra.2008.08.015.
- [37] Jhooti P, Haas T, Kawel N, Bremerich J, Keegan J, and Scheffler K. “Use of respiratory biofeedback and CLAWS for increased navigator efficiency for imaging the thoracic aorta.” *Magn Reson Med*, 2011. **66**(6):1666–1673. doi:10.1002/mrm.22945.
- [38] Wang Y, Rossman PJ, Grimm Rc, Riederer SJ, and Ehman RL. “Navigator-Echo-based Real-Time Respiratory Gating and Triggering for Reduction of Respiration Effects in Three-dimensional Coronary MR Angiography.” *Radiology*, 1996. **198**:55–60.
- [39] Hor KN, Gottliebson WM, Carson C, Wash E, Cnota J, Fleck R, Wansapura J, Klimeczek P, Al-Khalidi HR, Chung ES, Benson DW, and Mazur W. “Comparison of Magnetic Resonance Feature Tracking for Strain Calculation With Harmonic Phase Imaging Analysis.” *JACC: Cardiovascular Imaging*, 2010. **3**(2):144–151. ISSN 1936878X. doi:10.1016/j.jcmg.2009.11.006.
- [40] Axel L and Dougherty L. “MR imaging of motion with spatial modulation of magnetization.” *Radiology*, 1989. **171**(3):841–845. ISSN 0033-8419. doi:10.1148/radiology.171.3.2717762.
- [41] Zerhouni EA, Parish DM, Rogers WJ, Yang A, and Shapiro EP. “Human heart: tagging with MR imaging—a method for noninvasive assessment of myocardial motion.” *Radiology*, 1988. **169**(1):59–63. ISSN 0033-8419. doi:10.1148/radiology.169.1.3420283.
- [42] Pelc LR, Sayre J, Yun K, Castro LJ, Herfkens RJ, Miller DC, and Pelc NJ. “Evaluation of myocardial motion tracking with cine-phase contrast magnetic resonance imaging.” *Investigative radiology*, 1994. **29**(12):1038–1042. ISSN 0020-9996. doi:10.1097/00004424-199412000-00005.
- [43] Osman NF, Sampath S, Atalar E, and Prince JL. “Imaging longitudinal cardiac strain on short-axis images using strain-encoded MRI.” *Magnetic Resonance in Medicine*, 2001. **46**(2):324–334. ISSN 07403194. doi:10.1002/mrm.1195.
- [44] Slomka PJ, Fieno D, Ramesh A, Goyal V, Nishina H, Thompson LE, Saouaf R, Berman DS, and Germano G. “Patient motion correction for multiplanar, multi-breath-hold cardiac cine MR imaging.” *J Magn Reson Imaging*, 2007. **25**(5):965–973. doi:10.1002/jmri.20909.
- [45] Swingen C, Seethamraju RT, and Jerosch-Herold M. “An approach to the three-dimensional display of left ventricular function and viability using MRI.” *Int J Cardiovasc Imaging*, 2003. **19**(4):325–336.

- [46] Wang Y, Riederer SJ, and Ehman RL. “Respiratory Motion of the Heart: Kinematics and the Implications for the Spatial Resolution in Coronary Imaging.” *Magnetic Resonance in Medicine*, 1995. **33**:713–719.
- [47] McLeish K, Hill DLG, Atkinson D, Blackall JM, and Razavi R. “A study of the motion and deformation of the heart due to respiration.” *Medical Imaging, IEEE Transactions on*, 2002. **21**(9):1142–1150. doi:10.1109/tmi.2002.804427.
- [48] Hamlet SM, Haggerty CM, Suever JD, Wehner GJ, Grabau JD, Andres KN, Vandsburger MH, Powell DK, Sorrell VL, and Fornwalt BK. “An interactive videogame designed to improve respiratory navigator efficiency in children undergoing cardiac magnetic resonance.” *Journal of Cardiovascular Magnetic Resonance*, 2016. **18**(1):54. ISSN 1532-429X. doi:10.1186/s12968-016-0272-z.
- [49] Hamlet SM, Haggerty CM, Suever JD, Wehner GJ, Andres KN, Powell DK, Zhong X, and Fornwalt BK. “Optimal configuration of respiratory navigator gating for the quantification of left ventricular strain using spiral cine displacement encoding with stimulated echoes (DENSE) MRI.” *Journal of magnetic resonance imaging : JMRI*, 2016. ISSN 1522-2586. doi:10.1002/jmri.25389.
- [50] Gilliam AD and Suever JD. “DENSEanalysis.”, 2016.
- [51] Suever JD, Wehner GJ, Haggerty CM, Jing L, Hamlet SM, Binkley CM, Kramer SP, Mattingly AC, Powell DK, Bilchick KC, Epstein FH, and Fornwalt BK. “Simplified post processing of cine DENSE cardiovascular magnetic resonance for quantification of cardiac mechanics.” *Journal of cardiovascular magnetic resonance : official journal of the Society for Cardiovascular Magnetic Resonance*, 2014. **16**:94. ISSN 1532-429X. doi:10.1186/s12968-014-0094-9.
- [52] Dytham C. *Choosing and Using Statistics: A Biologist’s Guide, 3rd Edition*. 3rd edition, 2011.
- [53] Bland J and Altman D. “Statistical methods for assessing agreement between two methods of clinical measurement.” *Lancet*, 1986. **1**:307–310.
- [54] Hamlet SM, Haggerty CM, Suever JD, Wehner GJ, Andres KN, Powell DK, Charnigo RJ, and Fornwalt BK. “Using a respiratory navigator significantly reduces variability when quantifying left ventricular torsion with cardiovascular magnetic resonance.” *Journal of Cardiovascular Magnetic Resonance*, 2017. **19**(1):25. ISSN 1532-429X. doi:10.1186/s12968-017-0338-6.
- [55] Pahlm US, Ubachs JFA, Heiberg E, Engblom H, Erlinge D, Götberg M, and Arheden H. “Regional wall function before and after acute myocardial infarction; an experimental study in pigs.” *BMC Cardiovascular Disorders*, 2014. **14**(1):1–10. ISSN 1471-2261.

- [56] Rüssel IK, Götte MJW, Bronzwaer JG, Knaapen P, Walter J, and Rossum ACV. “Left Ventricular Torsion.” *JACC: Cardiovascular Imaging*, 2011. **2**(5):648–655. ISSN 1936-878X. doi:10.1016/j.jcmg.2009.03.001.
- [57] Kaku K, Takeuchi M, Tsang W, Takigiku K, Yasukochi S, Patel AR, Mor-Avi V, Lang RM, and Otsuji Y. “Age-related normal range of left ventricular strain and torsion using three-dimensional speckle-tracking echocardiography.” *Journal of the American Society of Echocardiography*, 2014. **27**(1):55–64. ISSN 10976795. doi:10.1016/j.echo.2013.10.002.
- [58] Wehner GJ, Suever JD, Haggerty CM, Jing L, Powell DK, Hamlet SM, Grabau JD, Mojsejenko WD, Zhong X, Epstein FH, and Fornwalt BK. “Validation of in vivo 2D displacements from spiral cine DENSE at 3T.” *Journal of Cardiovascular Magnetic Resonance*, 2015. **17**(1):1–11. ISSN 1532-429X. doi:10.1186/s12968-015-0119-z.
- [59] Phan TT, Shivu GN, Abozguia K, Gnanadevan M, Ahmed I, and Frenneaux M. “Left ventricular torsion and strain patterns in heart failure with normal ejection fraction are similar to age-related changes.” *European Journal of Echocardiography*, 2009. **10**(6):793–800. ISSN 1532-2114. doi:10.1093/ejehocard/jep072.
- [60] Sorger JM, Wyman BT, Faris OP, Hunter WC, and McVeigh ER. “Torsion of the left ventricle during pacing with MRI tagging.” *J Cardiovasc Magn Reson*, 2003. **5**(4):521–530.
- [61] Grothues F, Smith GC, Moon JCC, Bellenger NG, Collins P, Klein HU, and Pennell DJ. “Comparison of interstudy reproducibility of cardiovascular magnetic resonance with two-dimensional echocardiography in normal subjects and in patients with heart failure or left ventricular hypertrophy.” *Am J Cardiol*, 2002. **90**(1):29–34. ISSN 0002-9149. doi:http://dx.doi.org/10.1016/S0002-9149(02)02381-0.
- [62] Broussard JL, Nelson MD, Kolka CM, Bediako IA, Paszkiewicz RL, Smith L, Szczepaniak EW, Stefanovski D, Szczepaniak LS, and Bergman RN. “Rapid development of cardiac dysfunction in a canine model of insulin resistance and moderate obesity.” *Diabetologia*, 2016. **59**(1):197–207. ISSN 0012-186X. doi:10.1007/s00125-015-3767-5.
- [63] Kramer SP, Powell DK, Haggerty CM, Binkley CM, Mattingly AC, Cassis La, Epstein FH, and Fornwalt BK. “Obesity reduces left ventricular strains, torsion, and synchrony in mouse models: a cine displacement encoding with stimulated echoes (DENSE) cardiovascular magnetic resonance study.” *Journal of cardiovascular magnetic resonance : official journal of the Society for Cardiovascular Magnetic Resonance*, 2013. **15**:109. ISSN 1532-429X. doi:10.1186/1532-429X-15-109.

- [64] Oxenham HC, Young AA, Cowan BR, Gentles TL, Occleshaw CJ, Fonseca CG, Doughty RN, and Sharpe N. “Age-Related Changes in Myocardial Relaxation Using Three-Dimensional Tagged Magnetic Resonance Imaging.” *Journal of Cardiovascular Magnetic Resonance*, 2003. **5**(3):421–430. ISSN 10976647. doi:10.1081/JCMR-120022258.
- [65] Setser RM, Kasper JM, Lieber ML, Starling RC, McCarthy PM, and White RD. “Persistent abnormal left ventricular systolic torsion in dilated cardiomyopathy after partial left ventriculectomy.” *Journal of Thoracic and Cardiovascular Surgery*, 2003. **126**(July):48–55. ISSN 00225223. doi:10.1016/S0022-5223(03)00050-3.
- [66] Garot J, Pascal O, Diébold B, Derumeaux G, Gerber BL, Dubois-Randé JL, Lima JaC, and Guéret P. “Alterations of systolic left ventricular twist after acute myocardial infarction.” *American journal of physiology Heart and circulatory physiology*, 2002. **282**(1):H357–H362. ISSN 0363-6135. doi:10.1152/ajpheart.00136.2001.
- [67] Reyhan ML, Wang Z, Kim HJ, Halnon NJ, Finn JP, and Ennis DB. “Effect of free-breathing on left ventricular rotational mechanics in healthy subjects and patients with duchenne muscular dystrophy.” *Magnetic resonance in medicine*, 2017. **77**(2):864–869. ISSN 1522-2594. doi:10.1002/mrm.26137.
- [68] Stuber M, Spiegel MA, Fischer SE, Scheidegger MB, Danias PG, Pedersen EM, and Boesiger P. “Single breath-hold slice-following CSPAMM myocardial tagging.” *MAGMA*, 1999. **9**(1-2):85–91.
- [69] Swoboda PP, Larghat A, Zaman A, Fairbairn TA, Motwani M, Greenwood JP, and Plein S. “Reproducibility of myocardial strain and left ventricular twist measured using complementary spatial modulation of magnetization.” *Journal of magnetic resonance imaging : JMRI*, 2014. **39**(4):887–94. ISSN 15222586. doi:10.1002/jmri.24223.
- [70] Moody WE, Taylor RJ, Edwards NC, Chue CD, Umar F, Taylor TJ, Ferro CJ, Young AA, Townend JN, Leyva F, and Steeds RP. “Comparison of magnetic resonance feature tracking for systolic and diastolic strain and strain rate calculation with spatial modulation of magnetization imaging analysis.” *Journal of magnetic resonance imaging : JMRI*, 2015. **41**(4):1000–1012. ISSN 1522-2586 (Electronic). doi:10.1002/jmri.24623.
- [71] Sigfridsson A, Haraldsson H, Ebberts T, Knutsson H, and Sakuma H. “In vivo SNR in DENSE MRI; temporal and regional effects of field strength, receiver coil sensitivity and flip angle strategies.” *Magnetic resonance imaging*, 2011. **29**(2):202–8. ISSN 1873-5894. doi:10.1016/j.j.mri.2010.08.016.
- [72] Gudbjartsson H and Patz S. “The Rician Distribution of Noisy MRI Data.” *Magn Reson Med*, 1995. **34**(6):910–914. ISSN 15378276. doi:10.1016/j.biotechadv.2011.08.021.Secreted.

- [73] Peters DC, Nezafat R, Eggers H, Stehning C, and Manning WJ. “2D free-breathing dual navigator-gated cardiac function validated against the 2D breath-hold acquisition.” *J Magn Reson Imaging*, 2008. **28**(3):773–777. ISSN 1878-5832. doi:10.1002/jmri.21417.
- [74] Potthast S, Mitsumori L, Stanescu LA, Richardson ML, Branch K, Dubinsky TJ, and Maki JH. “Measuring aortic diameter with different MR techniques: Comparison of three-dimensional (3D) navigated steady-state free-precession (SSFP), 3D contrast-enhanced magnetic resonance angiography (CE-MRA), 2D T2 black blood, and 2D cine SSFP.” *Journal of Magnetic Resonance Imaging*, 2010. **31**(1):177–184. ISSN 10531807. doi:10.1002/jmri.22016.
- [75] Markl M, Kilner PJ, and Ebbers T. “Comprehensive 4D velocity mapping of the heart and great vessels by cardiovascular magnetic resonance.” *J Cardiovasc Magn Reson*, 2011. **13**:7. doi:10.1186/1532-429X-13-7.
- [76] Harte JM, Golby CK, Acosta J, Nash EF, Kiraci E, Williams MA, Arvanitis TN, and Naidu B. “Chest wall motion analysis in healthy volunteers and adults with cystic fibrosis using a novel Kinect-based motion tracking system.” *Medical & biological engineering & computing*, 2016. ISSN 1741-0444 (Electronic). doi:10.1007/s11517-015-1433-1.
- [77] Heß M, Büther F, Gigengack F, Dawood M, and Schäfers KP. “A dual-Kinect approach to determine torso surface motion for respiratory motion correction in PET.” *Medical Physics*, 2015. **42**(5):2276–2286. ISSN 0094-2405. doi:10.1118/1.4917163.
- [78] Kim T, Pollock S, Lee D, O’Brien R, and Keall P. “Audiovisual biofeedback improves diaphragm motion reproducibility in MRI.” *Med Phys*, 2012. **39**(11):6921–6928. doi:10.1118/1.4761866.
- [79] Boettler P, Hartmann M, Watzl K, Maroula E, Schulte-moenting J, Knirsch W, and Dittrich S. “Heart Rate Effects on Strain and Strain Rate in Healthy Children.” *J Am Soc Echocardiogr*, 2005. **18**:1121–1130. ISSN 08947317. doi:10.1016/j.echo.2005.08.014.
- [80] Piran S, Bassett AS, Grewal J, Swaby JA, Morel C, Oechslin EN, Redington AN, Liu PP, and Silversides CK. “Patterns of cardiac and extracardiac anomalies in adults with tetralogy of Fallot.” *American heart journal*, 2011. **161**(1):131–137. ISSN 1535-7228. doi:10.1016/j.ahj.2010.09.015.
- [81] Pang J, Bhat H, Sharif B, Fan Z, Thomson LE, Labounty T, Friedman JD, Min J, Berman DS, and Li D. “Whole-heart coronary MRA with 100% respiratory gating efficiency: Self-navigated three-dimensional retrospective image-based motion correction (TRIM).” *Magn Reson Med*, 2014. **71**(1):67–74. doi:10.1002/mrm.24628.

- [82] Chen X, Salerno M, Yang Y, and Epstein FH. “Motion-compensated compressed sensing for dynamic contrast-enhanced MRI using regional spatiotemporal sparsity and region tracking: Block low-rank sparsity with motion-guidance (BLOSM).” *Magnetic Resonance in Medicine*, 2013. **1038**(November 2013):1028–1038. ISSN 07403194. doi:10.1002/mrm.25018.
- [83] Scott AD, Tayal U, Nilles-Vallespin S, Ferreira P, Zhong X, Epstein FH, Prasad SK, and Firmin D. “Accelerating cine DENSE using a zonal excitation.” *Journal of Cardiovascular Magnetic Resonance*, 2016. **18**(Suppl 1):O50. ISSN 1532-429X. doi:10.1186/1532-429X-18-S1-O50.

Sean Michael Hamlet

Vita

Education

- 2011–2012 **Master of Science in Electrical Engineering**,
University of Kentucky, Lexington, KY.
GPA - 4.0
- 2006–2010 **Bachelor of Science in Electrical Engineering**,
Western Kentucky University, Bowling Green, KY.
GPA - 4.0

Professional Positions

- 2013–2017 **Graduate Research Assistant**, *Cardiac Imaging Technology Lab*
University of Kentucky, Lexington, KY.
- 2013 **Electrical Engineering Hardware Student**, *Sensor Team*
Lexmark International, Inc., Lexington, KY.
- 2012 **Graduate Research Assistant**, *Center for Visualization and Virtual Environments*
University of Kentucky, Lexington, KY.
- 2012 **Electrical Engineering Hardware Student**, *Sensor Team*
Lexmark International, Inc., Lexington, KY.
- 2011–2012 **Teaching Assistant**, *EE280 - Design of Logic Circuits*
University of Kentucky, Lexington, KY.
- 2011 **Electrical Engineering Hardware Student**, *Sensor Team*
Lexmark International, Inc., Lexington, KY.
- 2009–2010 **Research Assistant**, *Applied Physics Institute*
Western Kentucky University, Bowling Green, KY.

Funding

- 2015–pres **Ruth L. Kirschstein Predoctoral Individual NRSA (NIH F31)**,
National Institutes of Health: National Heart, Lung, and Blood Institute,
April 15, 2015 (3 years of funding).

Honors and Awards

- 2013 Eta Kappa Nu Outstanding Electrical and Computer Engineering Graduate Student
- 2012–2013 Dr. Robert D. Hayest Fellowship
- 2012–2013 Lexmark Fellowship
 - 2013 *President*, Eta Kappa Nu (EE Honor Society) Beta Upsilon Chapter
 - 2012– Member, Eta Kappa Nu
- 2011–2012 Research Challenge Trust Fund Fellowship
- 2011–2012 Teaching Assistantship
 - 2010 Summa Cum Laude Graduate of WKU
 - 2010 Passed Fundamentals of Engineering (FE) Exam
 - 2010 Academic Excellence Award for the College of Engineering (WKU)
 - 2010 Only Student Leadership Representative for Electrical Engineering Department
 - 2010 *Charter President*, Tau Beta Pi (National Engineering Honor Society)
 - 2010– Member, Tau Beta Pi
 - 2009 IEEE Southeastern Conference Robotics Competition (7th Place)
 - 2009 *Treasurer*, IEEE
 - 2009 Attended National Convention as only student representative to bid for WKU EHS to become new Tau Beta Pi Chapter
- 2009–2010 *President*, WKU Engineering Honor Society
- 2009–2010 Member, WKU Engineering Honor Society
 - 2008– Member, IEEE
- 2006–2010 Ogden Scholarship
- 2006–2010 Regent's Scholarship
- 2006–2007 Siemens/NACO Buchanon Scholarship

Publications

- 2017 **Hamlet SM**, Haggerty CM, Suever JD, Wehner GJ, Andres KN, Powell DK, Charnigo RJ, and Fornwalt BK. Using a respiratory navigator significantly reduces variability when quantifying left ventricular torsion with cardiovascular magnetic resonance. *Journal of Cardiovascular Magnetic Resonance*. 2017, 19(1):25. doi: 10.1186/s12968-017-0338-6
- 2016 **Hamlet SM**, Haggerty CM, Suever JD, Wehner GJ, Grabau JD, Andres KN, Vandsburger MH, Powell DK, Sorrell VJ, and Fornwalt BK. An interactive videogame designed to improve respiratory navigator efficiency in children undergoing cardiac magnetic resonance. *Journal of Cardiovascular Magnetic Resonance*. 2016, 18(1):54. doi: 10.1186/s12968-016-0272-z

- 2017 **Hamlet SM**, Haggerty CM, Suever JD, Wehner GJ, Andres KN, Powell DK and Fornwalt BK. Optimal configuration of respiratory navigator gating for the quantification of left ventricular strain using spiral cine displacement encoding with stimulated echoes (DENSE) MRI. *Journal of Magnetic Resonance Imaging*. 2017, 45(3):786-794. doi: 10.1002/jmri.25389
- 2017 Suever JD, Wehner GJ, Jing L, Powell DK, **Hamlet SM**, Grabau JD, Mojsejenko WD, Andres KN, Haggerty CM, Fornwalt BK: Right Ventricular Strain, Torsion, and Dyssynchrony in Healthy Subjects Using 3D Spiral Cine DENSE Magnetic Resonance Imaging. *IEEE Transactions on Medical Imaging* 2017, 36(5):1076-1085.
- 2016 Jing L, Binkley CM, Suever JD, Umasankar N, Haggerty CM, Rich J, Nevius CD, Wehner GJ, **Hamlet SM**, Powell DK, Radulescu A, Kirchner HL, Epstein FH, Fornwalt BK: Cardiac remodeling and dysfunction in childhood obesity: a cardiovascular magnetic resonance study. *J Cardiovasc Magn Reson* 2016, 18:28.
- 2015 Wehner GJ, Grabau JD, Suever JD, Haggerty CM, Jing L, Powell DK, **Hamlet SM**, Vandsburger, MH, Zhong X, Fornwalt BK. 2D cine DENSE with low encoding frequencies accurately quantifies cardiac mechanics with improved image characteristics. *Journal of Cardiovascular Magnetic Resonance*. 2015, 17(1):93
- 2015 Wehner GJ, Suever JD, Haggerty CM, Jing L, Powell DK, **Hamlet SM**, Grabau JD, Mojsejenko WD, Zhong X, Epstein FH, Fornwalt BK. Validation of in vivo 2D displacements from spiral cine DENSE at 3T. *Journal of Cardiovascular Magnetic Resonance*. 2015, 17(1):5
- 2014 Suever JD, Wehner GJ, Haggerty CM, Jing L, **Hamlet SM**, Binkley CM, Kramer SP, Mattingly AC, Powell DK, Bilchick KC, Epstein FH, Fornwalt BK: Simplified post processing of cine DENSE cardiovascular magnetic resonance for quantification of cardiac mechanics. *Journal of Cardiovascular Magnetic Resonance* 2014, 16:94.
- 2012 **Hamlet SM**: Comparing Acoustic Glottal Feature Extraction Methods with Simultaneously Recorded High-Speed Video Features for Clinically Obtained Data.. *Theses and Dissertations–Electrical and Computer Engineering* 2012, Paper 12. http://uknowledge.uky.edu/ece_etds/12

International Conference Abstracts

- 2017 **Hamlet SM**, Haggerty CM, Suever JD, Wehner GJ, Andres KA, Powell DK, Charnigo RJ, Fornwalt BK, Using a respiratory navigator significantly reduces variability when quantifying left ventricular torsion from CMR, Society of Cardiovascular Magnetic Resonance Scientific Sessions, Washington, DC, February 2017.

- 2016 **Hamlet SM**, Suever JD, Grabau JD, Wehner GJ, Vandsburger MH, Andres KA, Powell DK, Sorrell VL, Fornwalt BK, An interactive videogame designed to optimize respiratory navigator efficiency in children undergoing cardiac magnetic resonance, Society of Cardiovascular Magnetic Resonance Scientific Sessions, Los Angeles, CA, January 2016.
- 2015 **Hamlet SM**, Andres KA, Wehner GJ, Suever JD, Powell DK, Zhong X, Epstein FH, Fornwalt BK, Patient-specific variability in breath-hold positions during cardiac magnetic resonance imaging has a negligible effect on quantification of cardiac mechanics, Society of Cardiovascular Magnetic Resonance Scientific Sessions, Nice, France, February 2015.
- 2015 **Hamlet SM**, Andres KA, Wehner GJ, Suever JD, Powell DK, Zhong X, Epstein FH, Fornwalt BK, The effect of respiratory gating strategy on left ventricular cardiac strains with DENSE magnetic resonance imaging, Society of Cardiovascular Magnetic Resonance Scientific Sessions, Nice, France, February 2015.
- 2014 **Hamlet SM**, Wehner GW, Suever JD, Powell DK, Haggerty CM, Jing L, Zhong X, Epstein FH, Fornwalt BK, Effect of Variable Breath-hold Positions During Cardiac Magnetic Resonance on Measures of Left Ventricular Mechanics, Society of Cardiovascular Magnetic Resonance Scientific Sessions, New Orleans, LA, January 2014.
- 2013 **Hamlet SM**, Donohue KD, Unnikrishnan H, Patel RR, Acoustic and High-Speed Video Synchronization of Clinical Recordings for Enhanced Feature Estimations, Proceedings of the 10 International Conference on Advances in Quantitative Laryngology, Voice and Speech Research, Cincinnati, OH, June 2013.
- 2009 **Hamlet SM**, Simpson M, Morrison T, Berry A, Lodmell M, Re-Engineering of a User-Controlled Robotic ATV Platform, 20th Annual Argonne Symposium for Undergraduates, Lemont, IL, November 2009.